Pile driving induced liquefaction instability in sandy soils

Rawsan Al-Djema

Pile driving induced liquefaction instability in sandy soils

By

Rawsan Al-Djema

in partial fulfilment of the requirements for the degree of

Master of Science
in Civil Engineering

at the Delft University of Technology,

to be defended publicly on Monday April 23, 2018.

Thesis Committee

prof. dr. A. V. Metrikine (chairman)	TU Delft, Structural Mechanics
dr. ir. A. Tsouvalas	TU Delft, Hydraulic Engineering
ir. L.J.M. Houben	TU Delft, Pavement Engineering
Ir. D.J. Jaspers Focks	Witteveen + Bos

TU Delft Witteveen + Bos

Abstract

Sandy soils are characterized by negligible cohesion (compared to clay) and limited drainage capacity (compared to gravel), which makes these soils susceptible to excess pore (water) pressure accumulation induced by short term dynamic loading cycles. Pile driving subjects the soil to such type of dynamic loading. Accumulation of excess pore water pressure continuous until contact between the sand particles is lost, a process known as soil liquefaction.

This research investigates two soil configurations which are vulnerable to pore pressure accumulation and subsequent liquefaction induced by pile driving: slopes and confined aquifers. Slopes are vulnerable because of their geometry. Limited accumulation of excess pore pressures might be sufficient to induce sliding failure. Confined aquifers are vulnerable because of the lack of drainage boundaries. This can result in significant excess pore pressure accumulation in the aquifer.

Pile driving induced liquefaction instability is modelled by considering the pile-soil-plug interaction, the emission, propagation and attenuation of waves into the soil domain and the resulting generation of excess pore pressures. Two models are developed for this purpose.

The first is an cylindrically symmetric damped elastic pile-soil-plug model. This model calculates the vertical and radial displacements in the soil domain as a function of space and time. Shear stresses, which are the driving parameter for the second model, are then calculated as a function of the spatial derivatives of the two displacement components.

The second (liquefaction) model is a combination of the governing differential equation for cylindrically symmetric soil consolidation and an empirical model describing generation of excess pore pressures as a function of shear stress amplitudes. The output of this model is the steady state relative overpressure distribution. The relative overpressure distribution can then be used as input into slope stability analysis software in order to investigate whether a slope failure will occur given the reduced soil strength.

The biggest uncertainty in the second model is the coupling with the first model. This coupling is achieved by adjusting the elastic shear stresses (which are unrealistic and can therefore not be directly used as input for the liquefaction model) calculated in the first model. Three variables are defined for this purpose. Analysis of the sensitivity of these variables show that the variable β, which is the ratio between yield shear stress and initial effective stress of a liquefied interface, is the most sensitive and therefore most uncertain variable in the model. Experimental validation of β is recommended to the increase accuracy of the liquefaction model.

Acknowledgements

I would like to thank my company supervisor Dirk-Jan Jaspers Focks for always being available and for encouraging me whenever I got stuck. I thank Apostolos Tsouvalas for the detailed remarks on the final draft of the report and Andrei Metrikine for steering me in the right direction during the progress meetings. I would also like to thank mister Houben for helping out with organizational matters.

Content

1 Introduction

1.1 Problem statement

Pile driving is a strongly dynamical process (figure 1.1). First energy is transmitted from the impact hammer to the pile. This energy is carried down the pile by a stress wave. As time progresses the amplitude of the stress wave attenuates because of energy losses at the pile-soil interface. Some energy is dissipated by friction when the pile is slipping, while the remaining energy is carried by waves into the soil domain (for example conical shear waves originating from the pile shaft and spherical compression waves originating from the pile toe).

This thesis will consider instability in saturated loosely packed sand. Loose packing is an inefficient arrangement of the particles. The spaces between the particles (voids) are filled with water in case of saturated soils. The oscillating motion of the waves propagating into the soil domain results in shear stresses, which shake the sand and force the sand particles into a denser arrangement. This causes a reduction in void volume, resulting in excess pore pressures. These excess pore pressures will accumulate if the frequency of the loading is high enough and the drainage capacity of the sand is low enough (final step in figure 1.1). Accumulation continuous until the excess pore pressures become equal to the initial effective stress between the sand particles (overburden stress – hydrostatic water pressure). Once this stage is reached, the effective stress between the particles will equal zero. The contact between the particles is lost and the sand behaves similar to a viscous fluid. This process is called liquefaction.

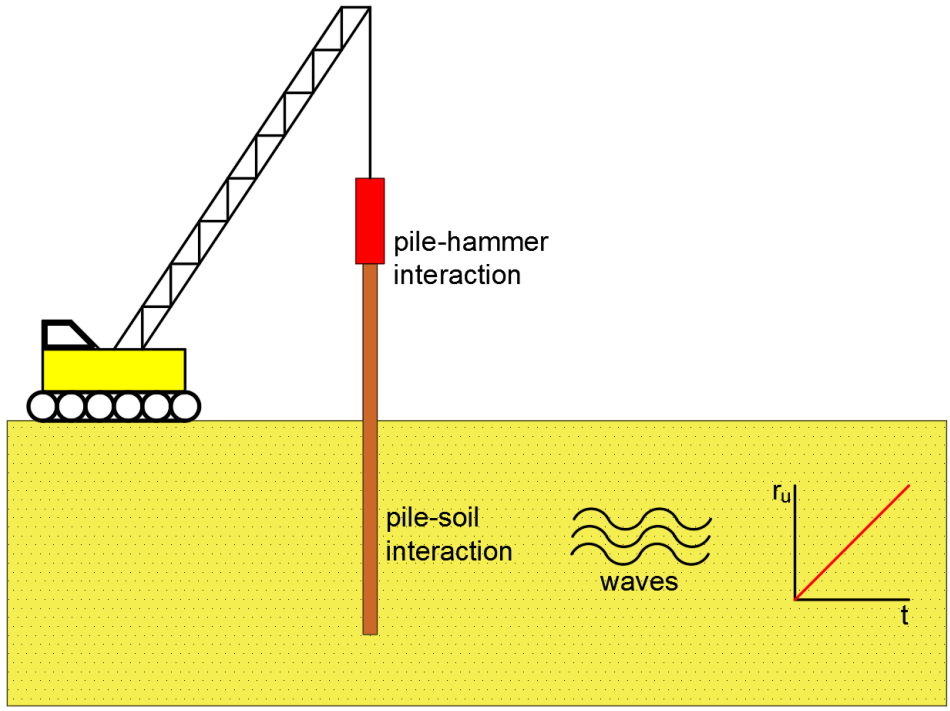

Figure 1.1: Problem statement

Two types of pile driving induced liquefaction instability cases will be considered in this thesis. It is important to note that the definition of liquefaction instability in this thesis is not strictly instability induced by liquefaction (excess pore pressure = initial effective stress), but rather instability induced by excess pore pressures in general. The first case is instability in slopes (figure 1.2). Embankment structures in ports commonly consist of a sand core because they are often constructed on reclaimed land. The core is constructed by spraying or rainbowing the sand layer by layer. This results in loosely packed sand with limited effective stress. Limited accumulation in excess pore water pressure induced by pile driving may degrade the resistance of the soil along a certain circle trajectory to become smaller than the imposed loading, initiating collapse (figure 1.2).

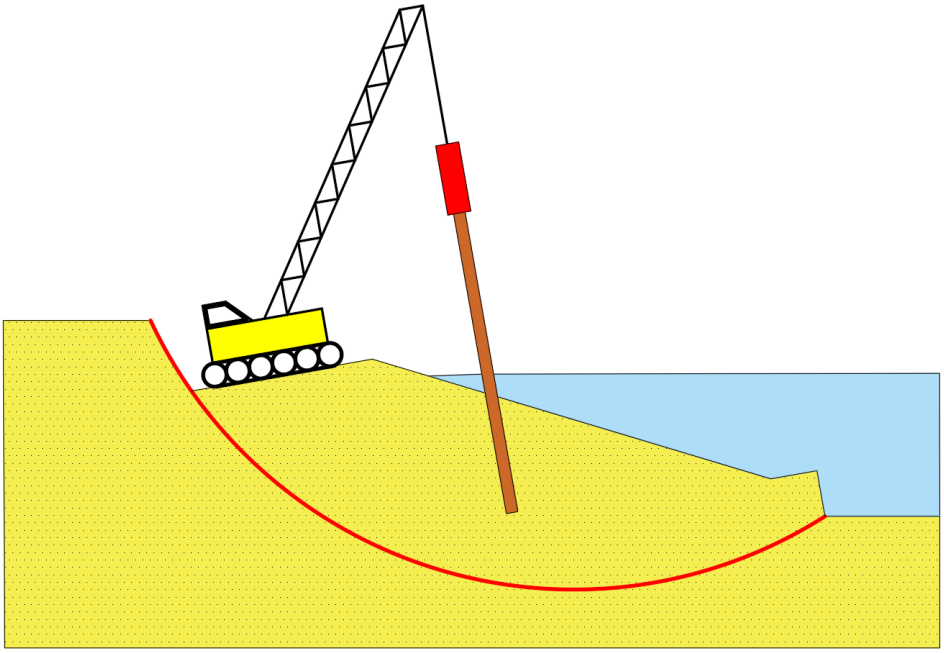

Figure 1.2: Pile driving induced liquefaction instability in slopes

The second case of liquefaction induced instability is a confined aquifer (figure 1.3). The figure shows a sand layer (the aquifer) confined between two impermeable clay layers. Pile driving results in excess pore water pressure in the sand layer, which cannot dissipate easily because of the impermeable upper and lower boundaries. This can result in significant accumulation in excess pore pressures. As a consequence the upper clay layer will not be evenly supported anymore, resulting in cracks. Water flows to the surface through these cracks. This is a very dangerous type of failure if a building pit is located at the surface.

Combinations of both slopes and confined aquifers might exist as well in practice.

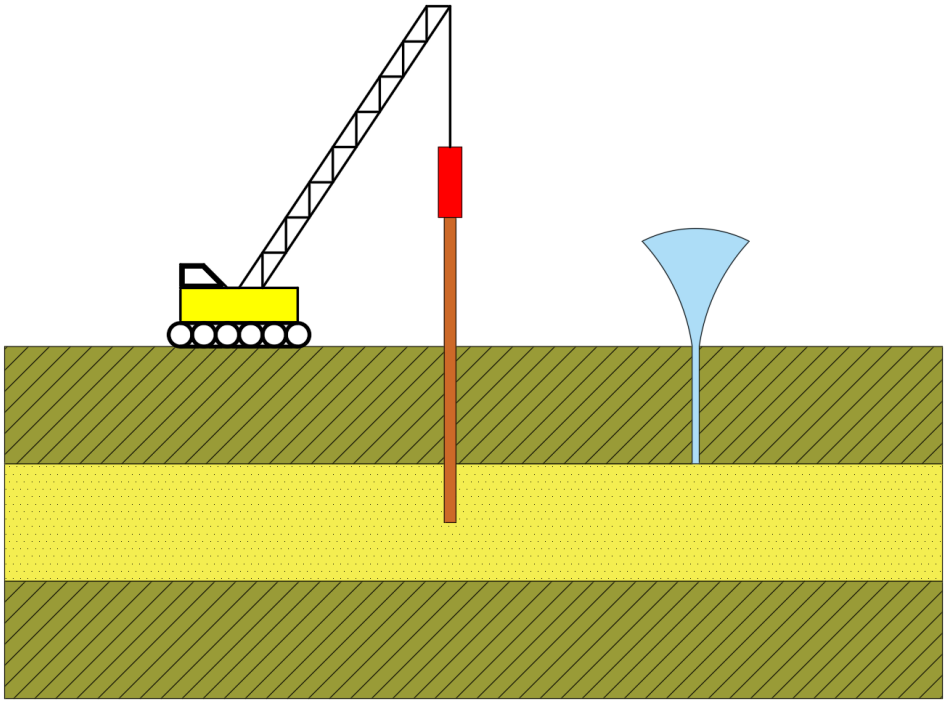

Figure 1.3: Pile driving induced liquefaction instability in confined aquifers

1.2 Objectives

Various models (analytical, empirical or numerical) exist for describing specific processes like pile driving, wave propagation in soils and excess pore pressure accumulation. A comprehensive framework is lacking. This thesis aims to set up such a comprehensive framework by combining separate models into one integrated model capable of predicting pile driving induced liquefaction instability. The output desired from the final model is a plot which shows the excess pore pressure distribution surrounding the pile. This will help practicing engineers to assess if pile driving induced liquefaction instability might pose a risk and whether more advanced analysis is required.

1.3 Outline

The literature study consists of chapter 2 and 3. Chapter 2 will discuss important background theory. Equations of motion for one and three dimensional elastic media will be presented. This is followed by a discussion of the types of waves propagating in elastic media and waves emanating from the pile-soil interface. The process of liquefaction is elaborated in more detail; and the chapter ends with presenting numerical methods in the time domain for solving partial differential equations in later chapters. Chapter 3 discusses existing pile driving models: the Smith model (soil is represented by a rheological model), the van den Berghe-Holeyman model (soil is represented by rigid cylinders) and the Salgado et al. model (soil is represented by thin slices).

Chapters 4 and 5 present a cylindrically symmetric damped elastic pile-soil-plug model. Chapter 4 presents the simplified model, neglecting radial displacement; while the full (soil) equations are solved in chapter 5. Results presented in chapter 4 will mainly focus on demonstrating the influence of different model components. The results in chapter 5 will focus on influence of soil layering and on the differences with the simplified model.

The final chapter, chapter 6, presents the liquefaction model. The governing equations for the model will be derived and the coupling with the pile-soil-plug model will be discussed. Uncertainties in the coupling are quantified by variables, of which the sensitivity will be analysed.

1.4 Input tables

Tables with input variables used in this report are all assembled in this section for the convenience of the reader. Each chapter will refer to one or multiple of these tables.

Input table 1.1: hammer

mass	m_H	20000	kg
impact velocity	$v_{0,H}$	5	m/s
cushion stiffness	$k_{c,H}$	10^{10}	N/m
hammer height	L_H	8	m

Input table 1.1

Input table 1.2: pile

external diameter	d_P	2	m
thickness	t_P	$40 * 10^{-3}$	m
cross-sectional area	A_P	$1244 * 10^{-4}$	m^2
Young's modulus	E_P	$200 * 10^9$	N/m^2
density	ρ_P	7850	kg/m^3
wave velocity	c_{Pile}	5047.54	m/s
Impedance	Z_P	$4.93 * 10^6$	Ns/m

Input table 1.2

Input table 1.3: pile driving (values apply for medium sand)

shaft quake	Q_{shaft}	$2.5 * 10^{-3}$	m
toe quake	Q_{toe}	$2.5 * 10^{-3}$	m
shaft static limit	τ_s	$5 * 10^4$	N/m^2
toe static limit	p_{lim}	$8 * 10^6$	N/m^2
shaft damping ratio	J_{shaft}	0.16	s/m
toe damping ratio	J_{toe}	0.5	s/m

Input table 1.3

Input table 1.4: soil

	shear modulus	*bulk modulus*	*density*	*shear wave velocity*	*compression wave velocity*
	G	K	ρ	c_s	c_c
	N/m^2	N/m^2	kg/m^3	m/s	m/s
soft clay	$35 * 10^6$	$3600 * 10^6$	1600	148	1510
firm clay	$110 * 10^6$	$5000 * 10^6$	1800	247	1691
loose saturated sand	$70 * 10^6$	$3800 * 10^6$	1700	203	1513
medium saturated sand	$150 * 10^6$	$5900 * 10^6$	2000	274	1746

Input table 1.4

Input table 1.5: liquefaction modelling

empirical constant	a	0.48	–
empirical constant	b	5	–
empirical constant	θ	0.7	–
ratio between yield shear stress and initial effective stress for zero relative overpressure	α	0.18	–
ratio between yield shear stress and initial effective stress for unity relative overpressure	β	0.1	–
ratio between the increase in amount of shear cycles and the decrease of resistance at the pile-soil interface	γ	1	–
initial relative density	I_D	0.5	–
coefficient of vertical consolidation	c_V	0.1	m^2/s
coefficient of horizontal consolidation	c_H	0.1	m^2/s
time interval between subsequent blows	t_i	1	s

Input table 1.5

Sign convention

$$s \rightarrow scalar$$

$$\boldsymbol{v} \rightarrow vector$$

$$[M] \rightarrow matrix$$

2 Background theory

This chapter presents all necessary background theory for this thesis. The equations of motion of elastic media and numerical solution procedures will be extensively used in the next chapters.

2.1 Wave mechanics

2.1.1 The wave equation

The wave equation for rods under axial load N (for example piles) can be derived by considering a slice of rod having a length Δx, displacement u, density ρ and cross-sectional area A:

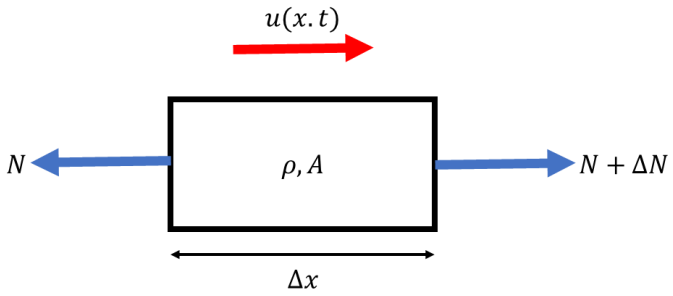

Figure 2.1: Force equilibrium of a pile slice

Using figure 2.1, the equation of motion can be derived from equilibrium:

$$\rho A \Delta x \frac{\partial^2 u}{\partial t^2} = N + \Delta N - N = \Delta N \tag{2.1}$$

Dividing both sides by Δx and taking the limit of Δx to 0 results in:

$$\frac{\partial^2 u}{\partial t^2} - \frac{1}{\rho A}\frac{\partial N}{\partial x} = 0 \tag{2.2}$$

The constitutive and kinematic relations (for linear rods) read:

$$N = EA\varepsilon = EA\frac{du}{dx} \tag{2.3}$$

E is the Young's modulus of the rod and ε is the strain of the rod. The final form of the (linear) wave equation for rods is obtained by substituting equation 2.3 into equation 2.2:

$$\frac{\partial^2 u}{\partial t^2} - \frac{E}{\rho}\frac{\partial^2 u}{\partial u^2} = \frac{\partial^2 u}{\partial t^2} - c^2\frac{\partial^2 u}{\partial u^2} = 0 \tag{2.4}$$

In this equation parameter c is the wave propagation velocity. The solution of the wave equation was first proposed by D'Alembert:

$$u(x,t) = u^+(x - ct) + u^-(x + ct) \tag{2.5}$$

It describes two waves travelling in opposite direction, with a constant velocity equal to the wave propagation velocity (figure 2.2). This underlines the significance of this parameter. While propagating the waves keep their shape, no distortion is observed. Such a wave is called non-dispersive.

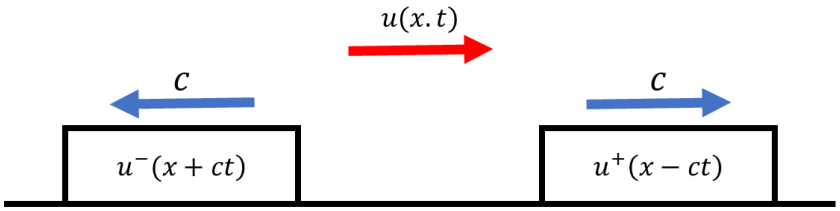

Figure 2.2: Wave equation solution visualized

In section 2.3 it will become clear that the wave equation is also suitable for modelling one dimensional wave propagation in soils, either in compression or shear. The only difference is the definition of the wave propagation velocity.

2.1.2 Impedance

The impedance relates normal force and velocity (Holsher, 2016). The definition of normal force and velocity reads:

$$v(x,t) = \frac{\partial u(x,t)}{\partial t} \tag{2.6}$$

$$N(x,t) = EA\frac{\partial u(x,t)}{\partial x} \tag{2.7}$$

Substituting u^+ or u^- from equation 2.5 into equations 2.6 and 2.7 and performing some algebraic manipulations yields:

$$N^+ = -\frac{EA}{c}v^+ = -Zv^+ \tag{2.8}$$

$$N^- = \frac{EA}{c}v^- = Zv^- \tag{2.9}$$

N^+ and v^+ relate to u^+ and N^- and v^- relate to u^-. Z is the impedance. The importance of the impedance is illustrated by an example:

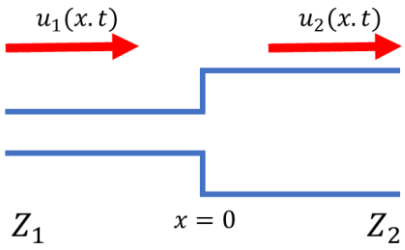

Figure 2.3: Sudden change in impedance

Suppose an incident wave is travelling towards an interface with a discontinuity in the impedance, as illustrated in figure 2.3. To determine the reflected and transmitted wave as a function of the incident wave, two interface conditions need to be formulated:

$$v_i + v_r = v_t \tag{2.10}$$

$$N_i + N_r = N_t \rightarrow -Z_1 v_i + Z_1 v_r = -Z_2 v_t \tag{2.11}$$

Solving equation 2.10 and 2.11 yields:

$$v_r = \frac{Z_1 - Z_2}{Z_1 + Z_2} v_i \tag{2.12}$$

$$N_r = \frac{Z_2 - Z_1}{Z_1 + Z_2} N_i \tag{2.13}$$

$$v_t = \frac{2Z_1}{Z_1 + Z_2} v_i \tag{2.14}$$

$$N_t = \frac{-2Z_2}{Z_1 + Z_2} \tag{2.15}$$

This shows the importance of the impedance:

- If $Z_1 \ll Z_2$, the incident wave is travelling to a very stiff (almost fixed) boundary. The velocity will change sign upon reflection, while the normal force keeps its sign.
- If $Z_1 \gg Z_2$, the incident wave is travelling to a very weak (almost open ended) boundary. In this case the velocity will keep its sign upon reflection, while the normal force changes sign.

2.1.3 Non-reflective boundary

A non-reflective boundary fully absorbs the incoming wave energy, therefore no reflection occurs. A simple non-reflective boundary consisting of a dashpot at the end of a one dimensional rod (figure 2.4) Is considered.

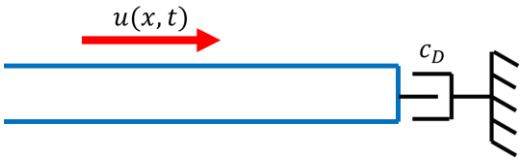

Figure 2.4: Non-reflective boundary

The boundary condition reads:

$$Z(v_r - v_i) = -c_D(v_i + v_r) \tag{2.16}$$

And therefore:

$$v_r = \frac{Z - c_D}{Z + c_D} v_i \tag{2.17}$$

No reflection occurs if the dashpot constant is equal to the impedance of the rod. The importance of the impedance as a dynamic parameter is again underlined. This simple non-reflective boundary will be extensively used in the various models presented in the upcoming chapters.

2.2 Pile driving

2.2.1 Impact pile driving

Several types of hammers exist for impact pile driving(Deckner, 2013), the most important are:

- drop hammers: the hammer is pulled to a certain height and dropped on top of the pile.
- diesel hammers: igniting diesel causes an explosion raising op a piston, which then falls on top of the pile.
- hydraulic hammers: the lifting of the hammer is assisted by hydraulic devices.

Deckner also distinguishes between light and heavy impact hammers, the latter having a weight larger than the total weight of the pile. The usual blow rate of heavy hammers is 30-60 bpm (blows per minute), while light hammers have rates of 300-1000 bpm.

Massarsch & Fellenius (2008) proposes a simple method of modelling the hammer impact. A simple rectangular pulse represents the impact. The height of the pulse (impact velocity) is equal to:

$$v_{impact} = \frac{\sqrt{2gh_0}}{1 + \frac{Z_p}{Z_H}} \tag{2.18}$$

In which h_0 is the drop height of the hammer, Z_p the impedance of the pile (section 2.4) and Z_H the impedance of the hammer. It is observed that according to Massarsch & Fellenius, the mass of the hammer does not affect the magnitude of the pulse. Massarsch & Fellenius also propose to add a reduction factor, accounting for the energy transmission loss upon hammer impact. The width of the pulse is equal to the time needed for the stress wave to travel up and down the hammer (Massarsch & Fellenius, 2008):

$$t_{pulse} = \frac{2L_H}{c_H} \tag{2.19}$$

L_H is the hammer height and c_H the wave propagation velocity in the hammer (section 2.3).

A more sophisticated method is proposed by Deeks & Randolph (1993) as shown in figure 2.5.

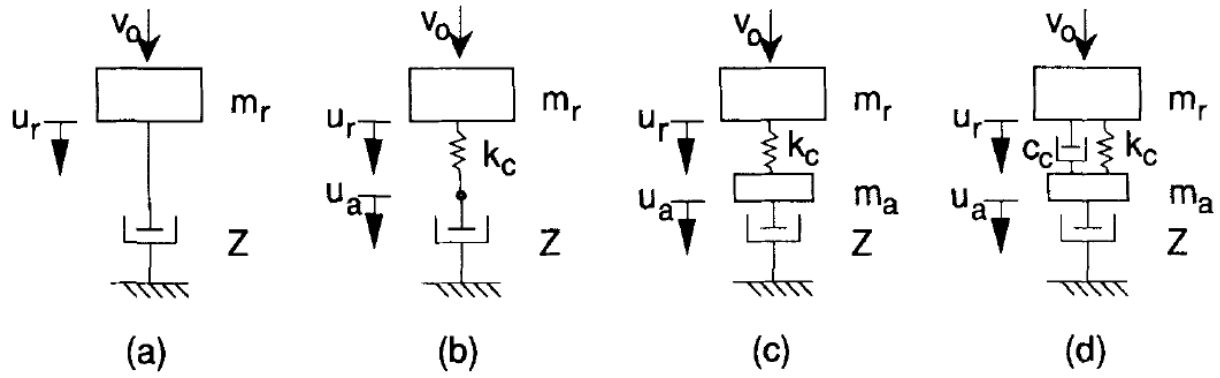

Figure 2.5: Deeks & Randolph (1993) models for hammer impact

Model (d) is the most complex, taking every single component into account. The pile is modelled as a dashpot, with Z being the pile impedance. The mass of the pile cap m_a is taken into account and the

cushion is attributed both stiffness k_c and damping c_c. The hammer is represented by its mass m_r and initial velocity $v_0 = \sqrt{2gh_0}$. To make a comparison with the Massarsch & Fellenius model, model (b) is chosen, the analytical solution of the impact velocity for this model is (Holscher, 2016):

$$v_{impact}(t) = v_0 \frac{\alpha}{\sqrt{\omega^2 - \alpha^2}} e^{-\alpha t} \sin(\sqrt{\omega^2 - \alpha^2}\, t) \tag{2.20}$$

$$\alpha = \frac{k_c}{2Z_P} \; and \; \omega = \sqrt{\frac{k_c}{m_r}} \tag{2.21}$$

Values of $v_{impact} < 0$ are not allowed, since the hammer cannot pull the pile. The input parameters are chosen according to tables 1.1 (pile) and 1.2 (hammer). The impedance of the hammer is assumed equal to the impedance of the pile. The following plot shows the results of both methods:

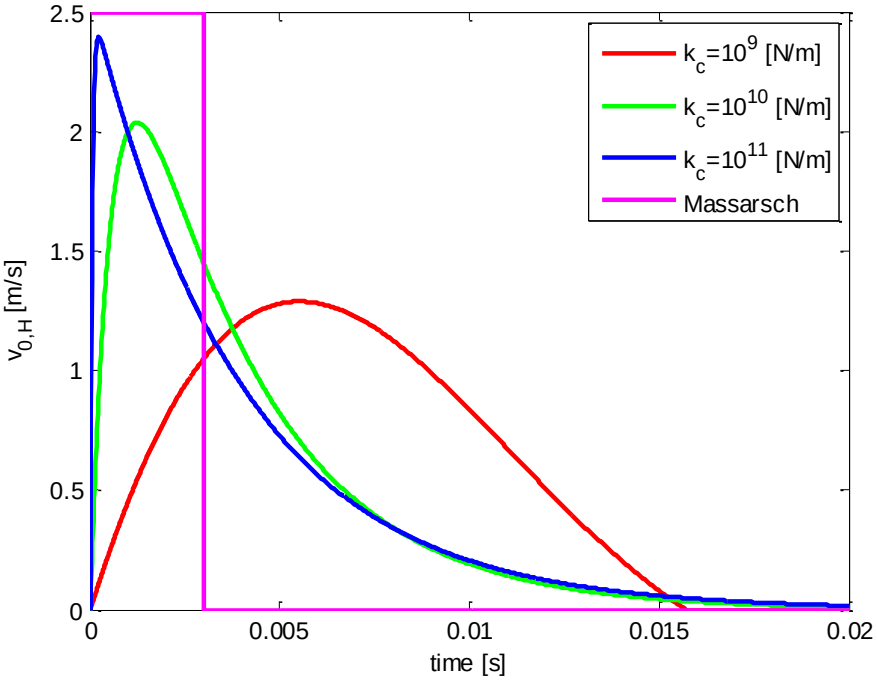

Figure 2.6: Impact velocity on top of the pile as a function of time using different methods and cushion stiffness

It is clear that higher cushion stiffness results in higher peak impact velocity at the pile head. The Deeks & Randolph method is preferred over the Massarsch & Fellenius method, because of the more realistic representation of the hammer impact.

2.2.2 Vibratory pile driving

The process of vibratory pile driving is depicted in figure 2.7. Two sets of eccentric masses are placed symmetrically with respect to the symmetry axis of the vibrator. The masses on each side of the symmetry axis rotate in opposite direction, therefore cancelling out the horizontal component of their centrifugal force and resulting in a harmonic vertical component over time (van den Berghe, 2001). The total vertical force exerted on the pile is the sum of the harmonic force excited by the rotating mases and the total static weight of the vibrator (including bias mass).

The loading frequency ranges between 1300 and 1800 rpm (rounds per minute) and the centrifugal force amplitude is up to 4600 kN (van den Berghe 2001). Figure 2.8 shows an example of vibratory pile driving loading, with centrifugal force amplitude of 3000 kN, static load of 1500 kN and frequency of 1500 rpm.

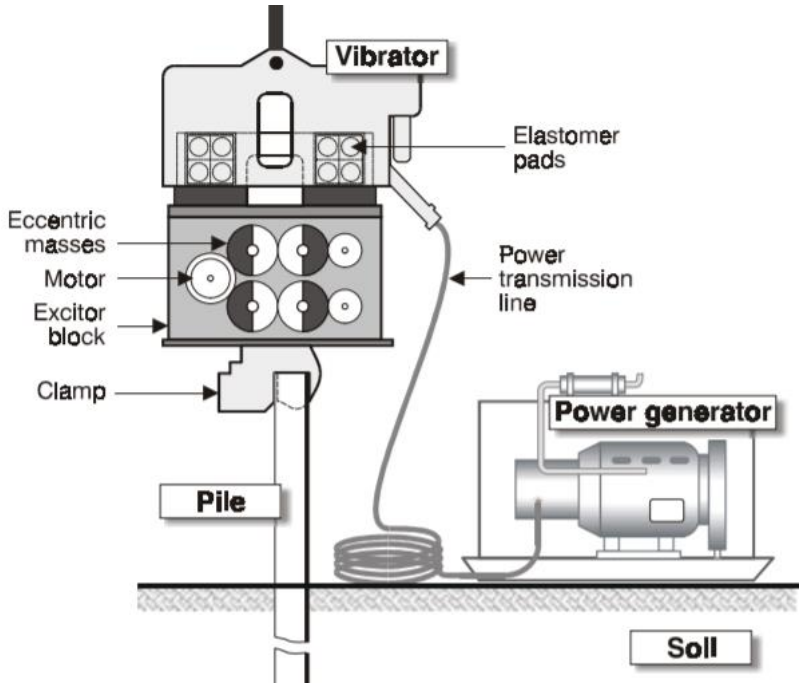

Figure 2.7: Vibratory pile driving scheme (Holeyman, 2000)

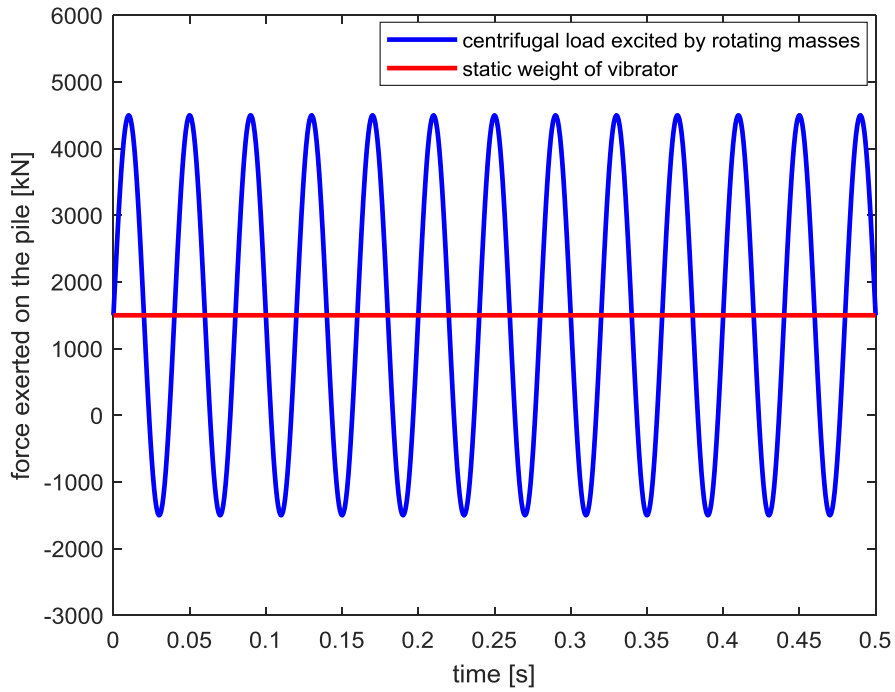

Figure 2.8: Example of vibratory pile driving loading

2.3 Soil behaviour

2.3.1 Soil properties

This thesis considers elastic behaviour of soils. A set of three variables is required for describing elastic soil behaviour: density, shear modulus and bulk modulus.

The soil density depends on the porosity of the soil. The shape of the soil particles (for example rounded or angular), the sorting of the particles and their arrangement (for example loose or dense) will determine the porosity (van Tol, 2006). The density of non-porous mineral is around $2650\ kg/m^3$. Table 2.1 gives estimates for soil density of various types of soil used in this thesis.

	porosity $(\%)$	density (kg/m^3)
loose saturated sand	55	1700
medium saturated sand	40	2000
soft clay	60	1600
firm clay	50	1800

Table 2.1: Soil density (van Tol, 2006)

The shear modulus of soil strongly depends on the strain rate. According to Deckner (2013), plastic soils (like clay) subjected to high strain rates tend to suffer smaller degradation of the shear modulus compared to non-plastic soils (like sand). When modelling soil as an elastic material, these effects are not considered. This makes choosing the shear modulus very sensitive to error. Table 2.2 lists an estimated range of the shear modulus for different types of soil considered in this thesis.

	shear modulus (MPa)
loose saturated sand	15-110
medium saturated sand	70-250
soft clay	10-65
firm clay	55-190

Table 2.2: Soil shear modulus (Head & Jardine, 1992)

The upcoming sections will show that both shear and bulk modulus can be derived from the shear and compression wave velocity of the soil.

2.3.2 Equations of motion of an elastic medium

A detailed derivation of the equation of motion of an elastic medium can be found in Holscher (2016). The final form of the equation is given:

$$\rho \frac{\partial^2 \boldsymbol{u}}{\partial t^2} = \left(K + \frac{1}{3}G\right) \nabla\nabla \cdot \boldsymbol{u} + G\nabla^2 \boldsymbol{u} \tag{2.22}$$

In which G is the shear modulus, K is the bulk modulus and ρ is the density. The nabla operator (in Cartesian coordinates) is defined as follows:

$$\nabla = \begin{bmatrix} \frac{\partial}{\partial x_1} \\ \frac{\partial}{\partial x_2} \\ \frac{\partial}{\partial x_3} \end{bmatrix} \tag{2.23}$$

Holscher (2016) also defines a relationship between stresses and strains in elastic soils:

$$\sigma_{ij} = \left(K - \frac{2}{3}G\right) \varepsilon_{kk}\delta_{ij} + 2G\varepsilon_{ij} \tag{2.24}$$

δ_{ij} is the Kronecker delta. The strains are derivatives of the displacements:

$$\varepsilon_{ij} = \frac{1}{2}\left(\frac{\partial u_i}{\partial x_j} + \frac{\partial u_j}{\partial x_i}\right) \tag{2.25}$$

2.3.3 Waves in elastic media

2.3.3.1 Compression waves

A compression wave is a repeated cycle of particle compressions and dilations in the direction of the wave propagation (figure 2.9).

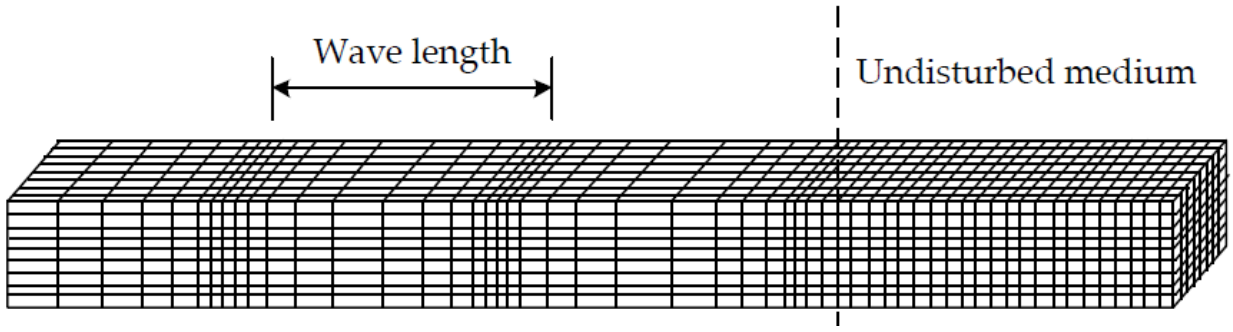

Figure 2.9: Compression wave (Deckner, 2013)

Consider one-dimensional wave propagation. Because both particle motion and wave propagation is along the same axis (say the x_1 axis), the derivatives and displacements along the other axes are equal to zero:

$$u_2 = u_3 = \frac{\partial}{\partial x_2} = \frac{\partial}{\partial x_3} = 0 \tag{2.26}$$

This simplifies the equation of motion in the previous section:

$$\rho\frac{\partial^2 u_1}{\partial t^2} = \left(K + \frac{1}{3}G\right)\frac{\partial^2 u_1}{\partial x_1^2} + G\frac{\partial^2 u_1}{\partial x_1^2} = \left(K + \frac{4}{3}G\right)\frac{\partial^2 u_1}{\partial x_1^2} \tag{2.27}$$

The equation of motion has reduced to the wave equation (section 2.1.1). Apparently the propagation velocity of compression waves is equal to:

$$c_p = \sqrt{\frac{K + \frac{4}{3}G}{\rho}} \tag{2.28}$$

$K + \frac{4}{3}G$ is often denoted as the compression modulus or odometer modulus.

2.3.3.2 Shear waves

Shear waves are characterized by a periodic particle motion perpendicular to the axis of wave propagation (figure 2.10).

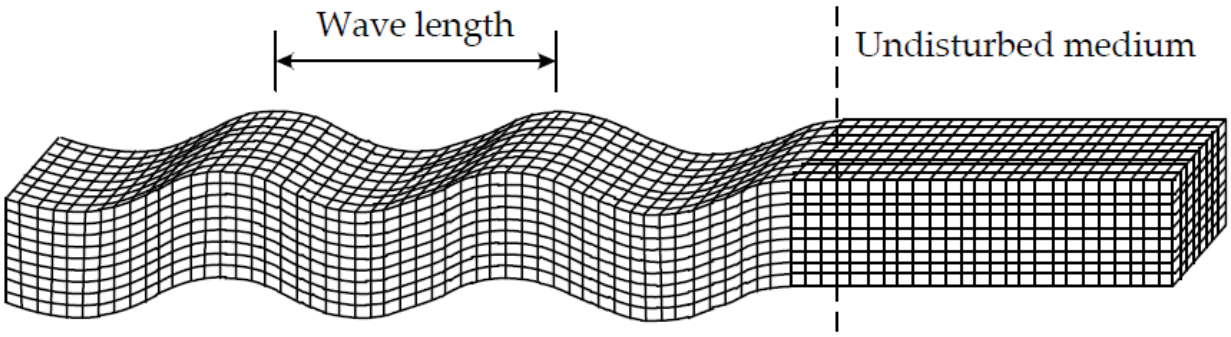

Figure 2.10: Shear wave (Deckner, 2013)

Consider again one-dimensional wave propagation. If the wave is propagating along the $x_1$axis and the particles are oscillating along the x_2 axis, then:

$$u_1 = u_3 = \frac{\partial}{\partial x_2} = \frac{\partial}{\partial x_3} = 0 \tag{2.29}$$

The equation of motion of elastic soils reduces to:

$$\rho \frac{\partial^2 u_2}{\partial t^2} = G \frac{\partial^2 u_2}{\partial x_1^2} \tag{2.30}$$

The propagation wave velocity of shear waves is equal to:

$$c_s = \sqrt{\frac{G}{\rho}} \tag{2.31}$$

This underlines the importance of the shear modulus as a shear stiffness parameter. Head & Jardine (1992) give a range of values for both compression and shear wave velocity (table 2.3).

	compression wave velocity (m/s)	shear wave velocity (m/s)
clay	1450-1900	80-500
saturated sand	1400-1800	100-400

Table 2.3: Estimated values for shear and compression wave velocity (Head & Jardine, 1992)

2.3.3.3 Rayleigh waves

Rayleigh waves are formed when compression waves hit the surface at an angle larger than the critical angle, according to Massarsch & Fellenius (2008). This critical angle is equal to:

$$\theta_{crit} = \sin^{-1}\left(\frac{c_s}{c_p}\right) \tag{2.32}$$

c_s is the shear wave velocity and c_p is the compression wave velocity.

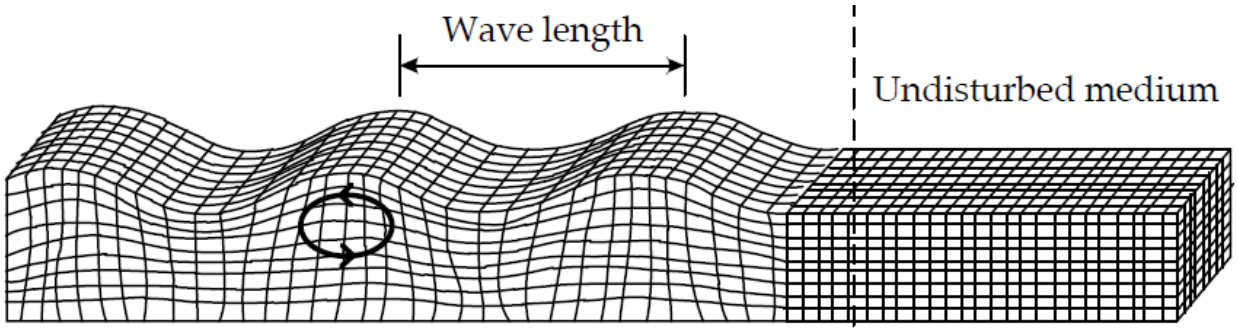

Figure 2.11: Rayleigh wave (Deckner, 2013)

Rayleigh waves are a combination of shear and compression waves (figure 2.11). The particles show an orbital motion, with orbit size decreasing down the surface (Deckner, 2013). Figure 2.12 depicts this behaviour, from the figure it is also clear that the vertical orbital component is always larger compared to the horizontal component.

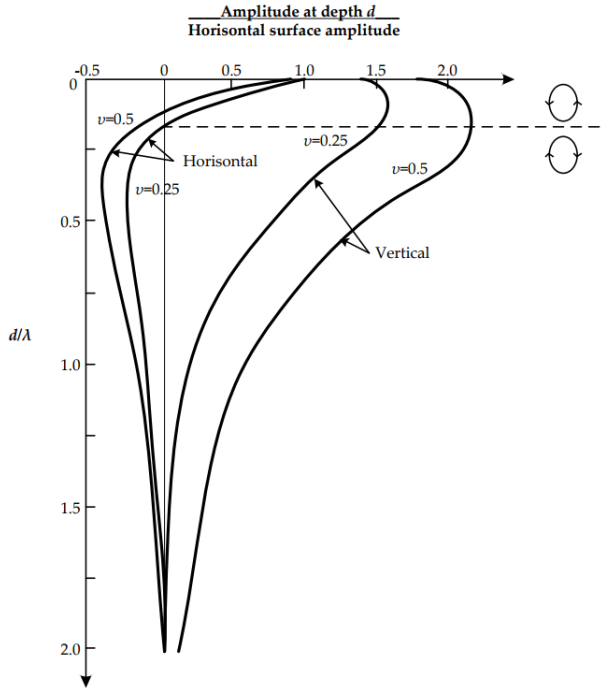

Figure 2.12: Horizontal and vertical component of Rayleigh waves as a function of depth (Deckner, 2013)

2.3.4 Waves emitted during pile driving

During pile driving the main type of wave emitted at the pile shaft-soil interface is a conical shear wave (Massarsch & Fellenius, 2008). This wave is the result of friction between the pile surface and the soil. At the pile toe-soil interface the main type of wave emitted into the soil is a spherical compression wave (Massarsch & Fellenius, 2008). This wave is formed when the pile toe presses against the underlying soil.

At a certain distance from the pile Rayleigh waves will be observed around the soil surface. This distance is equal to the critical angle defined in the previous section multiplied by the embedment depth of the pile. Figure 2.13 shows the different types of waves emitted during pile driving.

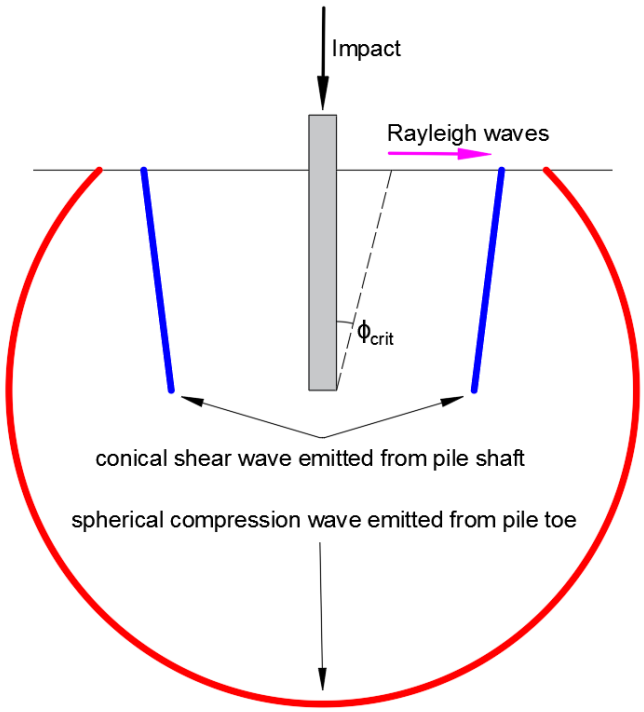

Figure 2.13: Waves emitted during pile driving

Aside from these waves, a minor cylindrical compression wave is emitted at the pile shaft-soil interface. This is caused by radial expansion of the pile shell. This radial expansion also causes a minor spherical shear wave to be emitted at the pile toe-soil interface.

2.3.5 Wave attenuation

Wave attenuation consists of two components: radiation damping and material damping (Holscher, 2016). Radiation damping is the decrease of wave energy per unit of volume over time, because of the wave spreading out over a larger volume. The type of source determines the rate of radiation damping. Holscher (2016), gives the following rates:

	attenuation of the wave amplitude as a function of the distance R from the source
cylindrical source	$\frac{1}{\sqrt{R}}$
spherical source	$\frac{1}{R}$

Table 2.4: Radiation damping for two different types of wave sources

Therefore spherical compression waves emitted at the pile toe attenuate much faster compared to conical shear waves emitted at the pile shaft.

Material damping is the loss of wave energy caused by soil behaviour (for example friction between particles or material plasticity). A simple expression for material damping is purposed by Massarsch & Fellenius (2008):

$$\Delta A = e^{-\alpha \Delta r}$$

In this expression ΔA is the decrease of wave amplitude over a distance Δr as a function of absorption coefficient α. The absorption coefficient has the following definition:

$$\alpha = \frac{2\pi D f}{c_s}$$

f is the frequency of the loading, c_s is the shear wave velocity and D the material damping coefficient. The material damping strongly depends on the strain imposed on the material and the material plasticity. Plastic soils like clay have lower material damping (and therefore weaker wave attenuation) compared to non-plastic soils like sand according to Deckner (2013) (figure 2.14).

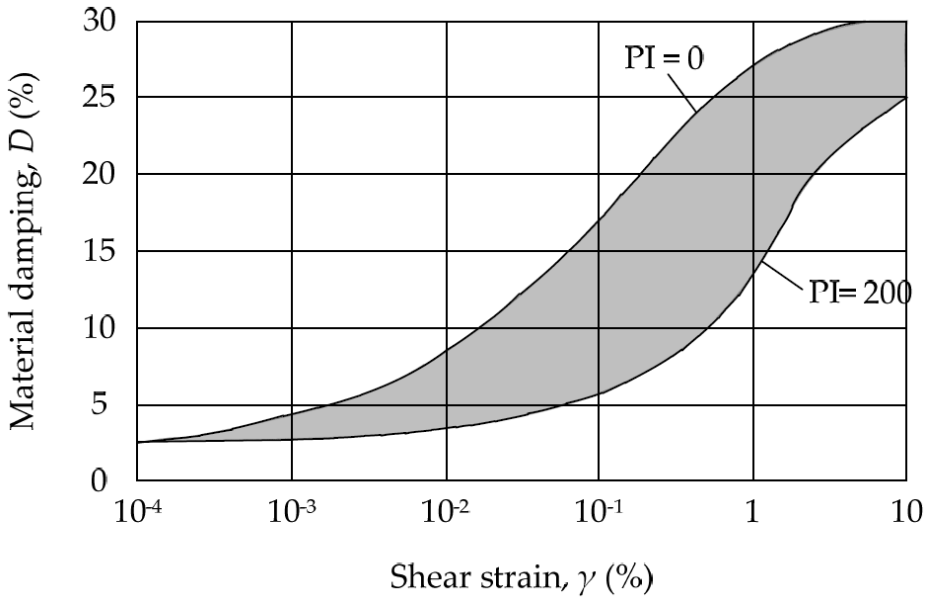

Figure 2.14: Material damping as a function of shear strain and material plasticity (Deckner, 2013)

2.4 Soil liquefaction

The effective soil stress (soil skeleton stress) is equal to the total stress minus the pore water pressure:

$$\sigma' = \sigma - p \tag{2.33}$$

If a dense soil is subject to dynamic loading (for example an earthquake or pile driving), shear stresses will cause dilation of the soil. The porosity increases. It is impossible for water to flow in and fill up the increased pore volume, because of the very short loading duration. This causes suction pressure in the pores, preventing dilation and increasing effective stress:

$$\sigma' = \sigma - (p - \Delta p_{suction}) \tag{2.34}$$

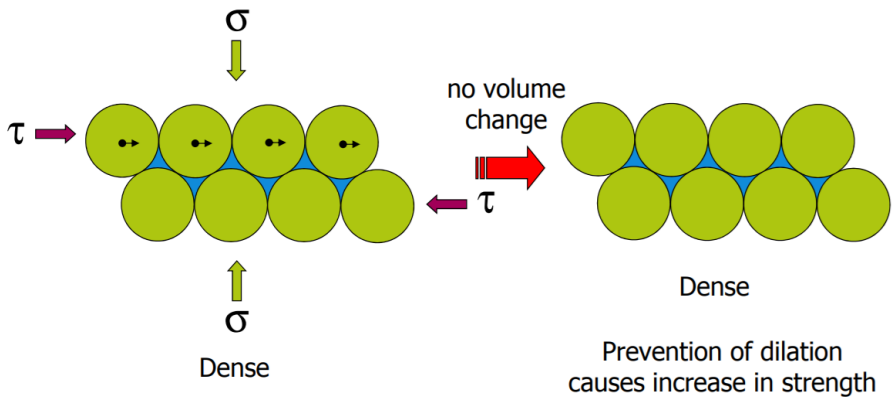

Figure 2.15: Dynamic loading acting on dense soil (Hicks, 2017)

In case of loose soils, shear stresses induced by dynamic loading cause contraction of the soil. The porosity decreases, but water cannot flow out during the short loading duration. This causes excess pore pressures in the pores, preventing contraction and decreasing effective stress:

$$\sigma' = \sigma - (p + \Delta p_{excess}) \tag{2.35}$$

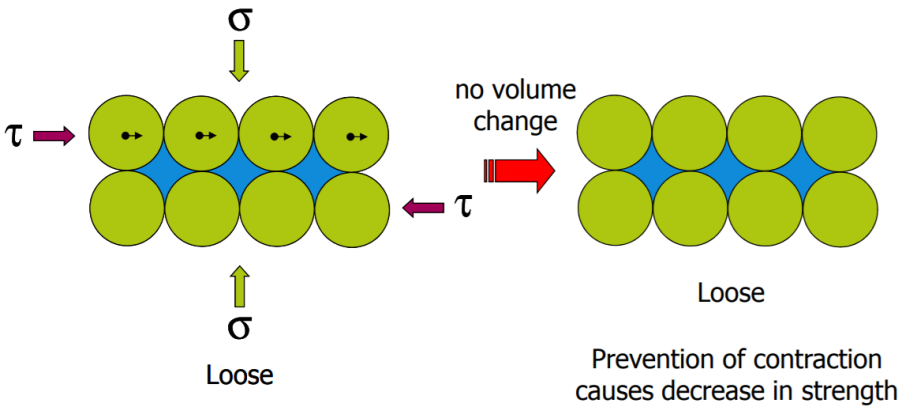

Figure 2.16: Dynamic loading acting on loose soil (Hicks, 2017)

The excess pore pressures will accumulate under sustained dynamic loading If the drainage capacity is insufficient. This is likely to be the case for sand (unless the sand is very coarse and close to being classified as gravel). Liquefaction occurs when the effective stress becomes equal to zero:

$$\sigma = (p + \Delta p_{excess}) \tag{2.36}$$

The soil does not process skeleton strength anymore. Contact between the particles is lost and the soil becomes a viscous fluid.

An empirical equation for the number of cycles resulting in soil liquefaction is proposed by Meijers (2007):

$$N_{cycles} = \left(\frac{0.48 * I_D * \sigma'_{v0}}{\Delta\tau}\right)^5 \tag{2.37}$$

The amount of cycles depends on initial relative soil density I_D, the initial effective stress σ'_{v0} and the amplitude of the shear stress $\Delta\tau$.

2.5 Numerical modelling

2.5.1 Newmark time integration scheme

In the upcoming chapters both discrete and continuous dynamic systems will be analysed in the time domain. Discrete dynamic systems are usually described by the following equation of motion:

$$[M]\ddot{\boldsymbol{u}} + [C]\dot{\boldsymbol{u}} + [K]\boldsymbol{u} = \boldsymbol{F} \tag{2.38}$$

$[M]$ is the mass matrix, $[C]$ the damping matrix, $[K]$ the stiffness matrix and $\boldsymbol{F}$ the forcing vector. These systems will be analysed using the Newmark time integration scheme. The scheme is derived starting with the definition of displacement, velocity and acceleration in the next time step (Gavin, 2016):

$$\boldsymbol{u}_{n+1} = \boldsymbol{u}_n + \Delta t\dot{\boldsymbol{u}}_n + \frac{\Delta t^2}{2}(2\beta\ddot{\boldsymbol{u}}_{n+1} + (1-2\beta)\ddot{\boldsymbol{u}}_n) \tag{2.39}$$

$$\dot{\boldsymbol{u}}_{n+1} = \dot{\boldsymbol{u}}_n + \Delta t(\gamma\ddot{\boldsymbol{u}}_{n+1} + (1-\gamma)\ddot{\boldsymbol{u}}_n) \tag{2.40}$$

$$\ddot{\boldsymbol{u}}_{n+1} = \frac{1}{\beta\Delta t^2}(\boldsymbol{u}_{n+1} - \boldsymbol{u}_n - \Delta t\dot{\boldsymbol{u}}_n) - \frac{(1-2\beta)}{2\beta}\ddot{\boldsymbol{u}}_n \tag{2.41}$$

For averaged acceleration, $\beta = 0.25$ and $\gamma = 0.5$. Substituting equation 2.41 into the equation 2.40 and performing some algebraic manipulations gives the following results:

$$\ddot{\boldsymbol{u}}_{n+1} = C_1(\boldsymbol{u}_{n+1} - \boldsymbol{u}_n) - C_2\dot{\boldsymbol{u}}_n + C_3\ddot{\boldsymbol{u}}_n \tag{2.42}$$

$$\dot{\boldsymbol{u}}_{n+1} = C_4(\boldsymbol{u}_{n+1} - \boldsymbol{u}_n) + C_5\dot{\boldsymbol{u}}_n + C_6\ddot{\boldsymbol{u}}_n \tag{2.43}$$

With the constants defined as:

$$C_1 = \frac{1}{\beta\Delta t^2}, C_2 = \frac{1}{\beta\Delta t}, C_3 = 1 - \frac{1}{2\beta}, C_4 = \frac{\gamma}{\beta\Delta t}, C_5 = 1 - \frac{\gamma}{\beta}, C_6 = \Delta t\left(1 - \frac{\gamma}{2\beta}\right) \tag{2.44}$$

The Newmark time integration scheme is obtained by substituting 2.42 and 2.43 into the equation of motion 2.38 and performing further algebraic manipulations:

$$\boldsymbol{u}_{n+1} = [M_a]^{-1}[\boldsymbol{F}_{n+1} + [M_b]\boldsymbol{u}_n + [M_c]\dot{\boldsymbol{u}}_n - [M_d]\ddot{\boldsymbol{u}}_n] \tag{2.45}$$

With the matrices defined as:

$$[M_a] = (C_1[M] + C_4[C] + [K]) \tag{2.46}$$

$$[M_b] = (C_1[M] + C_4[C]) \tag{2.47}$$

$$[M_c] = (C_2[M] - C_5[C]) \tag{2.48}$$

$$[M_d] = (C_3[M] + C_6[C]) \tag{2.49}$$

2.5.2 Finite difference method

Continuous dynamic systems are defined by partial differential equations (PDE), which contain both derivatives in time and space. These equations need to be discretized in space before solving numerically in time. This thesis will make use of finite difference approximations, which can be derived from Taylor series expansion (Mazumder, 2016). The approximations can be derived by considering a node of interest and all nodes surrounding it (figure 2.17).

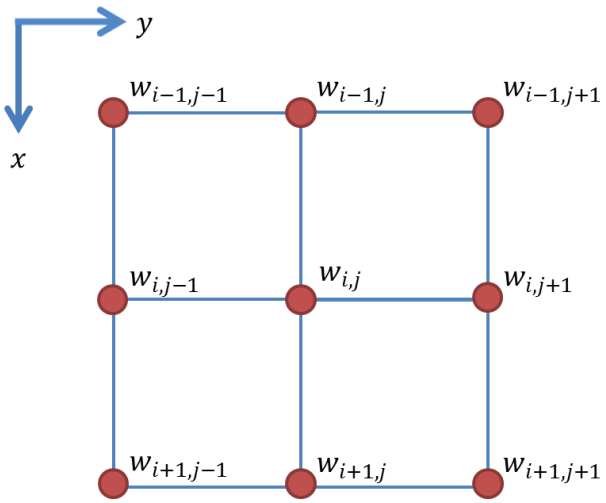

Figure 2.17: Finite difference grid

The Taylor series expansion for all surrounding nodes are listed below:

$$w_{i+1,j} = w_{i,j} + \Delta x \frac{\partial w}{\partial x}_{i,j} + \frac{1}{2}\Delta x^2 \frac{\partial^2 w}{\partial x^2}_{i,j} + \frac{1}{6}\Delta x^3 \frac{\partial^3 w}{\partial x^3}_{i,j} + O(\Delta x^4) \tag{2.50}$$

$$w_{i-1,j} = w_{i,j} - \Delta x \frac{\partial w}{\partial x}_{i,j} + \frac{1}{2}\Delta x^2 \frac{\partial^2 w}{\partial x^2}_{i,j} - \frac{1}{6}\Delta x^3 \frac{\partial^3 w}{\partial x^3}_{i,j} + O(\Delta x^4) \tag{2.51}$$

$$w_{i,j+1} = w_{i,j} + \Delta y \frac{\partial w}{\partial y}_{i,j} + \frac{1}{2}\Delta y^2 \frac{\partial^2 w}{\partial y^2}_{i,j} + \frac{1}{6}\Delta y^3 \frac{\partial^3 w}{\partial y^3}_{i,j} + O(\Delta y^4) \tag{2.52}$$

$$w_{i,j-1} = w_{i,j} - \Delta y \frac{\partial w}{\partial y}_{i,j} + \frac{1}{2}\Delta y^2 \frac{\partial^2 w}{\partial y^2}_{i,j} - \frac{1}{6}\Delta y^3 \frac{\partial^3 w}{\partial y^3}_{i,j} + O(\Delta y^4) \tag{2.53}$$

$$w_{i+1,j+1} = w_{i,j} + \Delta x \frac{\partial w}{\partial x}_{i,j} + \Delta y \frac{\partial w}{\partial y}_{i,j} + \frac{1}{2}\Delta x^2 \frac{\partial^2 w}{\partial x^2}_{i,j} + \frac{1}{2}\Delta y^2 \frac{\partial^2 w}{\partial y^2}_{i,j} + \Delta x \Delta y \frac{\partial^2 w}{\partial x \partial y}_{i,j} + O(\Delta x^3, \Delta y^3) \tag{2.54}$$

$$w_{i+1,j-1} = w_{i,j} + \Delta x \frac{\partial w}{\partial x}_{i,j} - \Delta y \frac{\partial w}{\partial y}_{i,j} + \frac{1}{2}\Delta x^2 \frac{\partial^2 w}{\partial x^2}_{i,j} + \frac{1}{2}\Delta y^2 \frac{\partial^2 w}{\partial y^2}_{i,j} - \Delta x \Delta y \frac{\partial^2 w}{\partial x \partial y}_{i,j} + O(\Delta x^3, \Delta y^3) \tag{2.55}$$

$$w_{i-1,j+1} = w_{i,j} - \Delta x \frac{\partial w}{\partial x}_{i,j} + \Delta y \frac{\partial w}{\partial y}_{i,j} + \frac{1}{2}\Delta x^2 \frac{\partial^2 w}{\partial x^2}_{i,j} + \frac{1}{2}\Delta y^2 \frac{\partial^2 w}{\partial y^2}_{i,j} - \Delta x \Delta y \frac{\partial^2 w}{\partial x \partial y}_{i,j} + O(\Delta x^3, \Delta y^3) \tag{2.56}$$

$$w_{i-1,j-1} = w_{i,j} - \Delta x \frac{\partial w}{\partial x}_{i,j} - \Delta y \frac{\partial w}{\partial y}_{i,j} + \frac{1}{2}\Delta x^2 \frac{\partial^2 w}{\partial x^2}_{i,j} + \frac{1}{2}\Delta y^2 \frac{\partial^2 w}{\partial y^2}_{i,j} + \Delta x \Delta y \frac{\partial^2 w}{\partial x \partial y}_{i,j} + O(\Delta x^3, \Delta y^3) \tag{2.57}$$

The O operator describes the order of the error. From these expansions, second order error approximations can be derived for single variable derivatives:

$$\frac{\partial w}{\partial x}_{i,j} = \frac{w_{i+1,j} - w_{i-1,j}}{2\Delta x} + O(\Delta x^2) \tag{2.58}$$

$$\frac{\partial^2 w}{\partial x^2}_{i,j} = \frac{w_{i+1,j} - 2w_{i,j} + w_{i-1,j}}{\Delta x^2} + O(\Delta x^2) \tag{2.59}$$

And for mixed derivatives:

$$\frac{\partial^2 w}{\partial x \partial y}_{i,j} = \frac{w_{i+1,j+1} - w_{i+1,j-1} - w_{i-1,j+1} + w_{i-1,j-1}}{4\Delta x \Delta y} + O(\Delta x^2, \Delta y^2) \tag{2.60}$$

An alternative expression for mixed derivatives is:

$$\frac{\partial^2 w}{\partial x \partial y}_{i,j} = \frac{w_{i+1,j+1} - w_{i+1,j} - w_{i,j+1} + 2w_{i,j} - w_{i-1,j} - w_{i,j-1} + w_{i-1,j-1}}{2\Delta x \Delta y} + O(\Delta x^2, \Delta y^2) \tag{2.61}$$

This alternative expression is more efficient if the PDE contains at least one single variable derivative with respect to x and one with respect to y.

Discretization in space reduces the PDE to a second order ordinary differential equation (ODE). The system of ODEs for elastic soil (section 2.3.2) will have the following form:

$$\frac{\partial^2}{\partial t^2}\boldsymbol{w} = [M]\boldsymbol{w} \tag{2.62}$$

$[M]$ is a matrix containing all discretization coefficients with respect to space. Various methods exist to integrate the system of ODEs forward in time. The simplest is using a second order error finite difference approximation:

$$\boldsymbol{w}^{n+1} = \Delta t^2 \left[[M] + \frac{2}{\Delta t^2}[I] \right] \boldsymbol{w}^n - \boldsymbol{w}^{n-1} \tag{2.63}$$

$[I]$ is the identity matrix. n+1, n and n-1 denote the next, current and previous time step. The disadvantage of this method is the use fixed time step. Matlab has various built in ODE solvers based on different numerical schemes, which perform time integration using variable time steps. These solvers solve first order ODEs, therefore the system of second order ODEs in equation 2.62 has to be transformed to state space description:

$$\begin{bmatrix} \frac{\partial}{\partial t}\boldsymbol{w} \\ \frac{\partial^2}{\partial t^2}\boldsymbol{w} \end{bmatrix} = \begin{bmatrix} [0] & [I] \\ [M] & [0] \end{bmatrix} \begin{bmatrix} \boldsymbol{w} \\ \frac{\partial}{\partial t}\boldsymbol{w} \end{bmatrix} \tag{2.64}$$

The following figure gives an overview of various Matlab ODE solvers:

MATLAB ODE Solvers

Solver	Problem type /Accuracy	Description
ode23	Non-stiff /Medium	One-step solver based on explicit Runge-Kutta (II and III) method. In general faster but less accurate than ode45
ode45	Non-stiff /Low	One-step solver based on explicit Runge-Kutta (IV and V) method. In general moderate accuracy
ode113	Non-stiff /Low to high	Multi-step solver based on Adams method
ode15s	Stiff /Moderate	Multi-step solver of variable order (I to V)
ode23s	Stiff /Low	One-step low order solver based on a modified Rosenbrock formula of order two
ode23t	Moderately stiff /Low	One-step solver based on trapezoidal rule
ode23tb	Stiff /Low	A low order solver, more efficient than ode15s
ode15i		Solves fully implicit differential equations, variable order method

Figure 2.18: Overview of Matlab ODE solvers (Raj, 2016)

3 Existing pile driving models

This chapter presents three existing pile driving models: the Smith model (soil is represented by a rheological model), the van den Berghe-Holeyman model (soil is represented by rigid cylinders) and the Salgado et al. model (soil is represented by thin slices).

3.1 Smith pile driving model

3.1.1 Model formulation

The pile driving model by Smith (Smith, 1960) divides the pile into discrete lumped masses, connected together by springs representing the internal stiffness of the pile. The soil is represented by a rheological model consisting of a spring (representing soil elasticity) in series with a slider (representing soil plasticity), which are placed in parallel with a dashpot (representing both friction and inertial damping).

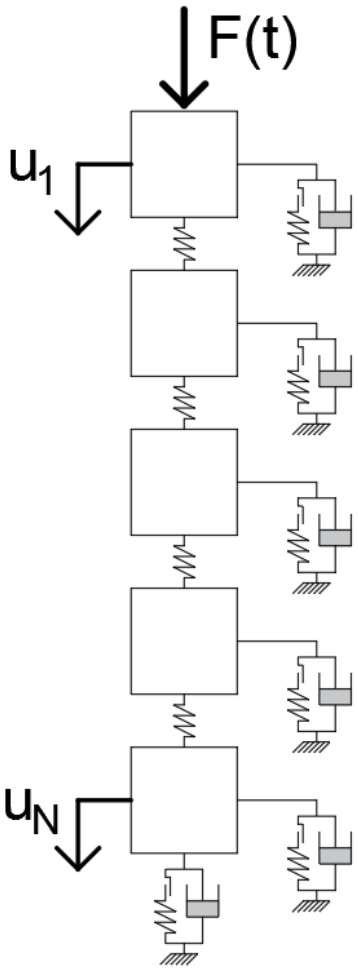

Figure 3.1: Smith pile driving model

The equation of motion for a pile divided in N lumped masses is:

$$[M]\ddot{\boldsymbol{u}} + [C]\dot{\boldsymbol{u}} + [K]\boldsymbol{u} = \boldsymbol{F} \tag{3.1}$$

With the matrices $[M]$, $[C]$, $[K]$ and $\boldsymbol{F}$ vector defined as:

$$[M] = \begin{bmatrix} m_1 & & & & \\ & m_2 & & & \\ & & \ddots & & \\ & & & m_{N-1} & \\ & & & & m_N \end{bmatrix} \tag{3.2}$$

$$[C] = [0] \tag{3.3}$$

$$[K] = \begin{bmatrix} k_1 & -k_1 & & & & & & \\ -k_1 & k_1 + k_2 & -k_2 & & & & & \\ & -k_2 & k_2 + k_3 & -k_3 & & & & \\ & & & \ddots & & & & \\ & & & & -k_{N-3} & k_{N-3} + k_{N-2} & -k_{N-2} & \\ & & & & & -k_{N-2} & k_{N-2} + k_{N-1} & -k_{N-1} \\ & & & & & & -k_{N-1} & k_{N-1} \end{bmatrix} \tag{3.4}$$

$$\boldsymbol{F} = \begin{bmatrix} F(t) - R_{shaft,1} \\ -R_{shaft,2} \\ \vdots \\ -R_{shaft,N-1} \\ -R_{shaft,N} - R_{toe} \end{bmatrix} \tag{3.5}$$

With the lumped mass equal to:

$$m_i = \frac{L_P A_P \rho_P}{N} \tag{3.6}$$

The internal stiffness is equal to:

$$k_i = \frac{E_P A_p N}{L_P} \tag{3.7}$$

L_P is the pile length, A_P is the cross-sectional area of the pile, ρ_P is the density of the pile and E_P is the Young's modulus of the pile.

$F(t) = v_{0,H}(t) Z_P$ Is the impact force on top of the pile. The shaft and toe resistances have the following definition (Randolph, 2003):

$$R_{shaft,i} = \frac{\pi d_P \tau_s L_p}{N} \begin{cases} \dfrac{u_i - u_{i,slip}}{Q_{shaft}} + J_{shaft}\dot{u}_i, & \left|u_i - u_{i,slip}\right| \le Q_{shaft} \\ \dfrac{u_i - u_{i,slip}}{\left|u_i - u_{i,slip}\right|} + J_{shaft}\dot{u}_i, & \left|u_i - u_{i,slip}\right| > Q_{shaft} \end{cases} \tag{3.8}$$

$$R_{toe} = A_p p_{lim} \begin{cases} 0, & u_N - u_{N,slip} < 0 \\ \dfrac{u_N - u_{N,slip}}{Q_{toe}} + J_{toe}\dot{u}_N, & 0 \le u_N - u_{N,slip} \le Q_{toe} \\ 1 + J_{toe}\dot{u}_N, & u_N - u_{N,slip} > Q_{toe} \end{cases} \tag{3.9}$$

In these equations, Q denotes the quake (the limit displacement at which a transition occurs from elastic to plastic behaviour), J denotes the damping ratio, τ_s and p_{lim} denote the static shear resistance of the

soil at the pile shaft and the static bearing capacity of the soil at the pile toe. d_P is the pile diameter. $u_{slip}$is the total slip accumulation. The soil cannot provide tension resistance at the pile toe, therefore toe resistance is zero for negative displacements. Figure 3.2 visualizes expression 4.8 and 4.9:

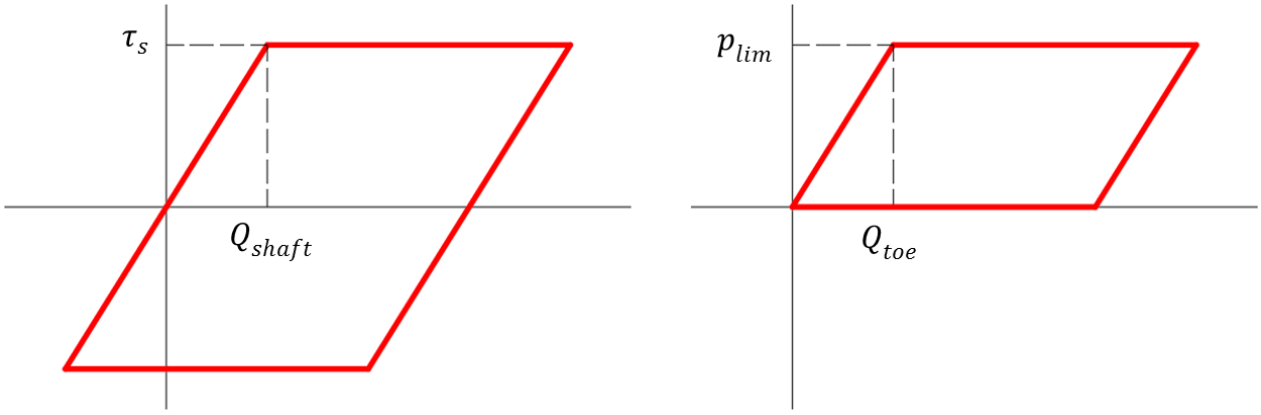

Figure 3.2: Resistance of pile shaft (left) and toe (right) as a function of displacement

3.1.2 Model results

The Smith pile driving model formulated in the previous section is implemented in Matlab using a Newmark time integration scheme (section 2.5.1). The Matlab code can be found in appendix B1. Averaging acceleration ($\beta = 0.25$ and $\gamma = 0.5$) is chosen for the analysis. The simple case of homogenous soil consisting of medium sand (input table 1.4) is considered. The input parameters are taken from input tables 1.1 (hammer), 1.2 (pile) and 1.3 (pile driving). The pile length is chosen to be 30 m and the pile is discretized in to 300 elements. To ensure stability of the Smith pile driving model, the time step should be chosen smaller than the time it takes the wave to travel between two pile nodes:

$$\Delta t < \frac{L_P}{N c_{Pile}} \tag{3.10}$$

$c_{pile} = \sqrt{\frac{E_P}{\rho_P}}$ is the wave propagation velocity in the pile. The pile is assumed to be fully embedded in the soil (end of driving phase). Figure 3.3 shows the stress wave travelling through the pile. The amplitude of the wave gradually decays as energy is dissipated by soil resistance. An important parameter for pile drivability is the pile set, which is shown in figure 3.4 at toe level. After some oscillations, the pile set reaches a stable value of 1.4 mm. The pile set strongly depends on the length of the pile (figure 3.5) and the static shear resistance of the soil at the pile shaft (figure 3.6). A less profound dependency exists with the static bearing capacity of the soil at the pile toe (figure 3.7). This less profound dependency might be explained by the fact that an open ended pile is considered for this calculation. The results show that longer piles driven in stiffer soils require heavier hammers.

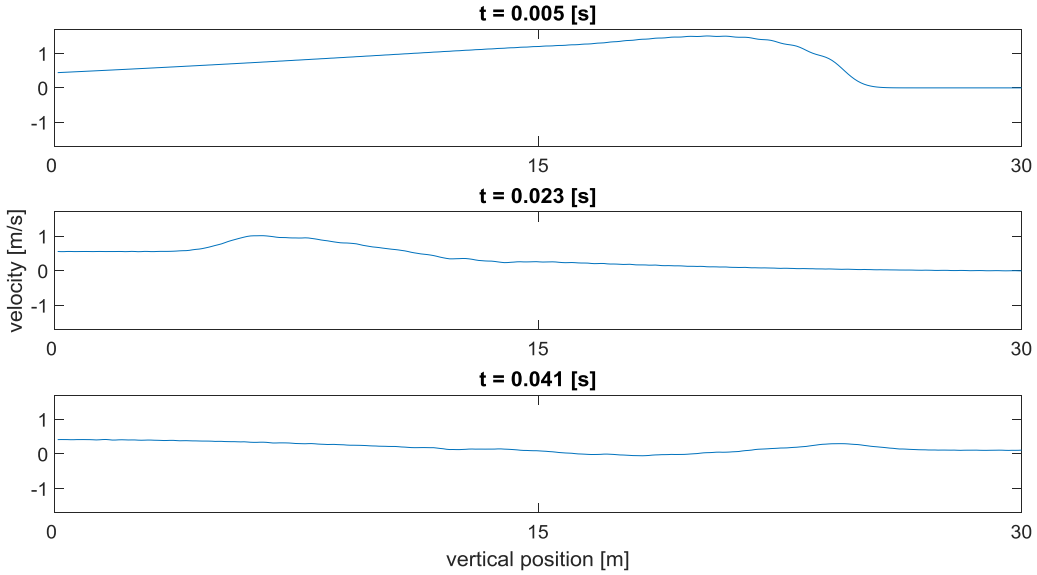

Figure 3.3: Stress wave travelling through the pile

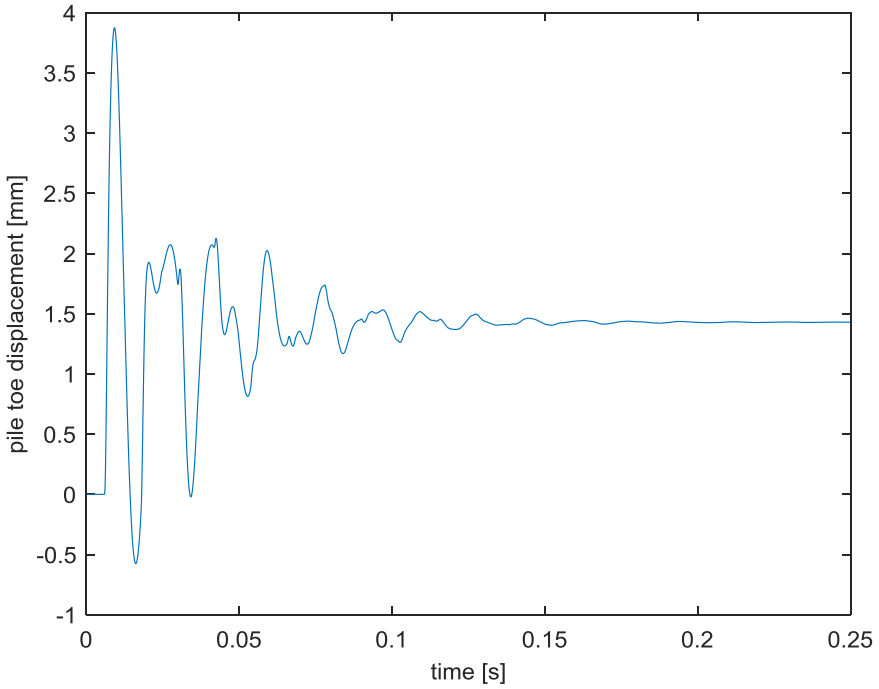

Figure 3.4: Pile toe displacement as a function of time

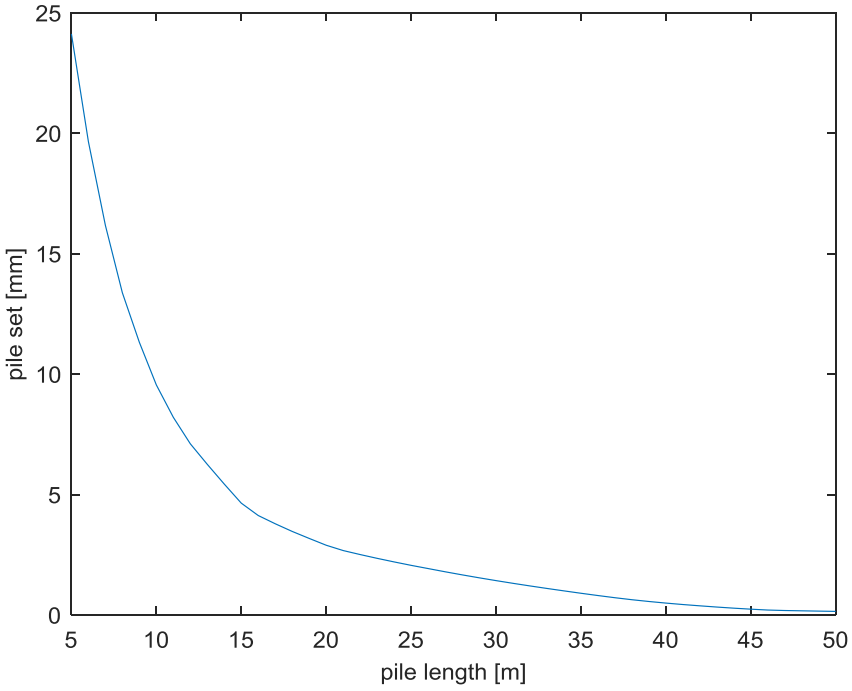

Figure 3.5: Pile set as a function of pile length (pile is fully embedded in the soil)

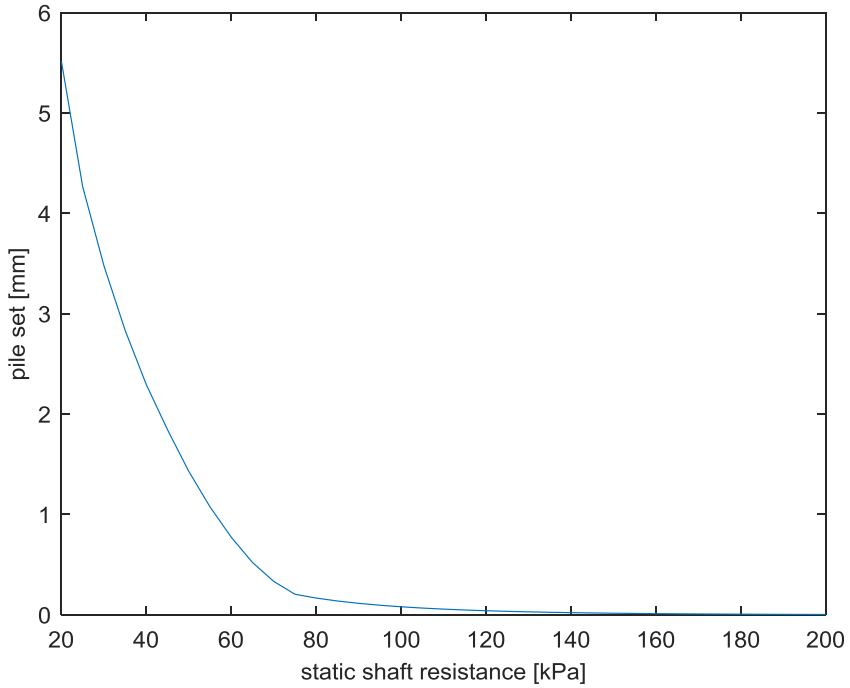

Figure 3.6: Pile set as a function of the static shear resistance of the soil at the pile shaft

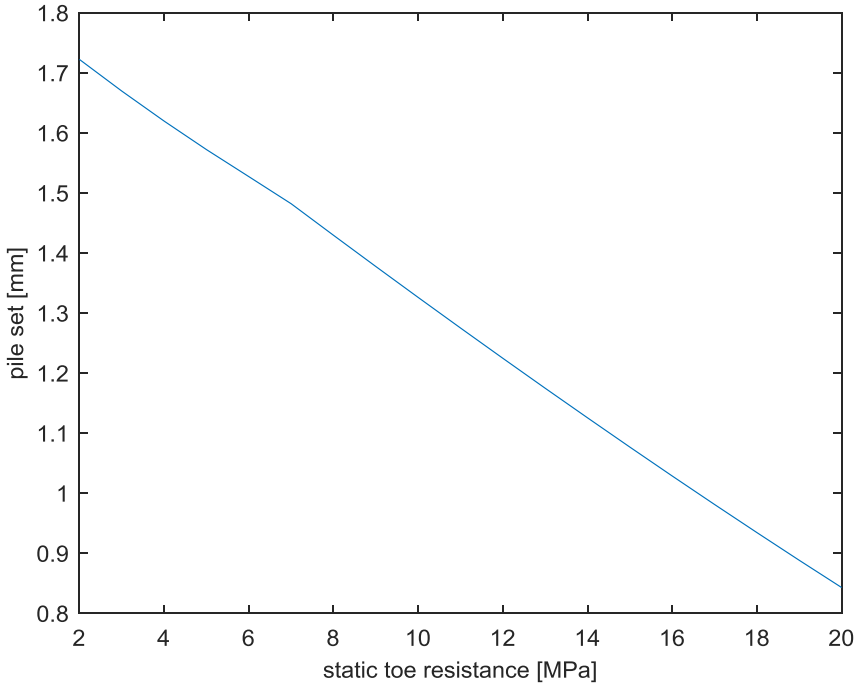

Figure 3.7: Pile set as a function the static bearing capacity of the soil at the pile toe

3.1.3 Other rheological soil models

Various rheological soil models have been developed to represent the shaft and toe resistance. Pile driving imposes large deformations in the soil. This results in a disturbed soil region in the vicinity of the pile. Complicated processes like strain softening, remolding and excess pore pressure development make this region hard to model (Massarsch & Fellenius, 2008). Gradual reduction of strength of the disturbed soil region during pile driving, will also reduce the emission of wave energy into the undisturbed region (Massarsch & Fellenius, 2008).

The biggest disadvantage of the Smith rheological soil model is that no distinction is made between viscous damping (by friction at the interface) and inertial damping (by accelerating the soil). Both components are lumped together and represented by a single dashpot. A second disadvantage is that input parameters like quake and damping ratio are required instead of meaningful soil properties like shear modulus and density. These disadvantages are solved by a more refined model presented by Simons & Randolph (1985). The model (shown in figure 3.8) clearly distinguishes between viscous and inertial damping. As long as the static capacity of the shaft is not reached, the slider will not activate. Therefore all energy is dissipated by inertial damping. Once the static shaft limit is reached, the pile starts slipping and viscous damping becomes dominant. The required input to determine shaft resistance and toe bearing capacity are the shear modulus and density of the soil.

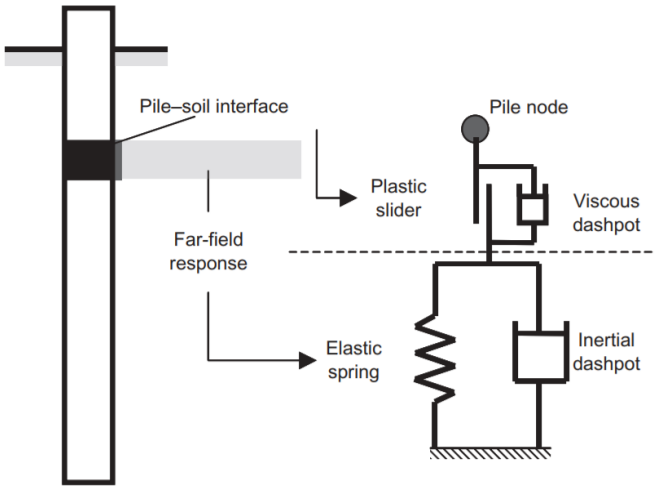

Figure 3.8: Simons and Randolph (1985) rheological soil model

Naggar & Novak (1994) present a rheological soil model with additional refinements (figure 3.9). This model defines three different zones: a slip zone under elastic-plastic influence, an inner (disturbed) region, where both elasto-plasticity and viscosity are significant and finally the undisturbed soil region, where stresses are assumed to be small and therefore no plasticity occurs. The dashpot in the undisturbed zone represents the inertial damping. Two point masses are added to account for the inertia of the soil after the energy input from the pile stops.

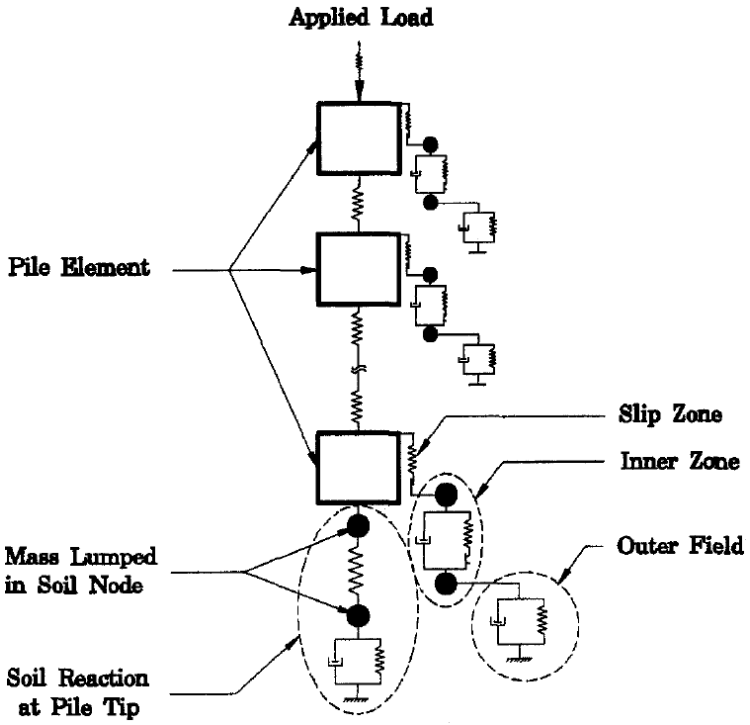

Figure 3.9: Naggar & Novak (1994) rheological soil model

Despite many rheological soil models being developed in the past decades, the Smith model remains the basis for many commercial pile driving packages, because of its simplicity and the familiarity of practicing engineers with the Smith input parameters (quake, damping ratio).

The aim of this theses is to gain understanding in wave propagation and pore pressure accumulation in soils induced by pile driving. The Smith pile driving model is not useful for this purpose, since the soil is represented by a rheological model. The upcoming models will therefore represent the soil as a continuum connected to the pile. The Smith model will be used for fine-tuning pile and hammer input parameters for the upcoming models.

3.2 Holeyman and van den Berghe pile driving model

This model was developed by Holeyman(1993) and refined by van den Berghe (2001). In this cylindrically symmetric model, the pile is assumed to be a rigid mass and the soil is discretised in radial direction into rigid cylinders (figure 3.10).

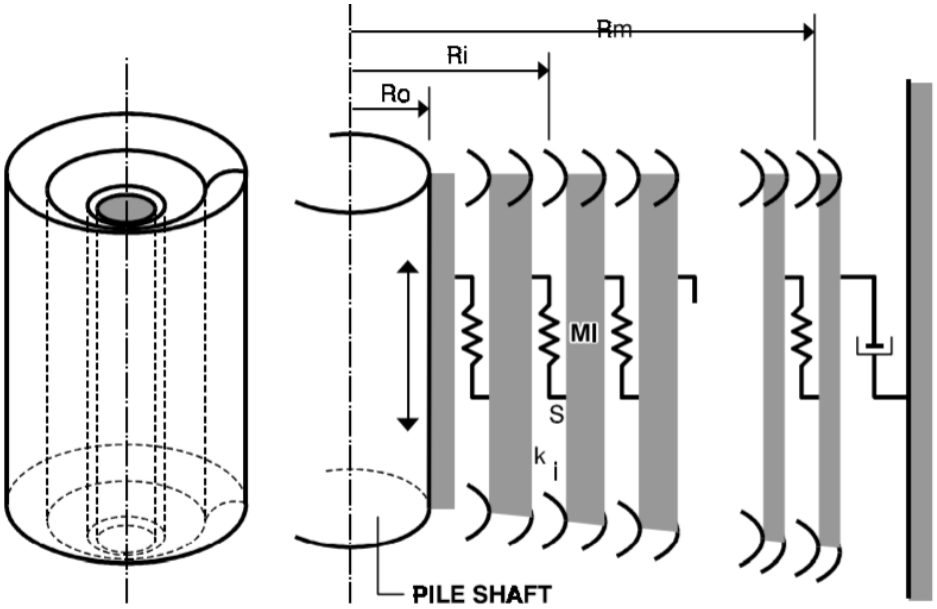

Figure 3.10: Cylindrically symmetric pile driving model with discretization in radial direction only (Holeyman, 1993)

The shear stiffness of the soil is represented by springs between each soil cylinder and between the pile and first soil cylinder. A dashpot is attached to the final soil cylinder to create a non-reflecting boundary (section 2.1.3). This model is in fact very similar to the Smith pile driving model, since the pile and the soil cylinders can be considered lumped masses (figure 3.11).

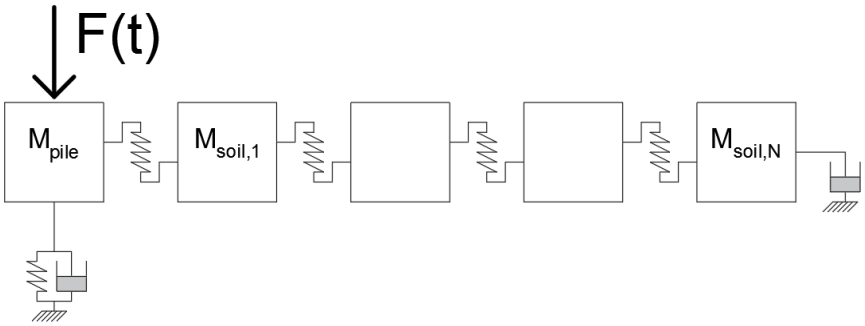

Figure 3.11: Dynamic scheme of the Holeyman and van den Berghe model

The spring and dashpot under the pile mass represent the base reaction. This model is an improvement compared to the Smith pile driving model, since the elastic behaviour of the soil under impact loading is calculated (displacements, shear stresses). The lack of discretization in vertical direction is however a big disadvantage, since no account can be taken for soil layering. Another disadvantage is that wave propagation the pile is neglected by assuming the pile to be a rigid mass. These disadvantages are solved by the model presented in the next section.

3.3 Salgado pile driving model

3.3.1 Model formulation

The Salgado pile driving model (Salgado et al., 2015) is based on the model of Holeyman and van den Berghe presented in the previous section. The soil and pile are discretized in both radial and vertical direction, allowing soil layering to be taken into account. The governing equation for the Salgado model is derived from the general equations of motion of an elastic medium (section 2.3.2). The model is cylindrically symmetric, which reduces the system of three governing equations to two governing equations (Verruijt, 2010):

$$\rho\frac{\partial^2 u}{\partial t^2} = \left(K+\frac{4}{3}G\right)\left(\frac{\partial^2 u}{\partial r^2}+\frac{1}{r}\frac{\partial u}{\partial r}-\frac{u}{r^2}\right)+\left(K+\frac{1}{3}G\right)\frac{\partial^2 w}{\partial r\partial z}+G\frac{\partial^2 u}{\partial z^2} \tag{3.11}$$

$$\rho\frac{\partial^2 w}{\partial t^2} = \left(K+\frac{4}{3}G\right)\frac{\partial^2 w}{\partial z^2}+\left(K+\frac{1}{3}G\right)\left(\frac{\partial^2 u}{\partial r\partial z}+\frac{1}{r}\frac{\partial u}{\partial z}\right)+G\left(\frac{\partial^2 w}{\partial r^2}+\frac{1}{r}\frac{\partial w}{\partial r}\right) \tag{3.12}$$

ρ is the soil density, G the soil shear modulus and K the soil bulk modulus. The first assumption of the Salgado pile driving model is that the radial displacement (u) can be neglected, which reduces the system of two governing equations to one governing equation:

$$\rho\frac{\partial^2 w}{\partial t^2} = \left(K+\frac{4}{3}G\right)\frac{\partial^2 w}{\partial z^2}+G\left(\frac{\partial^2 w}{\partial r^2}+\frac{1}{r}\frac{\partial w}{\partial r}\right) \tag{3.13}$$

The vertical discretization allows for another assumption: if the vertical discretization size is chosen small enough, the soil is assumed to behave as a stack of slices (figure 3.12), which do not interact which each other. No interaction between the slices implies that the axial stress ($\frac{\partial w}{\partial z}$) can be neglected, which yields the final form of the governing soil equation for the Salgado model:

$$\rho\frac{\partial^2 w}{\partial t^2} = G\left(\frac{\partial^2 w}{\partial r^2}+\frac{1}{r}\frac{\partial w}{\partial r}\right) \tag{3.14}$$

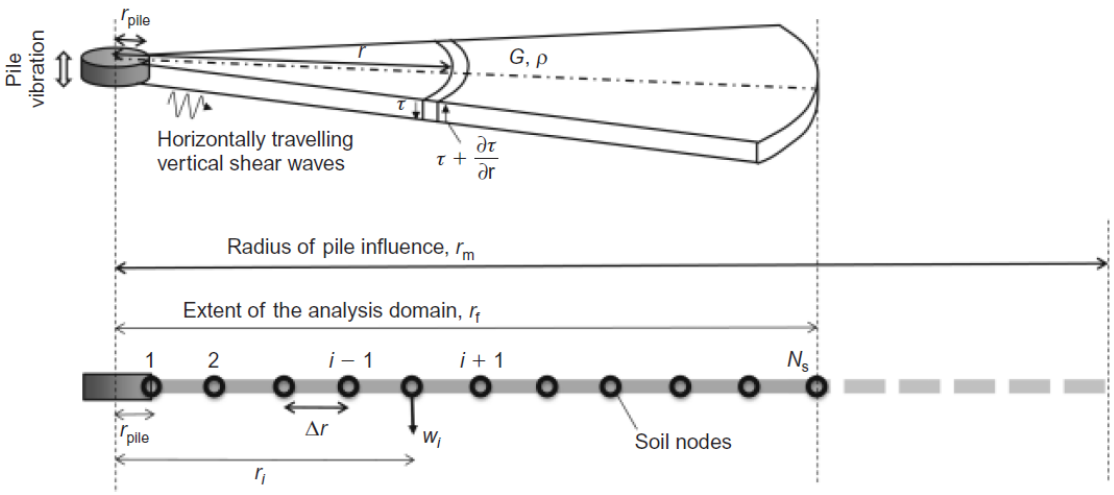

Figure 3.12: Thin slices approach (Salgado et al., 2015)

Because the axial stresses are neglected in the Salgado model, the soil slices will only be able to transfer shear waves. The shear waves are excited by the pile motion at the left boundary and an absorbing dashpot is placed at the right boundary (figure 3.13). Another implication of neglecting axial stresses, is that the soil resistance at the pile toe cannot be derived from the model. The base reaction is therefore represented by a spring and dashpot (figure 3.13).

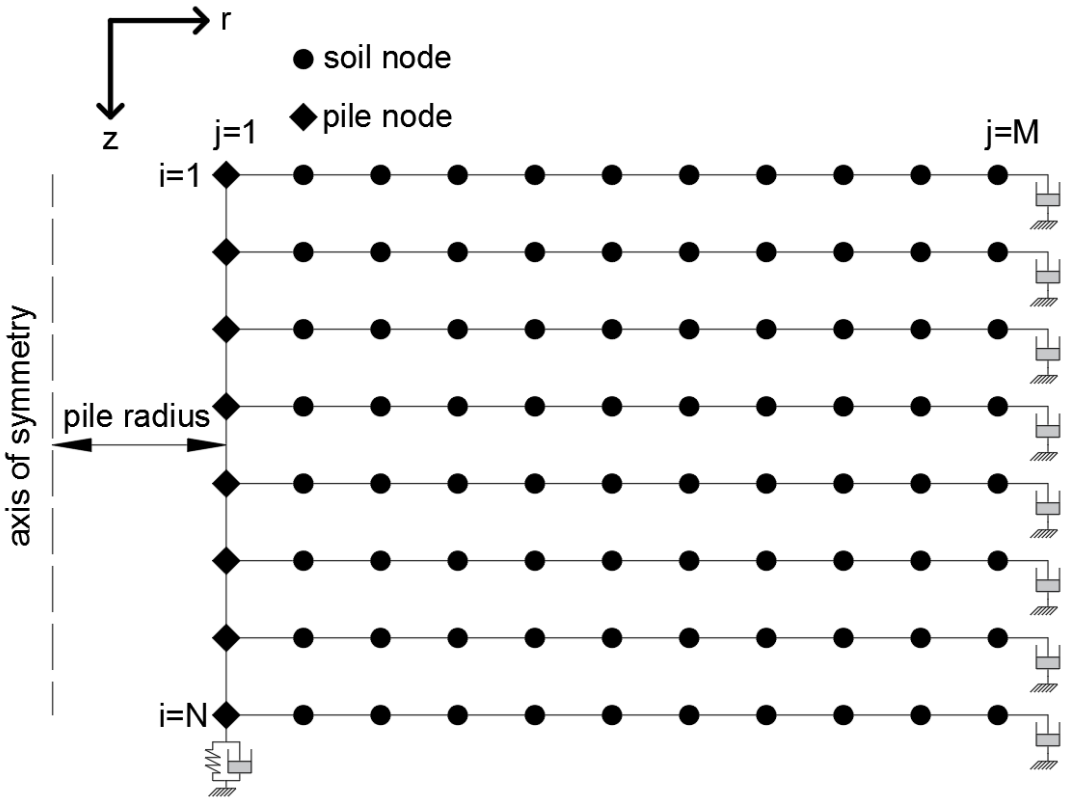

Figure 3.13: Salgado pile driving model grid

Salgado et al. (2015) solve the model using two different methods: the pile is solved with the Newmark time integration scheme and the soil is solved using finite difference grid for each soil slice. The models are coupled at each time step. This is a very inefficient solution procedure. This thesis follows a different approach: pile and soil are considered one single system and solved using 2D finite difference method.

The governing equation for the pile is (positions i and j can be found in figure 3.13):

$$\rho_p A_p \frac{\partial^2 w}{\partial r^2} = \pi d_P G \frac{\partial w}{\partial r} + E_p A_p \frac{\partial^2 w}{\partial z^2} \quad @i = 1{:}N, j = 1 \tag{3.15}$$

A_P is the cross-sectional area of the pile, ρ_P is the density of the pile, E_P is the Young's modulus of the pile and d_P is the pile diameter. The symbol : is used to denote 'up to and including'. The boundary condition at the pile head is:

$$E_p A_p \frac{\partial w}{\partial z} = -F_{imp}(t) \quad @i = 1, j = 1 \tag{3.16}$$

And at the pile base:

$$E_p A_p \frac{\partial w}{\partial z} = -R_{base}(t) \quad @i = N, j = 1 \tag{3.17}$$

The base reaction is defined in the same manner as the Smith pile driving model (section 3.1.1), but without plastic component:

$$R_{toe} = A_p p_{lim} \begin{cases} 0, & w_{base} < 0 \\ \frac{u_N}{Q_{toe}} + J_{toe}\dot{u}_N, & w_{base} \geq 0 \end{cases} \tag{3.18}$$

The governing equation for the soil reads:

$$\rho \frac{\partial^2 w}{\partial t^2} = G\left(\frac{\partial^2 w}{\partial r^2} + \frac{1}{r}\frac{\partial w}{\partial r}\right) \quad @i = 1{:}N, j = 2{:}M \tag{3.19}$$

The left soil interface condition reads:

$$w_{soil} = w_{pile} = w \quad @i = 1{:}N, j = 1 \tag{3.20}$$

And the right (non-reflective) boundary condition:

$$\frac{\partial w}{\partial r} = -\sqrt{\frac{\rho}{G}}\frac{\partial w}{\partial t} \quad @i = 1{:}N, j = M \tag{3.21}$$

Using finite difference approximations (section 2.5.2), the governing system of equations is turned into a state space system:

$$\begin{bmatrix} \frac{\partial}{\partial t}\boldsymbol{w} \\ \frac{\partial^2}{\partial t^2}\boldsymbol{w} \end{bmatrix} = \begin{bmatrix} [0] & [I] \\ [M_1] & [M_2] \end{bmatrix} \begin{bmatrix} \boldsymbol{w} \\ \frac{\partial}{\partial t}\boldsymbol{w} \end{bmatrix} + \boldsymbol{F} \tag{3.22}$$

$[M_1]$ and $[M_2]$ contain the discretization coefficients with respect to space and $\boldsymbol{F}$ contains the impact force at the pile head. The full derivation can be found in appendix A1.

3.3.2 Model results

The state space system presented in the previous section is implemented in Matlab and solved using ODE45, the full code can be found in appendix B2. To ensure stability of the Salgado pile driving model, the time step should be smaller than the time it takes the compression wave in the pile to travel between two pile nodes:

$$\Delta t < \frac{L_P}{N c_{Pile}} \tag{3.23}$$

L_P is the pile length and $c_{Pile} = \sqrt{E_P/\rho_P}$ is the compression wave velocity in the pile. This requirement is taken care of by the ODE45 solver. Additionally, the radial grid size Δr should be chosen small enough, allowing the shear waves to be transferred inside the soil:

$$\Delta r < \frac{c_s}{f_{load}} \tag{3.24}$$

c_s is the shear wave velocity in the soil and f_{load} is the frequency of the impact load by the hammer.

The input parameters are derived from input tables 1.1 (hammer), 1.2 (pile) and 1.4 (soil). First pile driving in homogenous soil consisting of loose sand is considered. The pile length is chosen to be 20 meter and the radial size of the soil domain is also 20 meter. The results are shown in figure 3.14. The upper part of the soil (closest to the hammer impact) shows the highest displacement amplitudes. The model has no material damping, so the attenuation of wave amplitude as it travels through the soil is purely due to geometrical damping.

Next layered soil is considered. The following layering is chosen (layer properties are taken from input table 1.4):

layer number	soil type	start height	end height
1	soft clay	0	5
2	loose sand	5	10
3	soft clay	10	15
4	medium sand	15	20

Table 3.1: Soil layering

The results are shown in figure 3.15. The soil layers have different shear moduli and therefore different wave propagation velocities. The absence of vertical interaction causes discontinuities at layer boundaries. The thin slices approach proposed by Salgado et al. (2015) is found to be unrealistic for layered soil.

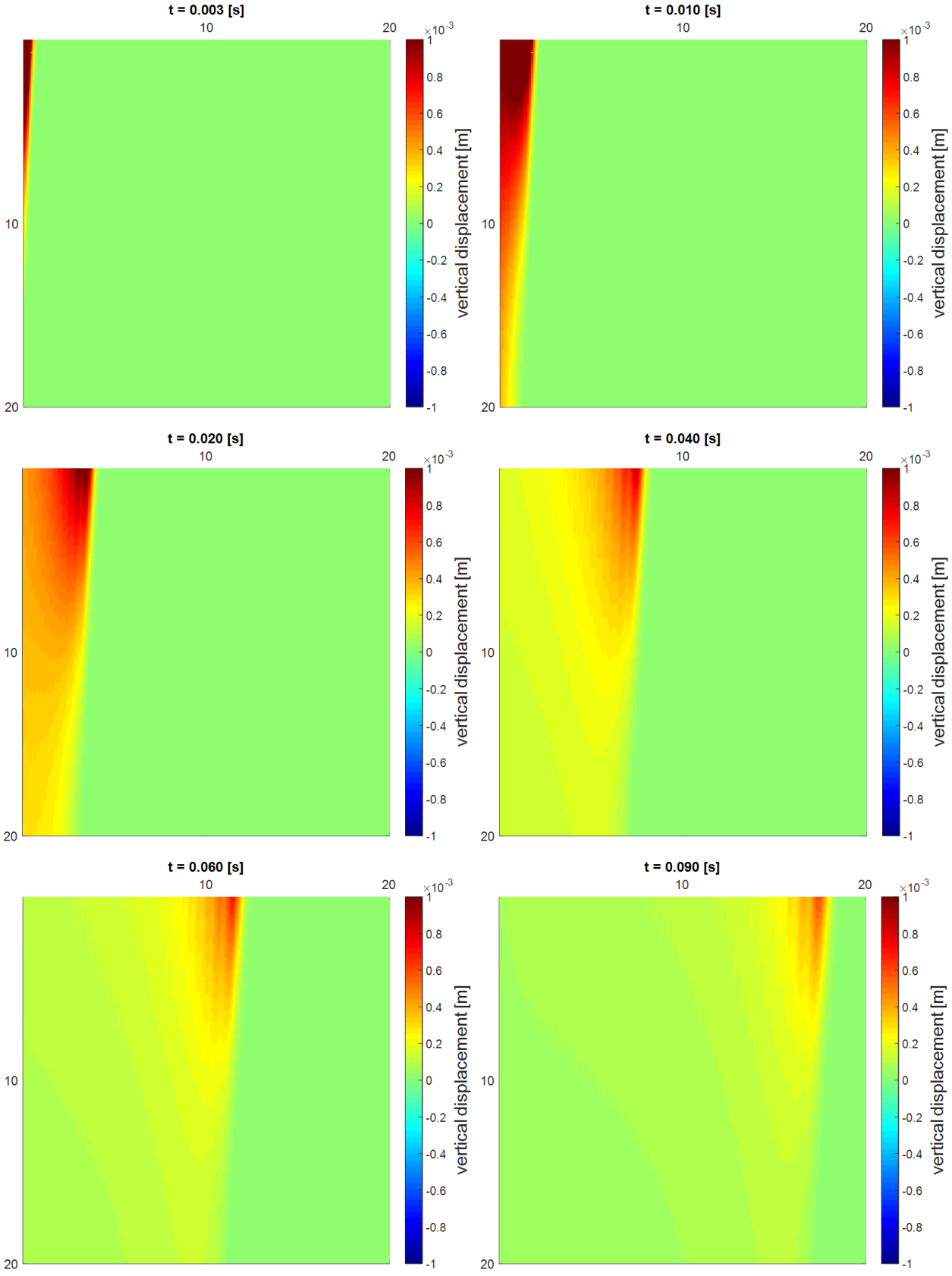

Figure 3.14 : Salgado pile driving model for homogenous soil

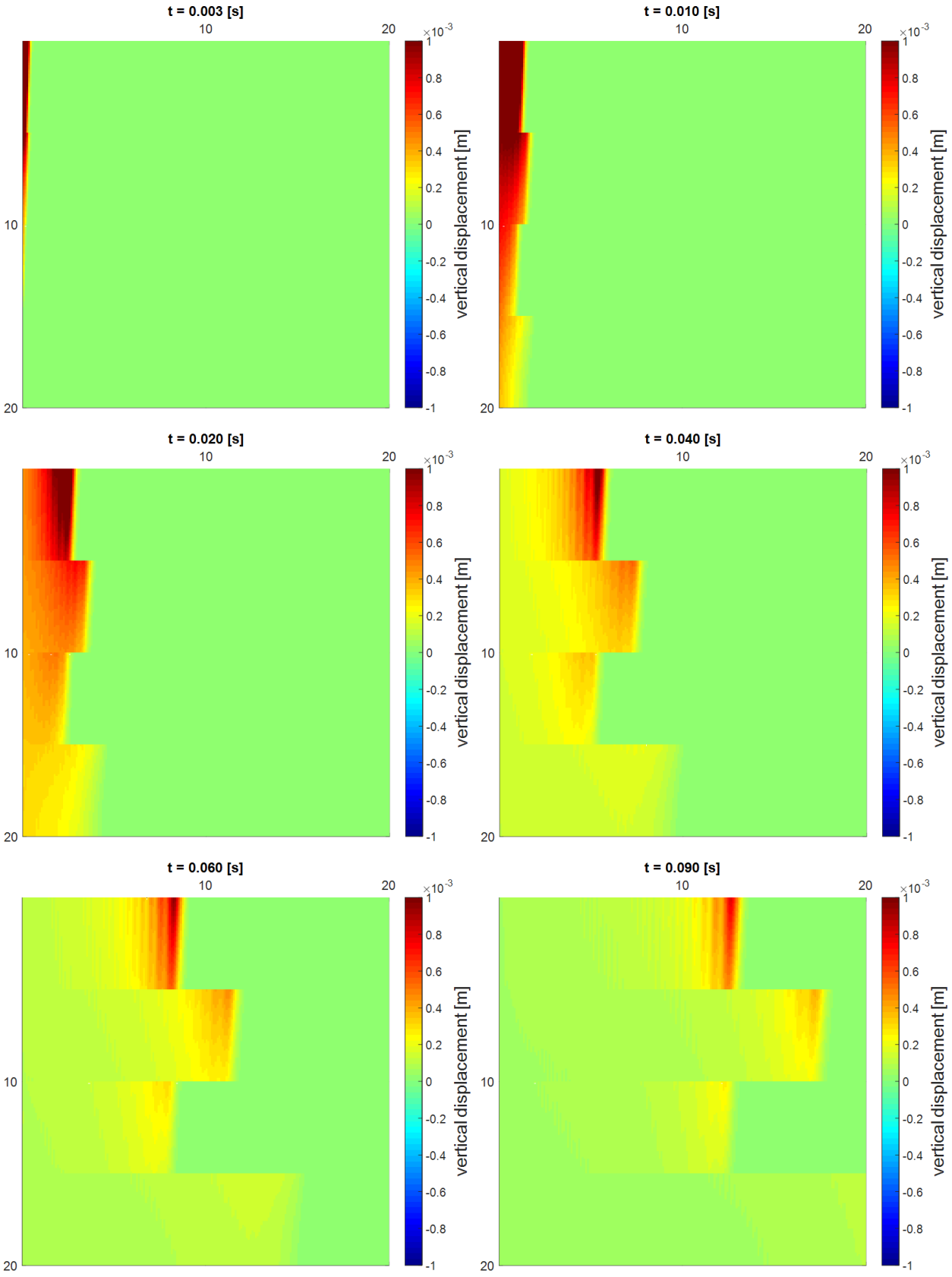

Figure 3.15: Salgado pile driving model for layered soil

3.3.3 Disadvantages of the Salgado pile driving model

The Salgado pile driving model seemed to be an improvement compared to the Holeyman & van den Berghe model, since the slices approach allows for soil layering to be taken into account. The results presented in this section show that the model gives unrealistic results for layered soil (because vertical interaction $\frac{\partial w}{\partial z}$ is neglected), taking away this advantage. Other disadvantages of this model are listed:

- The model neglects radial soil displacements, which might not be a valid assumption.
- It is not possible to derive the base reaction from this model, therefore the base reaction is modelled by a spring and dashpot.
- The soil plug is not taken into account.

The models presented in the upcoming chapters will try to resolve these disadvantages.

4 Simplified cylindrically symmetric damped elastic pile-soil-plug model neglecting radial displacement

This chapter presents a cylindrically symmetric damped elastic pile-soil-plug model. Vertical interaction, soil reaction at the pile toe and soil plug are taken into account. The radial displacement is neglected in this chapter and will be added in the next chapter.

4.1 Model formulation

Figure 4.1 gives the discretization map of the model and is used for the derivation of the governing equations of motion.

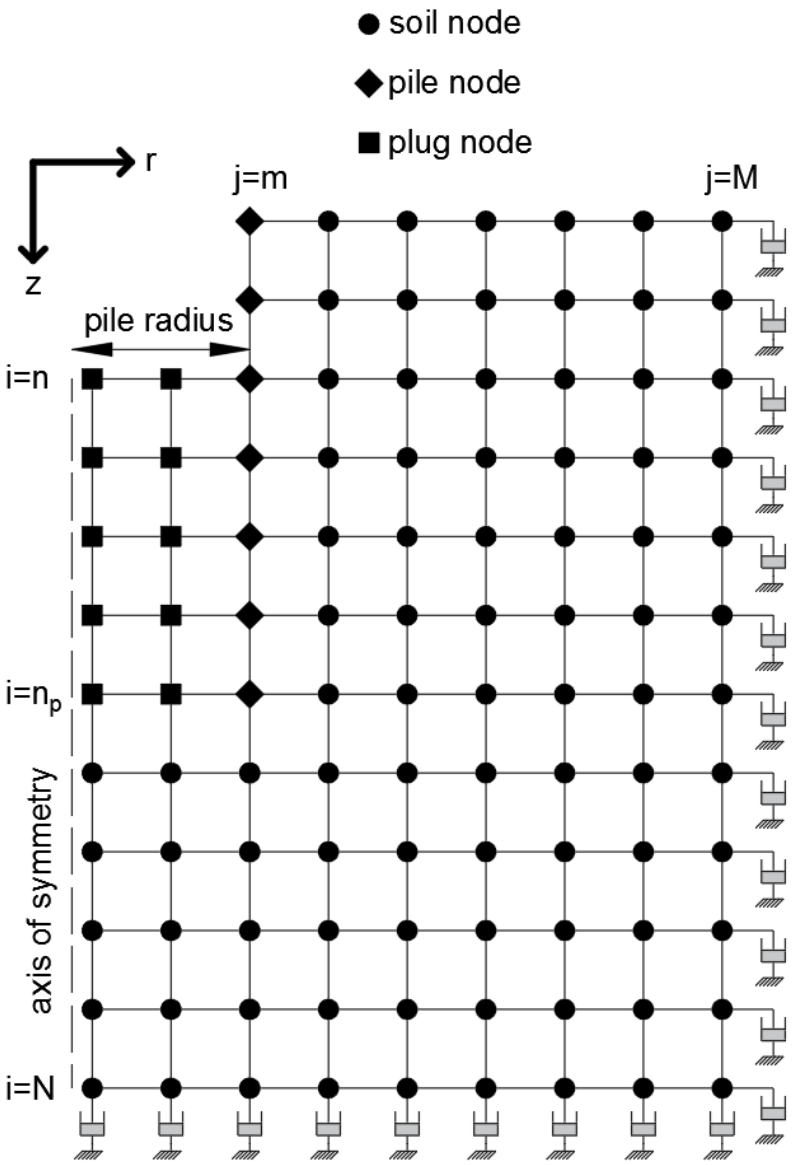

Figure 4.1: Model discretization map

The governing equation of motion of an elastic cylindrically symmetric elastic medium, neglecting radial displacement reads (Verruijt, 2010):

$$\rho \frac{\partial^2 w}{\partial t^2} = \left(K + \frac{4}{3}G\right)\frac{\partial^2 w}{\partial z^2} + G\left(\frac{\partial^2 w}{\partial r^2} + \frac{1}{r}\frac{\partial w}{\partial r}\right) \tag{4.1}$$

w is the vertical displacement, ρ is the soil density, G the soil shear modulus and K the soil bulk modulus. This equation is expanded with soil damping:

$$\frac{\partial^2 w}{\partial t^2} = \left(1 + \alpha\frac{\partial}{\partial t}\right)\left(\left(K + \frac{4}{3}G\right)\frac{\partial^2 w}{\partial z^2} + G\left(\frac{\partial^2 w}{\partial r^2} + \frac{1}{r}\frac{\partial w}{\partial r}\right)\right) \tag{4.2}$$

α is the damping coefficient. This will be the governing equation for the soil and plug nodes. For the axis of symmetry the following boundary condition holds:

$$\sigma_{rz} = G\frac{\partial w}{\partial r} = 0 \quad @i = n{:}N, j = 1 \tag{4.3}$$

Please note that damping is only applied at the internal nodes and not at the boundary nodes. The symbol : is used to denote 'up to and including'. The free surface boundary condition is:

$$\sigma_{zz} = \left(K + \frac{4}{3}G\right)\frac{\partial w}{\partial z} = 0 \quad @\, i = n, j = 1{:}m-1 \; and \; i = 1, j = m+1{:}M \tag{4.4}$$

The vertical non-reflective boundary condition:

$$\sigma_{rz} = G\frac{\partial w}{\partial r} = -\sqrt{G\rho}\frac{\partial w}{\partial t} \quad @i = 1{:}N, j = M \tag{4.5}$$

And the horizontal non-reflective boundary condition:

$$\sigma_{zz} = \left(K + \frac{4}{3}G\right)\frac{\partial w}{\partial z} = -\sqrt{\left(K + \frac{4}{3}G\right)\rho}\frac{\partial w}{\partial t} \quad @i = N, j = 1{:}M \tag{4.6}$$

The interface boundary conditions read:

$$w_{plug} = w_{pile} = w \quad @i = n{:}n_P, j = m \tag{4.7}$$

$$w_{soil} = w_{pile} = w \quad @i = 1{:}n_P, j = m \tag{4.8}$$

The equation of motion for the pile reads:

$$\rho_p A_p \frac{\partial^2 w}{\partial t^2} = \pi d_e G \frac{\partial w}{\partial r}|_{soil} + E_p A_p \frac{\partial^2 w}{\partial z^2} \quad @i = 1{:}n-1, j = m \tag{4.9}$$

Or:

$$\rho_p A_p \frac{\partial^2 w}{\partial t^2} = \pi d_e G \frac{\partial w}{\partial r}|_{soil} - \pi d_i G \frac{\partial w}{\partial r}|_{plug} + E_p A_p \frac{\partial^2 w}{\partial z^2} \quad @i = n{:}n_p, j = m \tag{4.10}$$

$|_{soil}$ denotes a single sided derivative to the right and $|_{plug}$ denotes a single sided derivative to the left. A_P is the cross-sectional area of the pile, ρ_P is the density of the pile, E_P is the Young's modulus of the pile, d_i is the internal pile diameter and d_e is the external pile diameter. The boundary condition at the pile head reads:

$$E_p A_p \frac{\partial w}{\partial z} = -F_{imp}(t) \quad @i = 1, j = m \tag{4.11}$$

$F_{imp}(t)$ is the hammer impact force as a function of time. The boundary condition at the pile toe reads:

$$\begin{aligned} E_p A_p \frac{\partial w}{\partial z} &= \frac{1}{4}\pi((d_n + \Delta r)^2 - (d_n - \Delta r)^2)\left(K + \frac{4}{3}G\right)\frac{\partial w}{\partial z}|_{soil} \\ &= \pi d_n \Delta r \left(K + \frac{4}{3}G\right)\frac{\partial w}{\partial z}|_{soil,V} \quad @i = n_P, j = m \end{aligned} \tag{4.12}$$

$|_{soil,V}$ is a single sided derivative downwards. $d_n = \frac{d_i + d_e}{2}$ is the nominal pile diameter. Δr is the radial grid size. Using finite difference approximations (section 2.5.2), the governing system of equations is discretized and transformed into a state space system of first order ordinary differential equations:

$$\begin{bmatrix} \frac{\partial}{\partial t}\boldsymbol{w} \\ \frac{\partial^2}{\partial t^2}\boldsymbol{w} \end{bmatrix} = \begin{bmatrix} [0] & [I] \\ [M_1] & [M_2] \end{bmatrix} \begin{bmatrix} \boldsymbol{w} \\ \frac{\partial}{\partial t}\boldsymbol{w} \end{bmatrix} + \boldsymbol{F} \tag{4.13}$$

$[M_1]$ and $[M_2]$ contain the discretization coefficients with respect to space, $[I]$ is the identity matrix and $\boldsymbol{F}$ contains the impact force at the pile head. The full derivation can be found in appendix A3.

4.2 Numerical aspects

The same stability requirements that are presented in section 3.3.2 hold for this model. Furthermore, to ensure transfer of compression waves into the soil, a third stability requirement is necessary:

$$\Delta z < \frac{c_p}{f_{load}} \tag{4.14}$$

Δz is the vertical grid size, c_p is the compression wave velocity in the soil and f_{load} is the frequency of the impact load by the hammer. It is also necessary to modify the equation of motion for the axis of symmetry, since:

$$\frac{1}{r}\frac{\partial w}{\partial r} = \frac{0}{0} \tag{4.15}$$

The modified expression is found using L'Hopital rule (Mazumder, 2016):

$$\frac{\partial^2 w}{\partial r^2} + \frac{1}{r}\frac{\partial w}{\partial r} = 2\frac{\partial^2 w}{\partial r^2} \quad @i = n{:}N, j = 1 \tag{4.16}$$

4.3 Model results

4.3.1 Soil damping

The model is implemented numerically in Matlab and solved using ODE45. The full code can be found in appendix B3. First the soil model without pile is investigated. The interface is excited by a prescribed harmonic displacement:

$$w_{interface} = 10^{-3}\sin(800t) \tag{4.17}$$

The soil is considered to be homogenous and consists of loose sand according to input table 1.3.

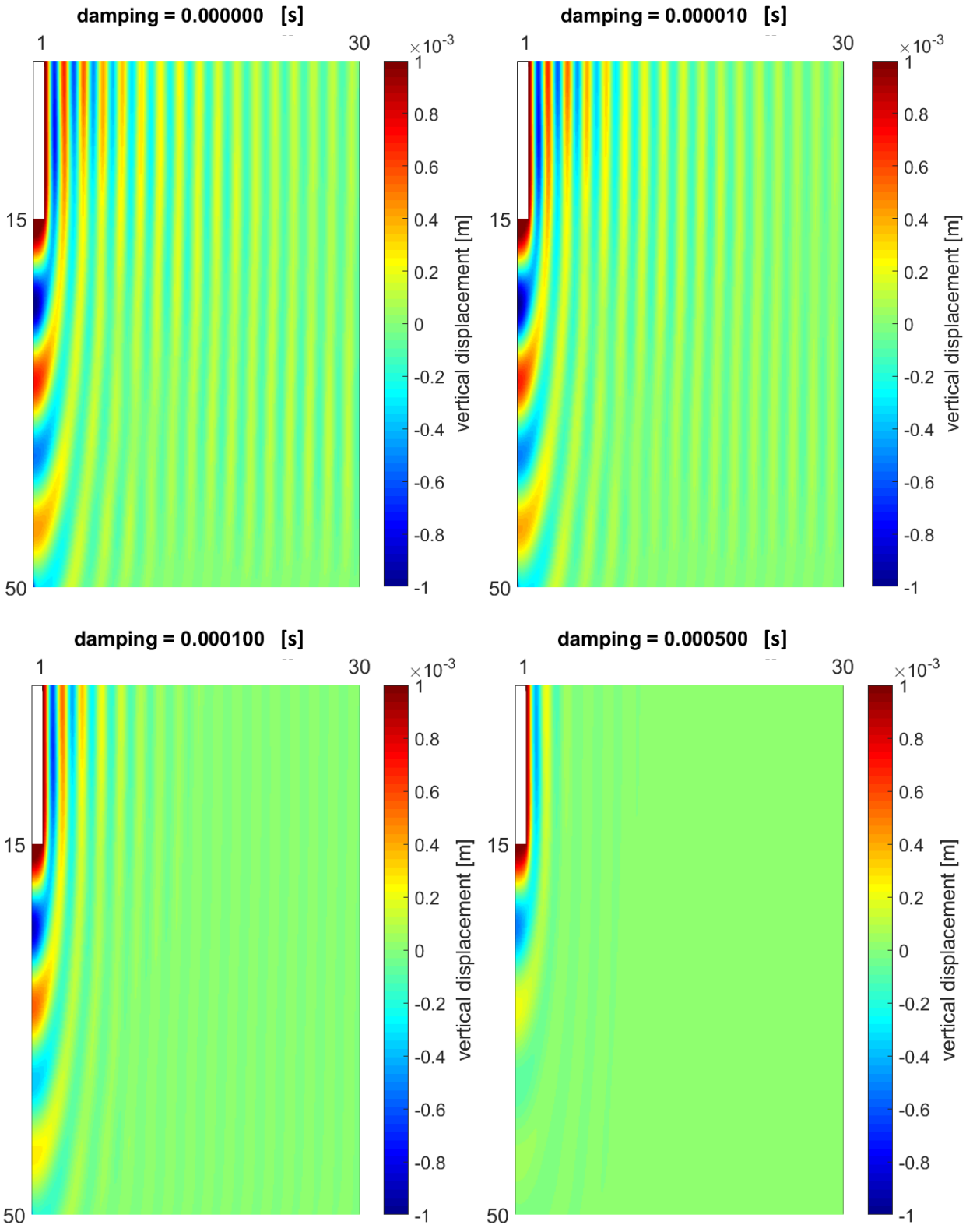

Figure 4.2: Vertical displacement field for various damping coefficients

The influence of damping coefficient α is shown in figure 4.2. The band is quite narrow. The damping is limited for $\alpha = 10^{-4}$, while $\alpha = 5 * 10^{-3}$ seems to give an overdamped solution.

4.3.2 Soil layering

Two types of soil layering are considered, with soil parameters according to input table 1.4:

layer	start height	end height	soil type first calculation	soil type second calculation
1	0	5	soft clay	firm clay
2	5	10	loose sand	loose sand
3	10	15	soft clay	firm clay
4	15	50	medium sand	medium sand

Table 4.1: soil layering for two comparison calculations

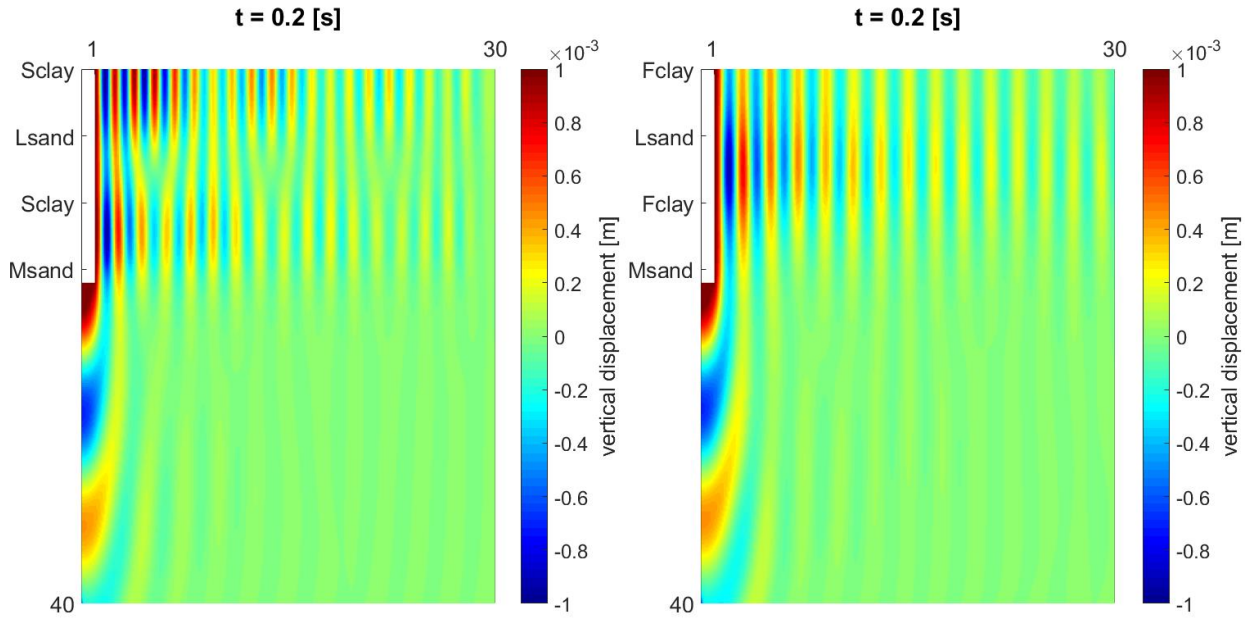

Figure 4.3: Displacement field for layered soil: loose sand between two soft clay layers

The results in figure 4.3 clearly show that lower stiffness results in higher displacements. Taking vertical interaction into account gives more realistic results for layered soil.

4.3.3 Soil plug

The pile is now added to the model to investigate the importance of the soil plug. The pile length is chosen to be 15 m, the radial domain size 15 m and the vertical domain size 35 m. Homogenous soil consisting of loose sand (input table 1.4) is chosen for the calculation. Hammer and pile properties are taken from input tables 1.1 and 1.2. The first calculation is carried out without soil plug and the second with a plug height of 12 m.

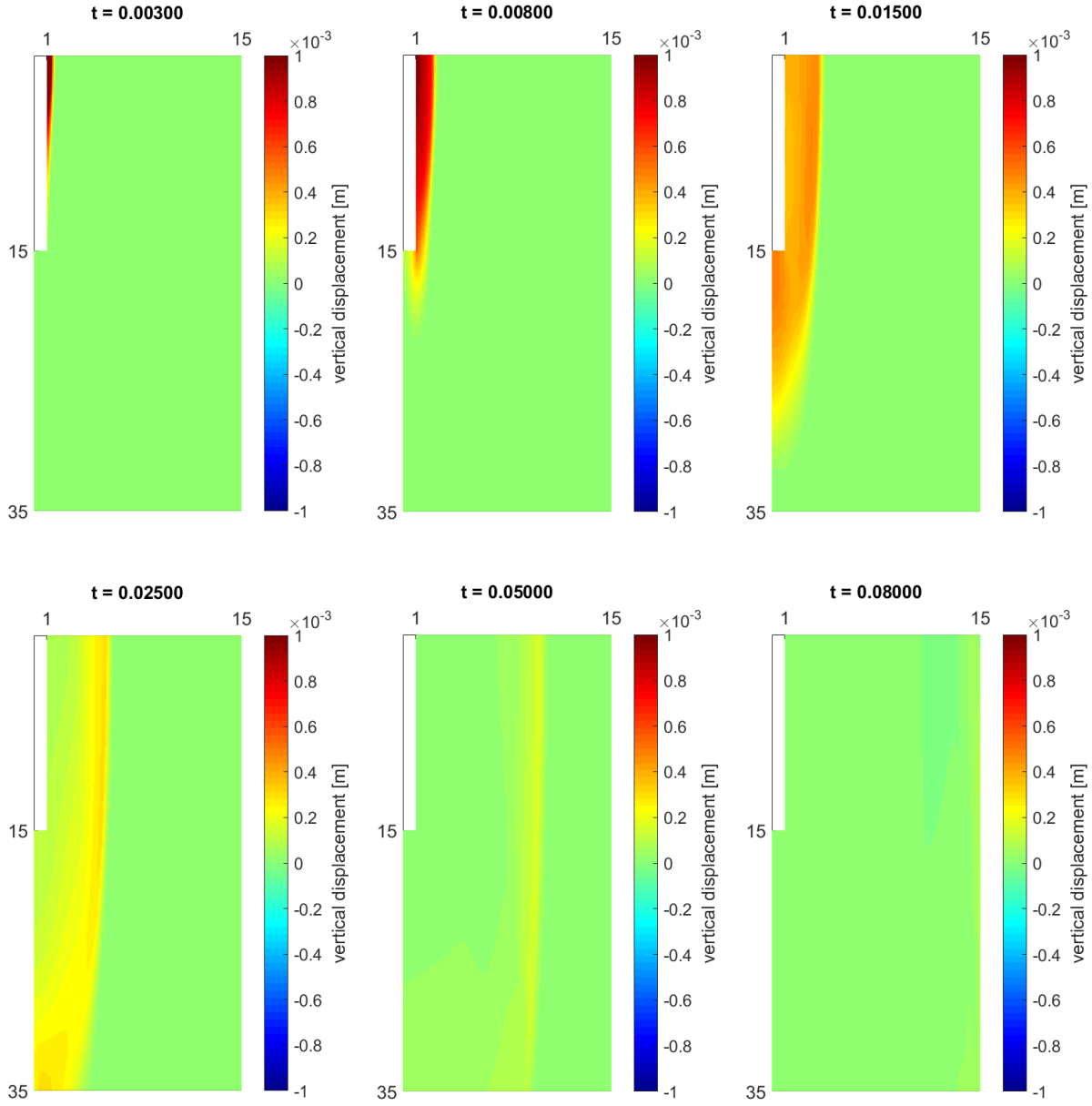

Figure 4.4: Pile-soil behavior after hammer impact with plug height equal to 0 m

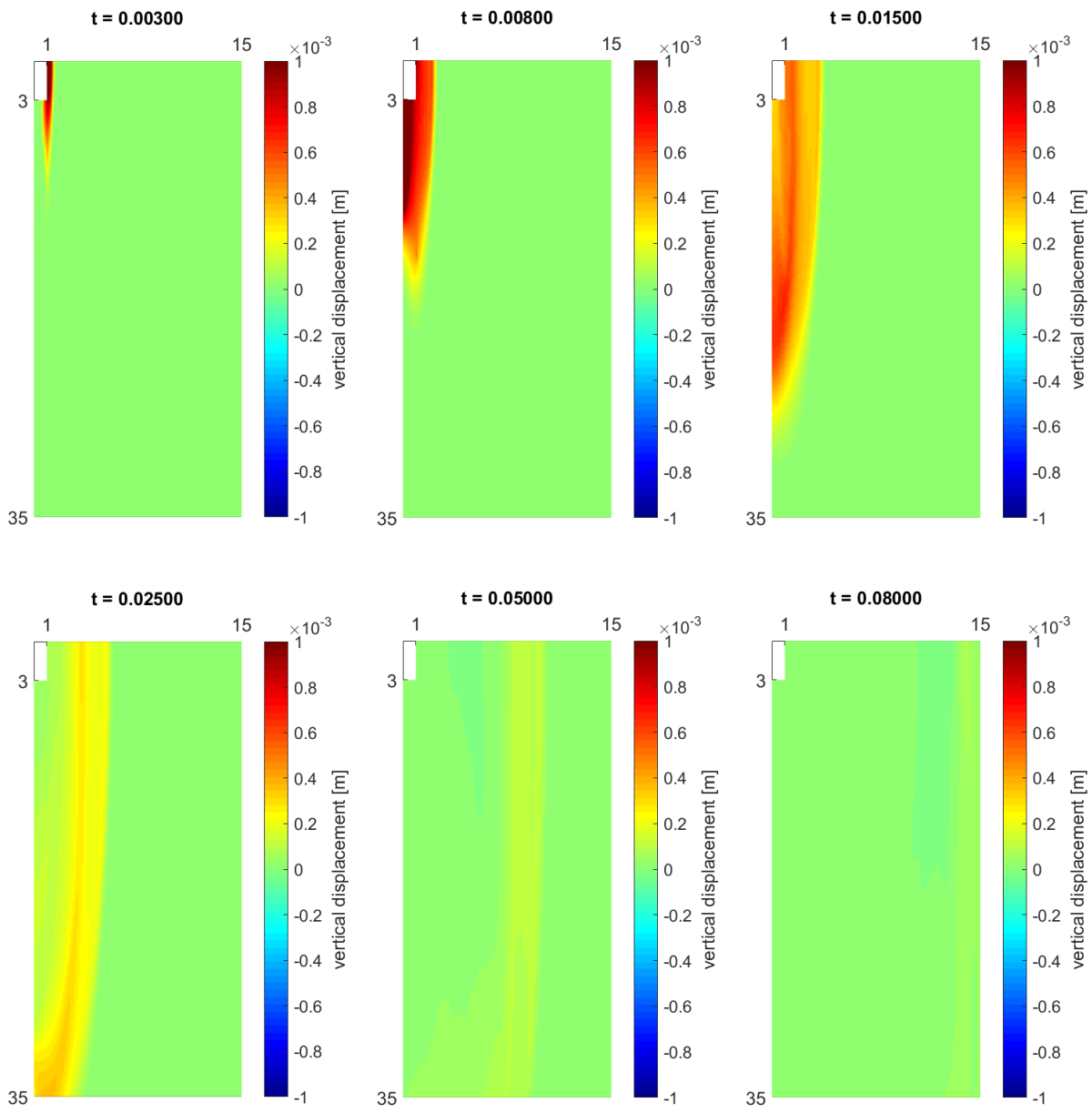

Figure 4.5: Pile-soil behavior after hammer impact with plug height equal to 12 m

The results in figures 4.4 and 4.5 show that the soil plug is important in the dynamic pile-soil behaviour. The plug delays and redistributes the emission of wave energy into the soil. If damping is present in the system, the plug will also absorb part of the wave energy.

4.3.4 Extending the pile above the surface

To study different phases of pile driving, it is important to understand the behaviour of the pile-soil-plug model when part of the pile is extended above the surface. For this purpose pile driving in loose sand (input table 1.4) is considered. 20 meter of the pile is above the surface and the remaining 10 meter below the surface. The results are shown in figure 4.6. Comparison with figure 4.4 shows that extending the pile above the surface will result in a longer period of time before the motion of the pile is damped out. The amount of displacement cycles increases.

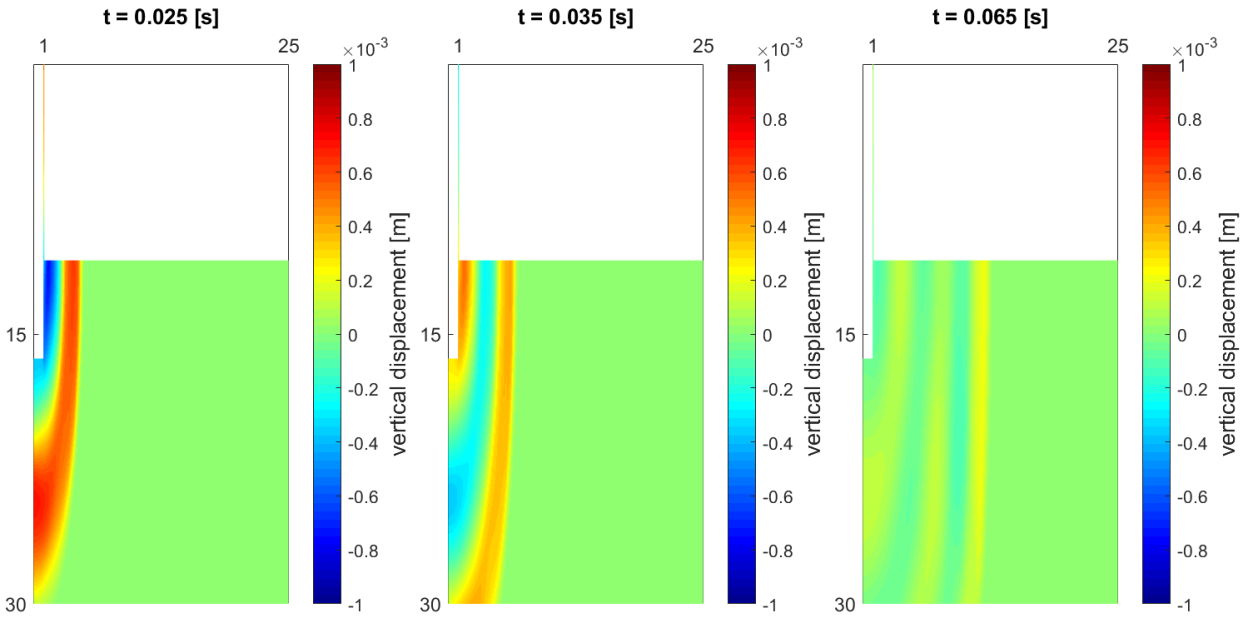

Figure 4.6: Behavior of pile-soil model with large part of the pile extended above the surface

4.3.5 Pile driving in a sloped soil structure

One of the main objectives of this thesis is to quantify vibrations and excess pore pressure accumulation induced by pile driving in embankments. Embankments are 3D rather than cylindrically symmetric. It is however possible to get an impression of the behaviour of a real slope by considering an cylindrically symmetric slope. The slope considered is 1/3 and consists of loosely packed sand (input table 1.4). The results are shown in figure 4.7. The results are very similar to the results shown in figure 4.4. This indicates that an cylindrically symmetric slope does not significantly alter the vibrations induced by pile driving. It is difficult to predict if this also holds for a real 3D slope.

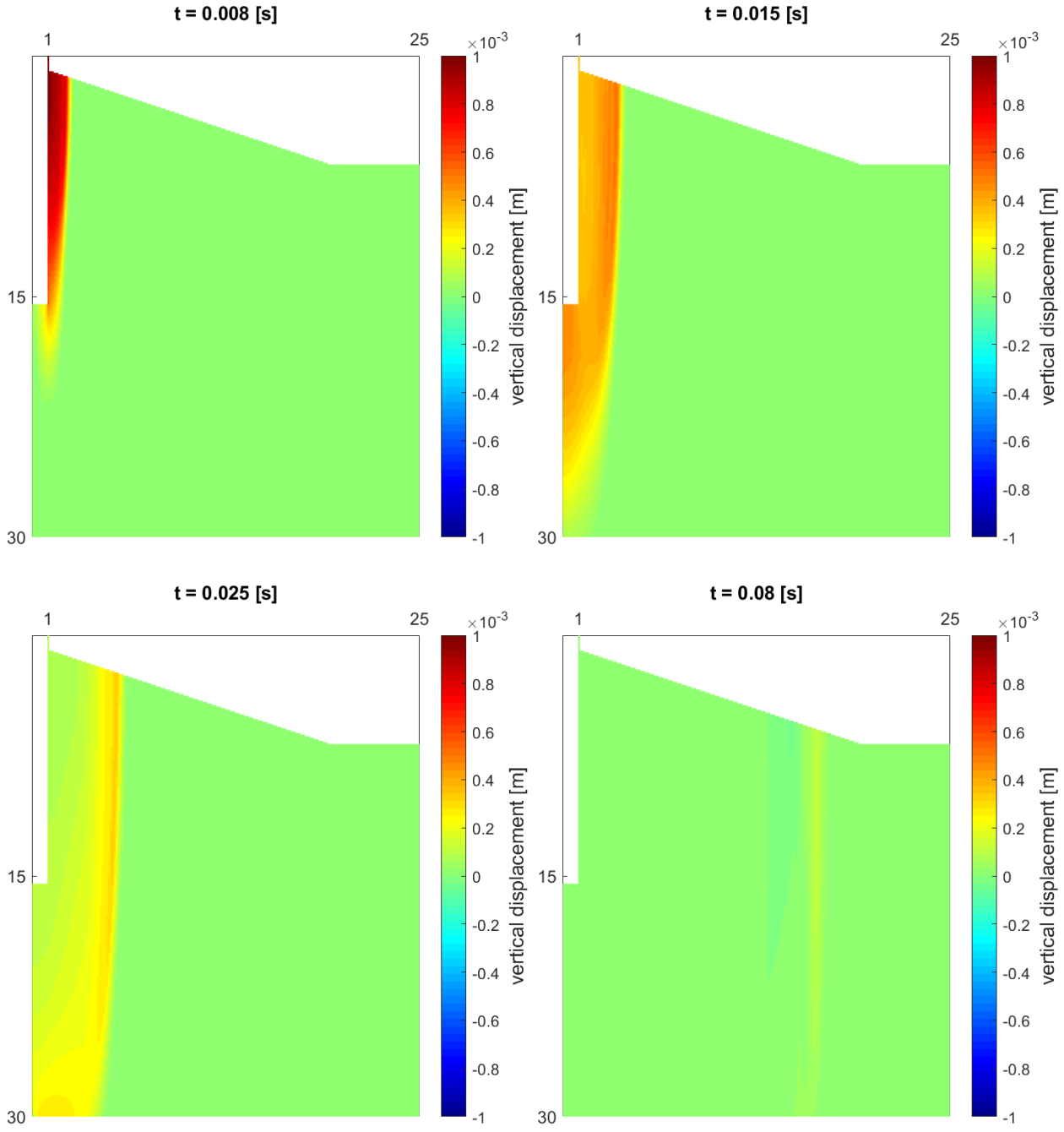

Figure 4.7: Pile driving in an cylindrically symmetric slope

5 Cylindrically symmetric damped elastic pile-soil-plug model

This chapter improves the model presented in chapter 4 by accounting for radial displacement, therefore solving the full soil equations. Radial displacement of the pile shell is also taken into account by introducing the Donnell thin shell theory.

5.1 Model formulation

The model in the previous chapter is expanded with radial displacement. The discretization map of the model is shown in figure 5.1.

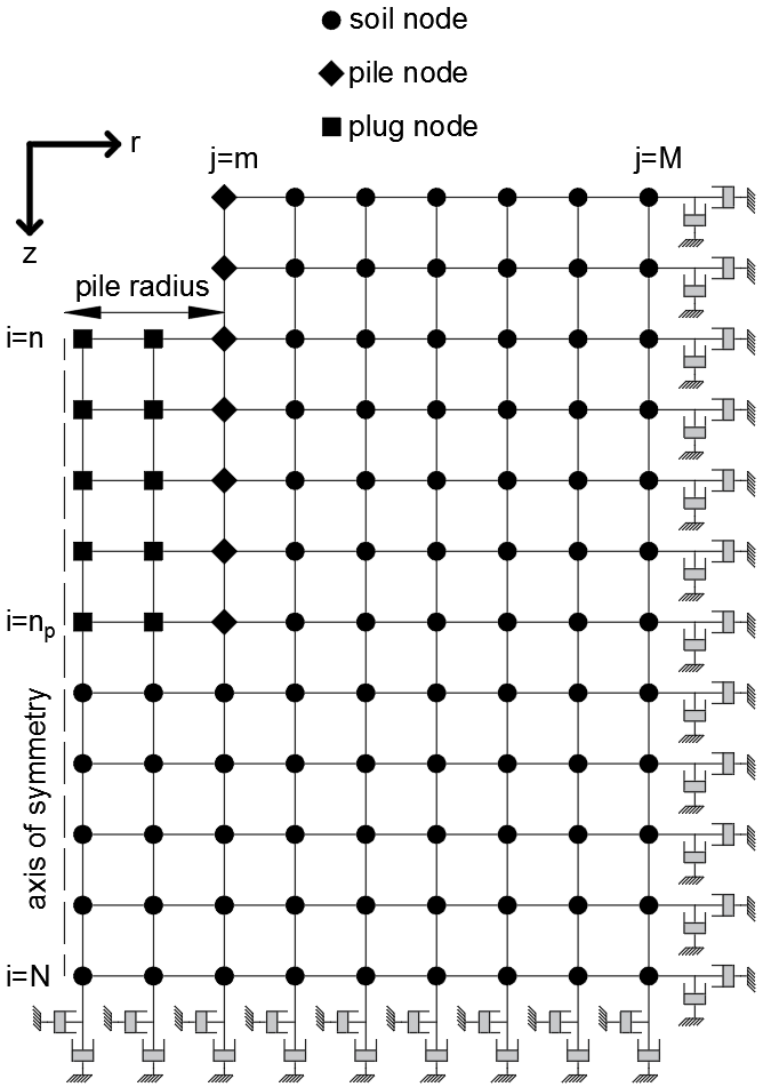

Figure 5.1: Model discretization map

The governing system of equations of an cylindrically symmetric elastic medium (Verruijt, 2010) expanded with soil damping read:

$$\rho\frac{\partial^2 u}{\partial t^2}=\left(1+\alpha\frac{\partial}{\partial t}\right)\left(\left(K+\frac{4}{3}G\right)\left(\frac{\partial^2 u}{\partial r^2}+\frac{1}{r}\frac{\partial u}{\partial r}-\frac{u}{r^2}\right)+\left(K+\frac{1}{3}G\right)\frac{\partial^2 w}{\partial r\partial z}+G\frac{\partial^2 u}{\partial z^2}\right) \tag{5.1}$$

$$\begin{aligned}\rho\frac{\partial^2 w}{\partial t^2}=\left(1+\alpha\frac{\partial}{\partial t}\right)\Bigg(&\left(K+\frac{4}{3}G\right)\frac{\partial^2 w}{\partial z^2}+\left(K+\frac{1}{3}G\right)\left(\frac{\partial^2 u}{\partial r\partial z}+\frac{1}{r}\frac{\partial u}{\partial z}\right)\\&+G\left(\frac{\partial^2 w}{\partial r^2}+\frac{1}{r}\frac{\partial w}{\partial r}\right)\Bigg)\end{aligned} \tag{5.2}$$

u is the radial displacement, w the vertical displacement, α is the damping coefficient, K the bulk modulus, G the shear modulus and ρ the density of the soil. For the axis of symmetry the following boundary conditions hold:

$$u=0 \quad @i=n{:}N, j=1 \tag{5.3}$$

$$\sigma_{rz}=G\left(\frac{\partial u}{\partial z}+\frac{\partial w}{\partial r}\right)=0 \quad @i=n{:}N, j=1 \tag{5.4}$$

Please note that damping is only applied at the internal nodes and not at the boundary nodes. The symbol : denotes 'up to and included'. The free surface boundary conditions:

$$\begin{aligned}\sigma_{zz}=\left(K+\frac{4}{3}G\right)\frac{\partial w}{\partial z}+\left(K-\frac{2}{3}G\right)\left(\frac{u}{r}+\frac{\partial u}{\partial r}\right)=0\\ @i=n, j=1{:}m-1 \; and \; i=1, j=m+1{:}M\end{aligned} \tag{5.5}$$

$$\sigma_{rz}=G\left(\frac{\partial u}{\partial z}+\frac{\partial w}{\partial r}\right)=0 \quad @i=n, j=1{:}m-1 \; and \; i=1, j=m+1{:}M \tag{5.6}$$

The vertical non-reflective boundary conditions read:

$$\sigma_{rr}=\left(K+\frac{4}{3}G\right)\frac{\partial u}{\partial r}+\left(K-\frac{2}{3}G\right)\left(\frac{u}{r}+\frac{\partial w}{\partial z}\right)=-\sqrt{\rho\left(K+\frac{4}{3}G\right)}\frac{\partial u}{\partial t} \quad @i=1{:}N, j=M \tag{5.7}$$

$$\sigma_{rz}=G\left(\frac{\partial u}{\partial z}+\frac{\partial w}{\partial r}\right)=-\sqrt{\rho G}\frac{\partial w}{\partial t} \quad @i=1{:}N, j=M \tag{5.8}$$

The horizontal non-reflective boundary read:

$$\begin{aligned}\sigma_{zz}=\left(K+\frac{4}{3}G\right)\frac{\partial w}{\partial z}+\left(K-\frac{2}{3}G\right)\left(\frac{u}{r}+\frac{\partial u}{\partial r}\right)=-\sqrt{\rho\left(K+\frac{4}{3}G\right)}\frac{\partial w}{\partial t}\\ @i=N, j=1{:}M\end{aligned} \tag{5.9}$$

$$\sigma_{rz}=G\left(\frac{\partial u}{\partial z}+\frac{\partial w}{\partial r}\right)=-\sqrt{\rho G}\frac{\partial u}{\partial t} \quad @i=N, j=1{:}M \tag{5.10}$$

The interface conditions read:

$$w_{pile} = w_{soil} = w \quad @i = 1{:}\,n_P, j = m \tag{5.11}$$

$$w_{pile} = w_{plug} = w \quad @i = n{:}\,n_P, j = m \tag{5.12}$$

$$u_{pile} = u_{soil} = u \quad @i = 1{:}\,n_P, j = m \tag{5.13}$$

$$u_{pile} = u_{plug} = u \quad @i = n{:}\,n_P, j = m \tag{5.14}$$

The pile equations are based on Donnell thin shell theory (Banks et al. 1995):

$$\frac{\partial^2 w}{\partial t^2} = \frac{E_P}{\rho_P(1-v_P^2)}\frac{\partial^2 w}{\partial z^2} + \frac{E_P v_P}{\rho_P(1-v_P^2)}\frac{1}{r}\frac{\partial u}{\partial z} \tag{5.15}$$

$$\frac{\partial^2 u}{\partial t^2} = -\frac{v_P E_P}{\rho_P(1-v_P^2)}\frac{1}{r}\frac{\partial w}{\partial z} - \frac{E_P}{\rho_P(1-v_P^2)}\frac{1}{r^2}u - \frac{E_P t_P^2}{12\rho_P(1-v_P^2)}\frac{\partial^4 u}{\partial z^4} \tag{5.16}$$

ρ_P is the density of the pile, E_P is the Young's modulus of the pile, $v_P$is the poison ratio of the pile and t_P is the thickness of the pile shell. The equations are modified to include dynamic soil resistance:

$$\frac{\partial^2 w}{\partial t^2} = \frac{E_P}{\rho_P(1-v_P^2)}\frac{\partial^2 w}{\partial z^2} + \frac{E_P v_P}{\rho_P(1-v_P^2)}\frac{1}{r}\frac{\partial u}{\partial z} + \frac{G}{\rho_P t_P}\frac{\partial w}{\partial r}|_{soil} + \frac{G}{\rho_P t_P}\frac{\partial u}{\partial z}|_{soil,V} \quad @i = 1{:}\,n-1, j = m \tag{5.17}$$

$$\frac{\partial^2 u}{\partial t^2} = -\frac{v_P E_P}{\rho_P(1-v_P^2)}\frac{1}{r}\frac{\partial w}{\partial z} - \frac{E_P}{\rho_P(1-v_P^2)}\frac{1}{r^2}u - \frac{E_P t_P^2}{12\rho_P(1-v_P^2)}\frac{\partial^4 u}{\partial z^4} + \frac{\left(K+\frac{4}{3}G\right)}{\rho_P t_P}\frac{\partial u}{\partial r}|_{soil} + \frac{\left(K-\frac{2}{3}G\right)}{\rho_P t_P}\left(\frac{u}{r} + \frac{\partial w}{\partial z}|_{soil,V}\right) \quad @i = 1{:}\,n-1, j = m \tag{5.18}$$

$$\frac{\partial^2 w}{\partial t^2} = \frac{E_P}{\rho_P(1-v_P^2)}\frac{\partial^2 w}{\partial z^2} + \frac{E_P v_P}{\rho_P(1-v_P^2)}\frac{1}{r}\frac{\partial u}{\partial z} + \frac{G}{\rho_P t_P}\frac{\partial w}{\partial r}|_{soil} - \frac{G}{\rho_P t_P}\frac{\partial w}{\partial r}|_{plug} \quad @i = n{:}\,n_P, j = m \tag{5.19}$$

$$\frac{\partial^2 u}{\partial t^2} = -\frac{v_P E_P}{\rho_P(1-v_P^2)}\frac{1}{r}\frac{\partial w}{\partial z} - \frac{E_P}{\rho_P(1-v_P^2)}\frac{1}{r^2}u - \frac{E_P t_P^2}{12\rho_P(1-v_P^2)}\frac{\partial^4 u}{\partial z^4} + \frac{\left(K+\frac{4}{3}G\right)}{\rho_P t_P}\frac{\partial u}{\partial r}|_{soil} - \frac{\left(K+\frac{4}{3}G\right)}{\rho_P t_P}\frac{\partial u}{\partial r}|_{plug} \quad @i = n{:}\,n_P, j = m \tag{5.20}$$

$|_{soil}$ denotes a single sided derivative to the right and $|_{plug}$ denotes a single sided derivative to the left. $|_{soil,V}$ is a single sided derivative downwards.

The boundary conditions at the pile head read:

$$\left(\frac{\partial w}{\partial z} + v_P \frac{u}{r}\right) = -\frac{1 - v_P^2}{E_p A_p} F_{imp}(t) \quad @i = 1, j = m \tag{5.21}$$

$$\frac{\partial^2 u}{\partial z^2} = 0 \quad @i = 1, j = m \tag{5.22}$$

$$\frac{\partial^3 u}{\partial z^3} = 0 \quad @i = 1, j = m \tag{5.23}$$

A_p is the cross-sectional area of the pile. In reality the moments and shear forces will not be zero at the pile head because the hammer will always hit the pile eccentrically and at an angle compared to the vertical axis. These loads are not axisymmetric and can therefore not be taken into account in this model. The boundary conditions at the pile toe read:

$$\left(\frac{\partial w}{\partial z} + v_P \frac{u}{r}\right) = \frac{\pi d_n \Delta r (1 - v_P^2)}{E_p A_p} \left(\left(K + \frac{4}{3}G\right) \frac{\partial w}{\partial z}\Big|_{soil,V} + \left(K - \frac{2}{3}G\right)\left(\frac{u}{r} + \frac{\partial u}{\partial r}\Big|_{soil}\right)\right) \quad @i = n_P, j = m \tag{5.24}$$

$$\frac{\partial^2 u}{\partial z^2} = 0 \quad @i = n_P, j = m \tag{5.25}$$

$$\frac{\partial^3 u}{\partial z^3} = 0 \quad @i = n_P, j = m \tag{5.26}$$

d_n is the nominal pile diameter. The moments and shear forces at the pile toe are not necessarily zero because of shear stress between the soil and the pile toe. This shear stress (which calculations show to be the same magnitude as the shear stresses observed along the shaft) is neglected, considering the small base area of open ended piles. The governing equations of motion, boundary and interface conditions are discretized with respect to space and transformed into a state space system:

$$\begin{bmatrix} \frac{\partial}{\partial t}\boldsymbol{d} \\ \frac{\partial^2}{\partial t^2}\boldsymbol{d} \end{bmatrix} = \begin{bmatrix} [0] & [I] \\ [M_1] & [M_2] \end{bmatrix} \begin{bmatrix} \boldsymbol{d} \\ \frac{\partial}{\partial t}\boldsymbol{d} \end{bmatrix} + \boldsymbol{F} \tag{5.27}$$

With:

$$\boldsymbol{d} = \begin{bmatrix} \boldsymbol{w} \\ \boldsymbol{u} \end{bmatrix} \tag{5.28}$$

$[M_1]$ and $[M_2]$ contain the discretization coefficients with respect to space, $[I]$ is the identity matrix and $\boldsymbol{F}$ contains the impact force at the pile head. The full derivation can be found in appendix A3. The state space system is numerically implemented in Matlab and solved using ODE 45 solver. The full code can be found in appendix B4.

5.2 Numerical aspects

The governing equation of motion for the axis of symmetry needs to be adjusted because of singularity. The same approach used in section 4.2 is implemented here. By using the fact that the radial

displacement is zero and applying the L'Hopital rule, the system of two governing equations reduces to one:

$$\rho \frac{\partial^2 w}{\partial t^2} = \left(1 + \alpha \frac{\partial}{\partial t}\right)\left(\left(K + \frac{4}{3}G\right)\frac{\partial^2 w}{\partial z^2} + \frac{\partial^2 u}{\partial r \partial z} + 2G\frac{\partial^2 w}{\partial r^2}\right) \quad @i = n{:}N, j = 1 \tag{5.29}$$

The convergence of the model is studied by considering the behaviour of soil system separately. The interface is excited by a harmonic vertical unity displacement (figure 5.2):

$$w_{interface} = 10^{-3}\sin(800t) \tag{5.30}$$

$$u_{interface} = 0 \tag{5.31}$$

Or a harmonic radial unity displacement (figure 5.3):

$$w_{interface} = 0 \tag{5.32}$$

$$u_{interface} = 10^{-3}\sin(800t) \tag{5.33}$$

Results in figure 5.2 show that the model converges for a grid size (both vertical and radial) of 2 cm. Various calculations with different ratio's between vertical and radial grid size show that the optimal ratio is approximately 2:1. Looking at the vertical displacement field at t=0.05 second for a grid size of 2 cm (figure 5.2 bottom left) and 10 cm (figure 5.2 top left), the difference seems to be twofold. The 10 cm plot has 2 concentrated diagonals, originating from the edges. The diagonals seem to divert displacements from the surface and from underneath the interface . For the 2 cm, the concentrated diagonals disappear. This results in Rayleigh waves at the surface being clearly distinguishable from the vertical shear waves and the disappearance of the stagnant zone underneath the interface.

Results in figure 5.3 show the development of pressure waves originating from the interface at two different instances: 0.005 s and 0.5 s. The complex interaction with the vertical displacement results in a chaotic displacement field.

Convergence of the coupled pile-soil-plug model is harder to determine, since it depends on many factors like soil and plug layering, embedment of the pile in the soil and the hammer impact characteristics. Calculations with different layering and grid sizes show that the optimal ratio between vertical and radial grid size for the coupled model is approximately 2:1. Recommended grid sizes are given in table 5.1, along with an indication of computation time and accuracy.

Δz [cm]	Δr [cm]	indication of computation time (running calculation on a laptop from 0 to 200 ms for a 50 m * 40 m domain size)	indication of accuracy
10	20	10 minutes	moderate
5	10	2 hours	high
2.5	5	8 hours	converged

Table 5.1: Recommended grid sizes for the coupled model

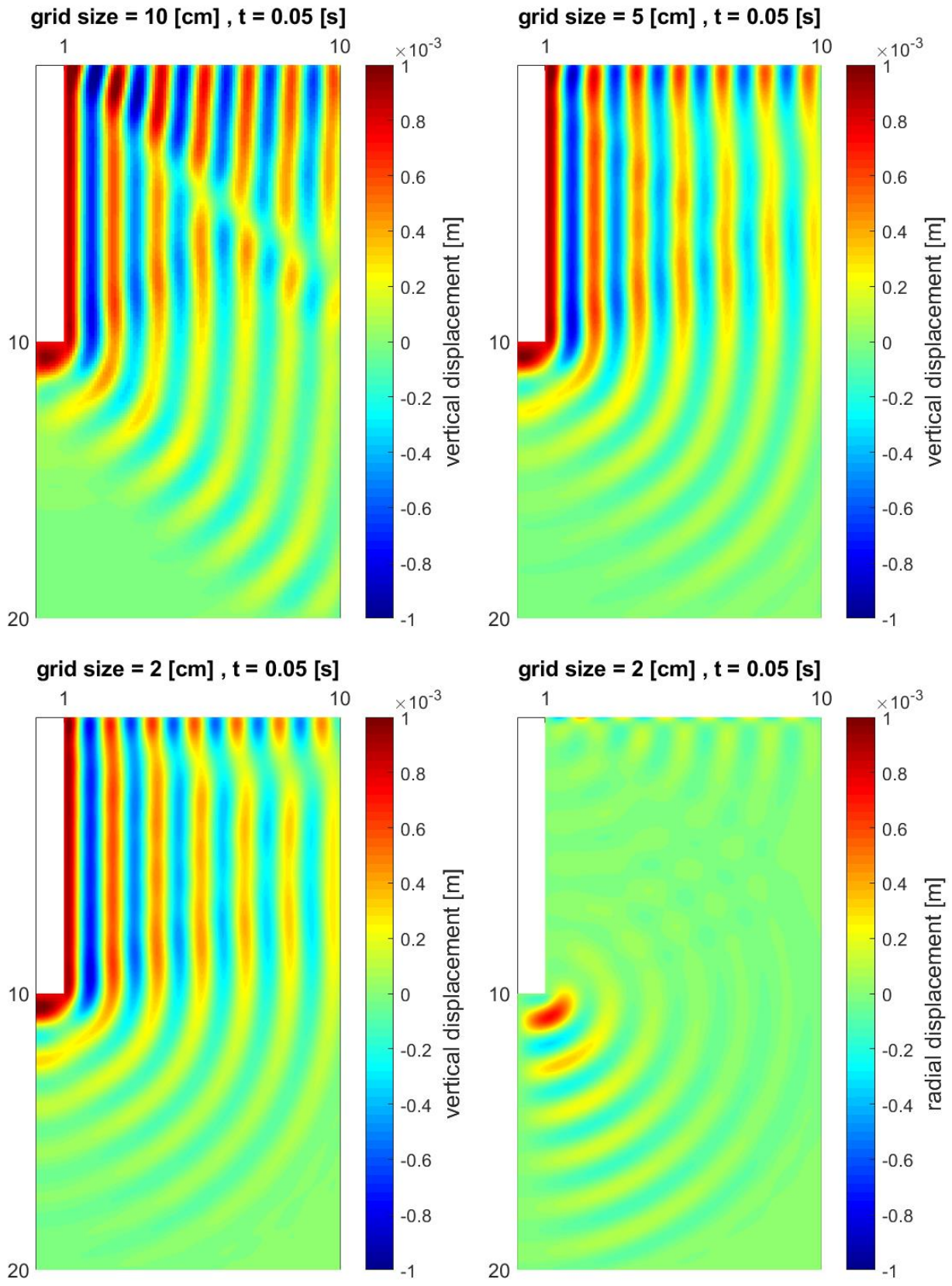

Figure 5.2: Behavior of the soil system under harmonic vertical unity excitation at the interface for various grid sizes

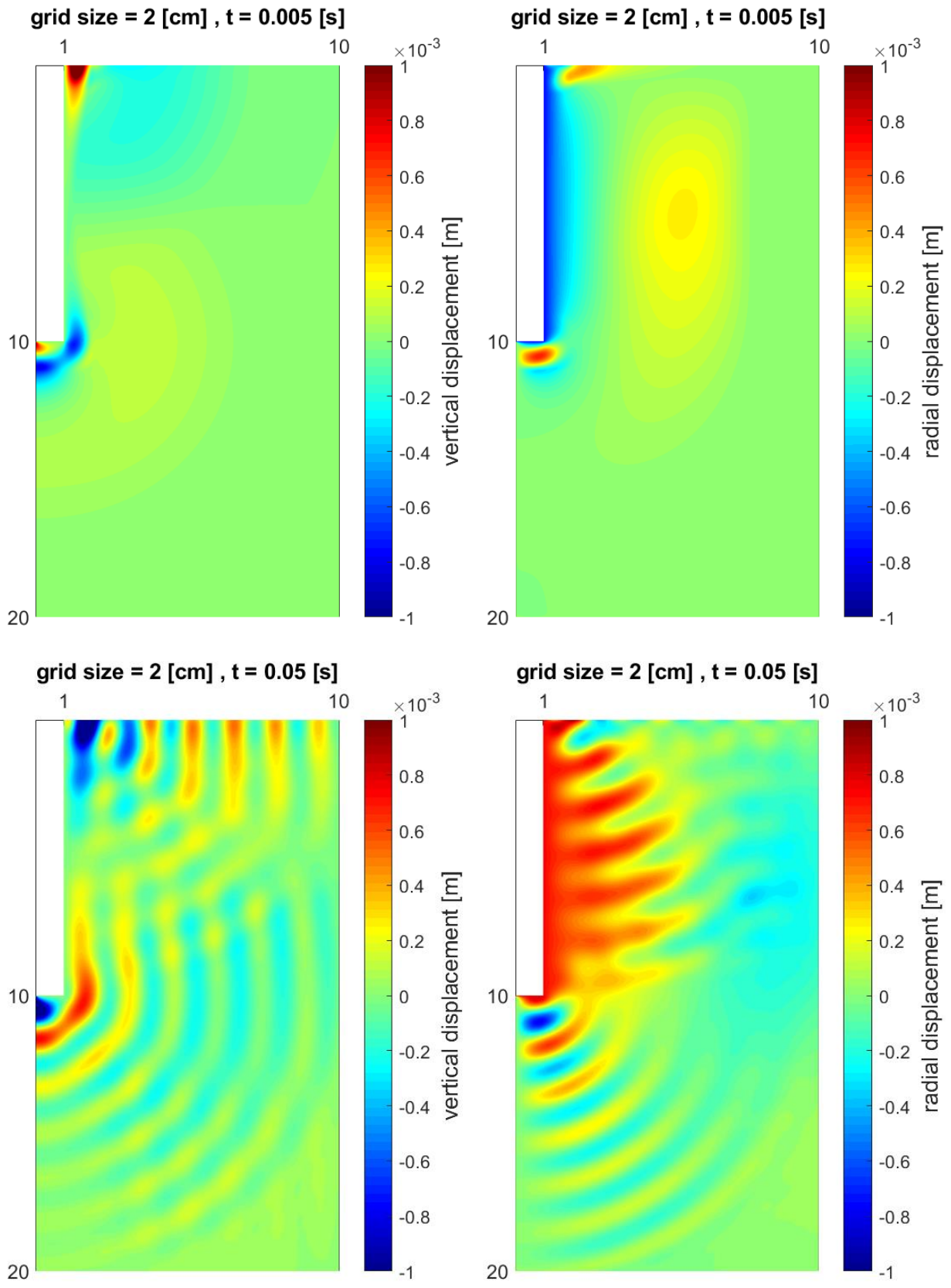

Figure 5.3: Behavior of the soil system under harmonic radial unity excitation at the interface at t=0.005 s and t=0.05 s

5.3 Confined aquifer modelling

The coupled pile-soil-plug model is first applied to investigate displacements and shear stresses for the confined aquifer problem. The aquifer consists of loose sand, confined by either soft or firm clay. Three different pile driving phases are considered , as shown in figure 5.4. The layering of the soil is given in table 5.2.

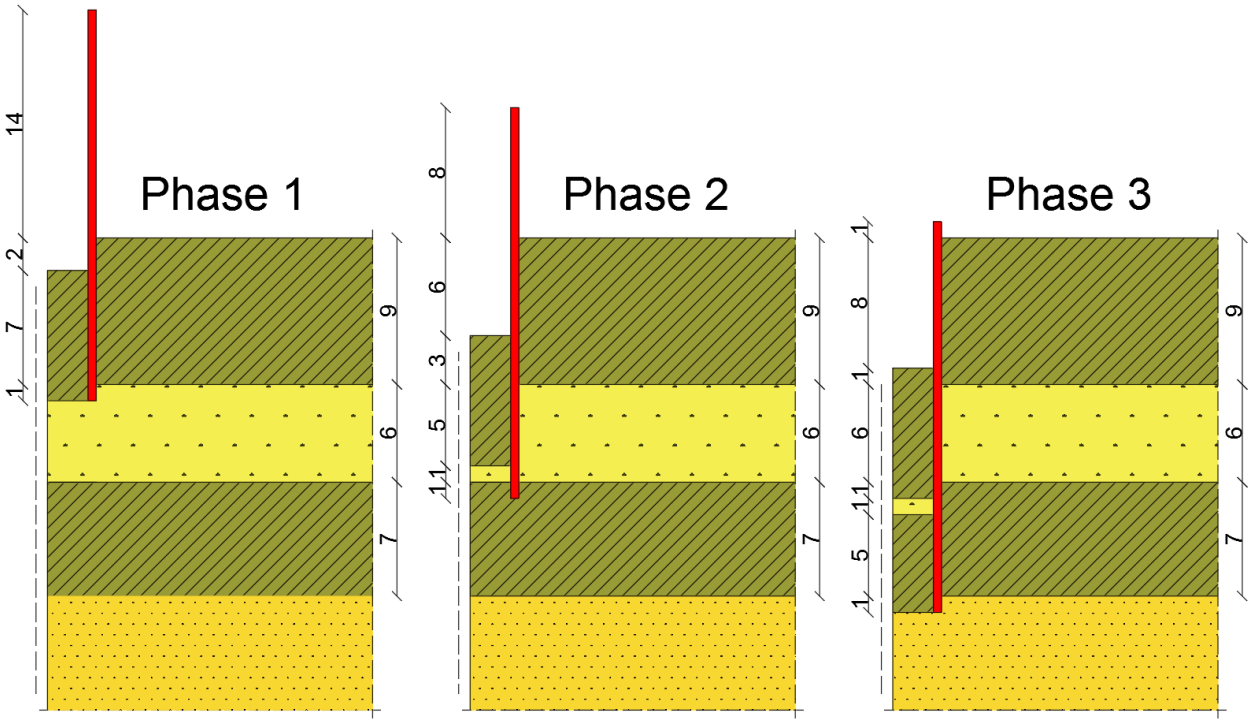

Figure 5.4: Three pile driving phases for the confined aquifer problem

layer	start height	end height	soil type first calculation
1	0	9	soft or firm clay
2	9	15	loose sand
3	15	22	soft or firm clay
4	22	50	medium sand

Table 5.2: Soil layering

The layering of the plug is different for each phase, as shown in figure 5.4. The damping coefficient used for all examples in this chapter is 0.0001. All other input values are derived from input tables 1.1 (hammer), 1.3 (pile) and 1.4 (soil).

Figure 5.5 shows a comparison between phase 1 and 3 for two firm confining clay layers. In phase 3, the pile is almost fully embedded in the soil, while in phase 1 most of the pile extends above the surface. This results in more displacement cycles, as was the case in section 4.3.4. The vertical shear waves in the sand layer clearly lag behind those in the top clay layer, because of lower shear wave propagation velocity. Weak displacement amplitudes are observed in the lower clay layer.

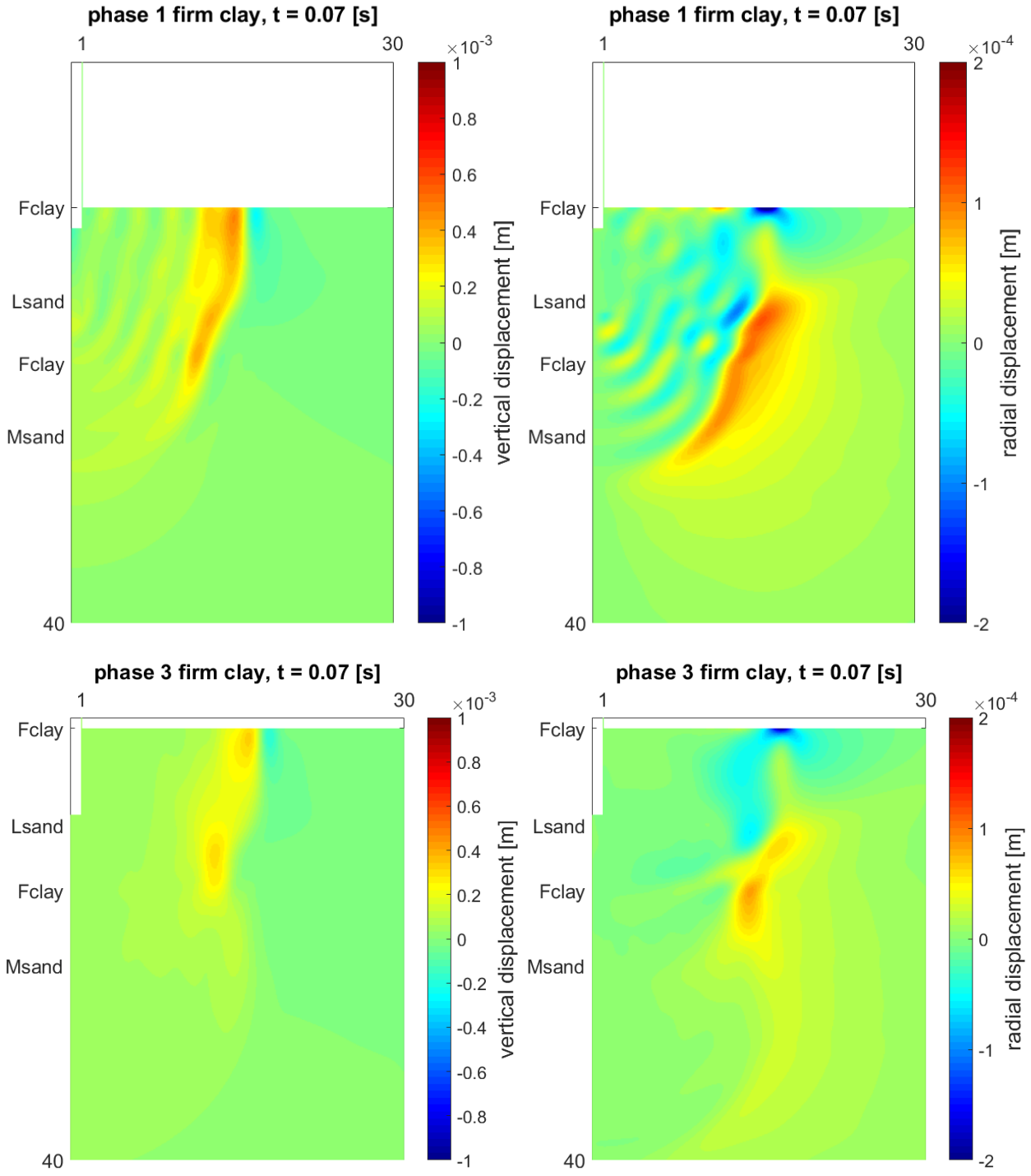

Figure 5.5: Comparison between phase 1 and 3 for loose sand confined by two firm clay layers

Figure 5.6 compares the shear stress as a function of time for the three different phases at various positions. In this case the aquifer is confined by two firm clay layers. The main wave front arrives at a certain point first in phase 3 and last in phase 1. This is because during phase 1 the wave first needs to travel the distance of the pile extended above the surface. Phase 3 is Cleary not the critical phase. Phase 1 generates most cycles, while phase 2 yields the highest average cycle amplitude. Chapter 6 will show that cycle amplitude (even if it is slightly larger), is more important for excess pore pressure generation.

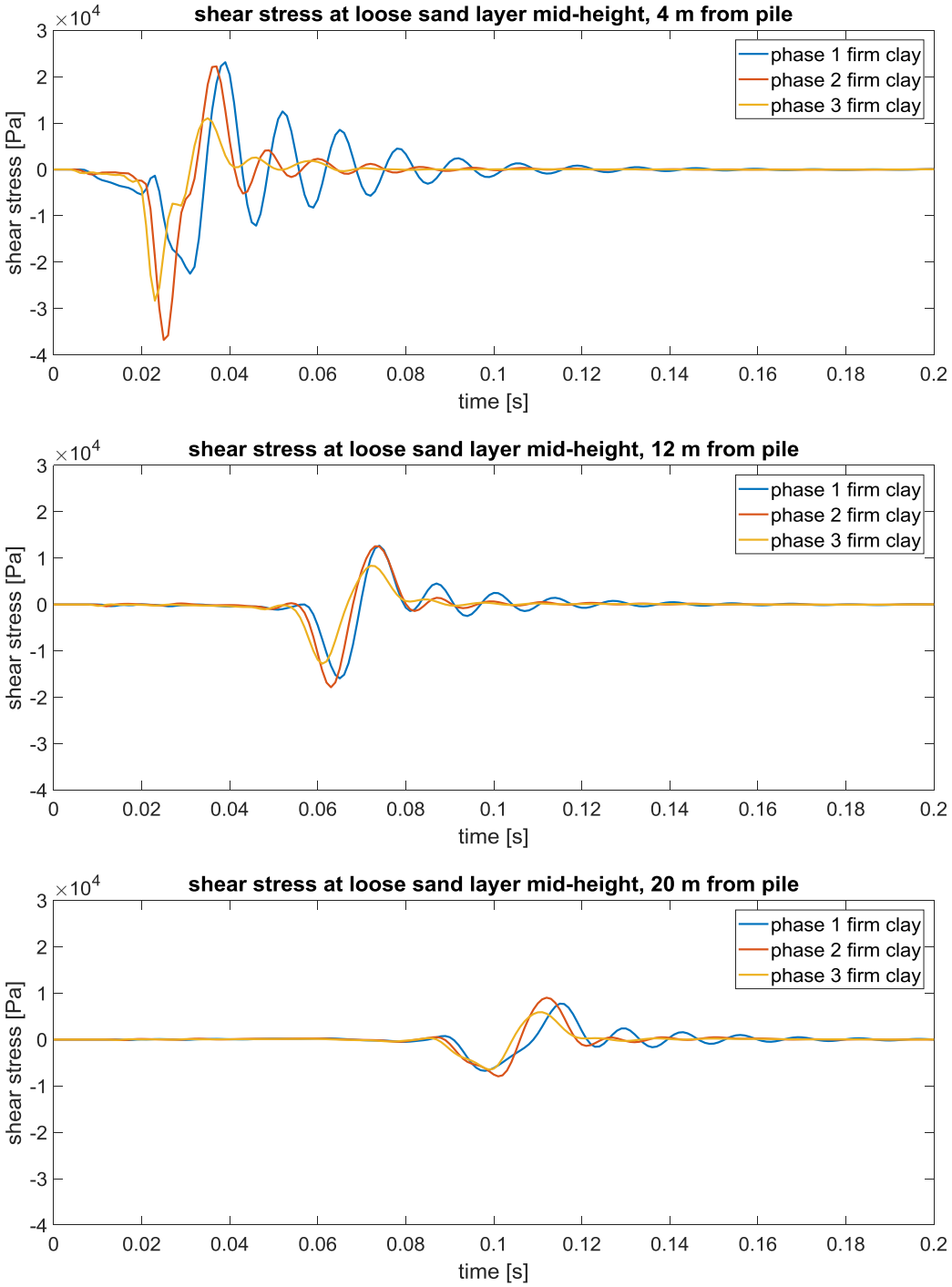

Figure 5.6: Shear stress as a function of time at various positions for the case of two firm confining clay layers

Figure 5.7 compares phase 2 with soft and firm confining clay layers. For the case of soft confining layers, the displacements are more severe because of the lower total stiffness of the system. Instead of lagging behind, the vertical shear waves in the loose sand layer are ahead in case of soft confining layers.

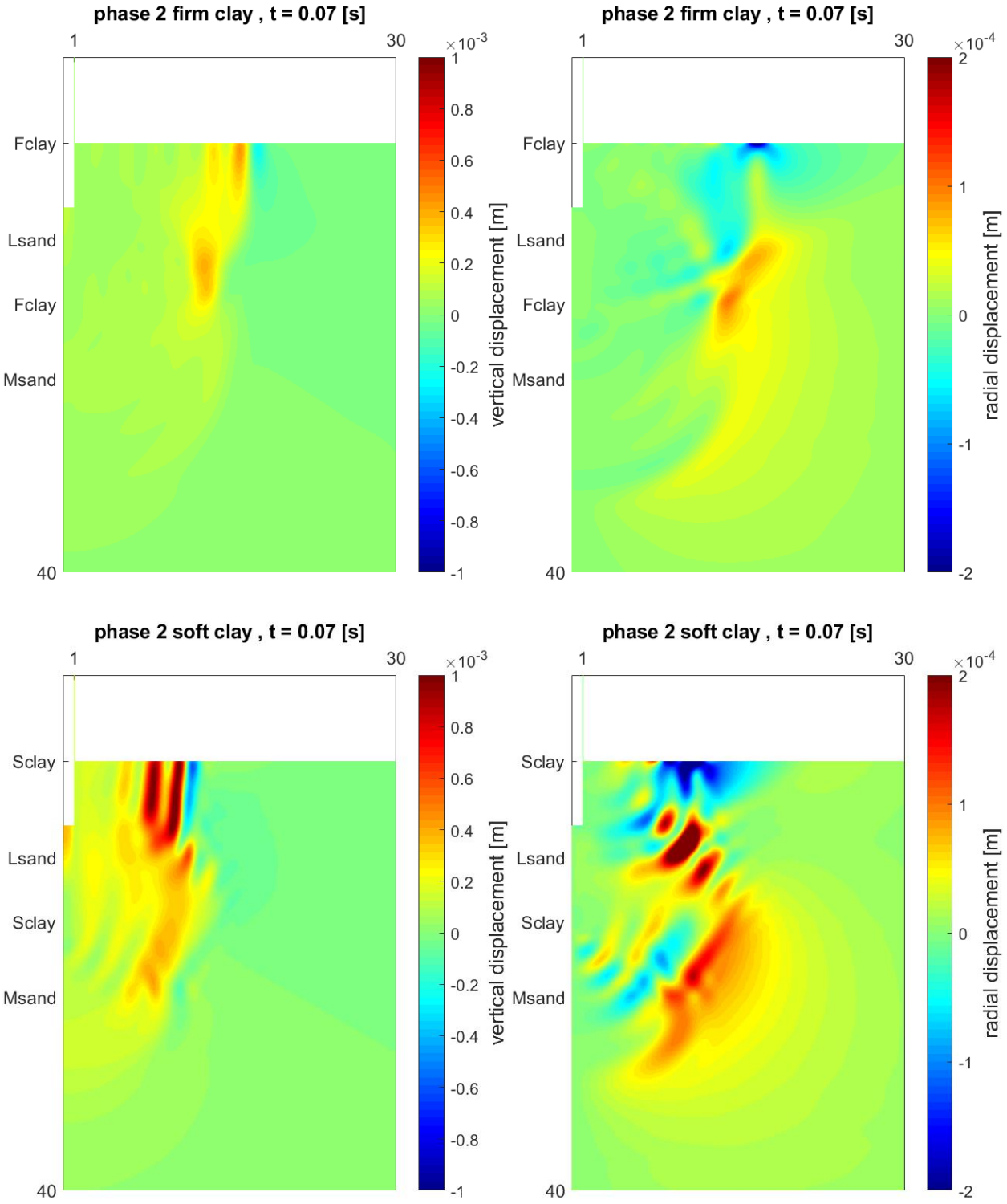

Figure 5.7: Comparison between soft and firm confining clay layers

Figure 5.8 shows the shear stresses for the three different phases at various positions for the case of soft confining layers. Compared to the case with firm confining layers, the shear stresses clearly shift toward the negative side. This is because of higher positive displacements as shown in figure 5.7. Phase 2 still has the higher average cycle amplitude and therefore it remains critical for excess pore pressure generation.

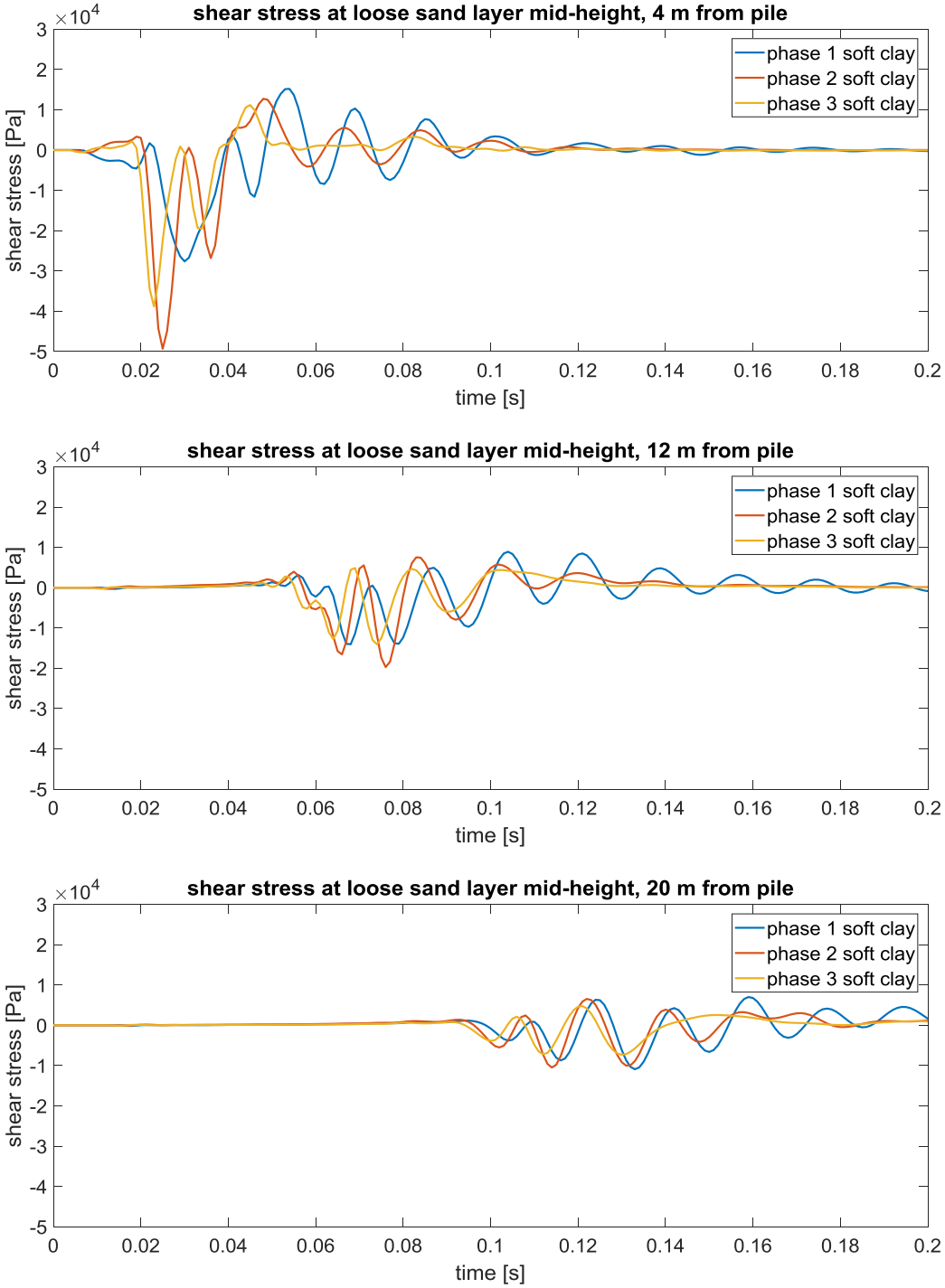

Figure 5.8: Shear stress as a function of time at various positions for the case of two soft confining clay layers

Figure 5.9 shows (for the case of firm confining layers) a comparison of shear stresses between the current model and the simplified model in the previous chapter. Two important observations can be made: the shear stress amplitudes decay much faster in the simplified model and the wave front arrives earlier. It is assumed that stronger interaction with the firm confining clay layers (higher shear wave propagation velocity) causes the wave front to arrive earlier (compared to the full equations model) at a random point in the sand layer for the simplified model.

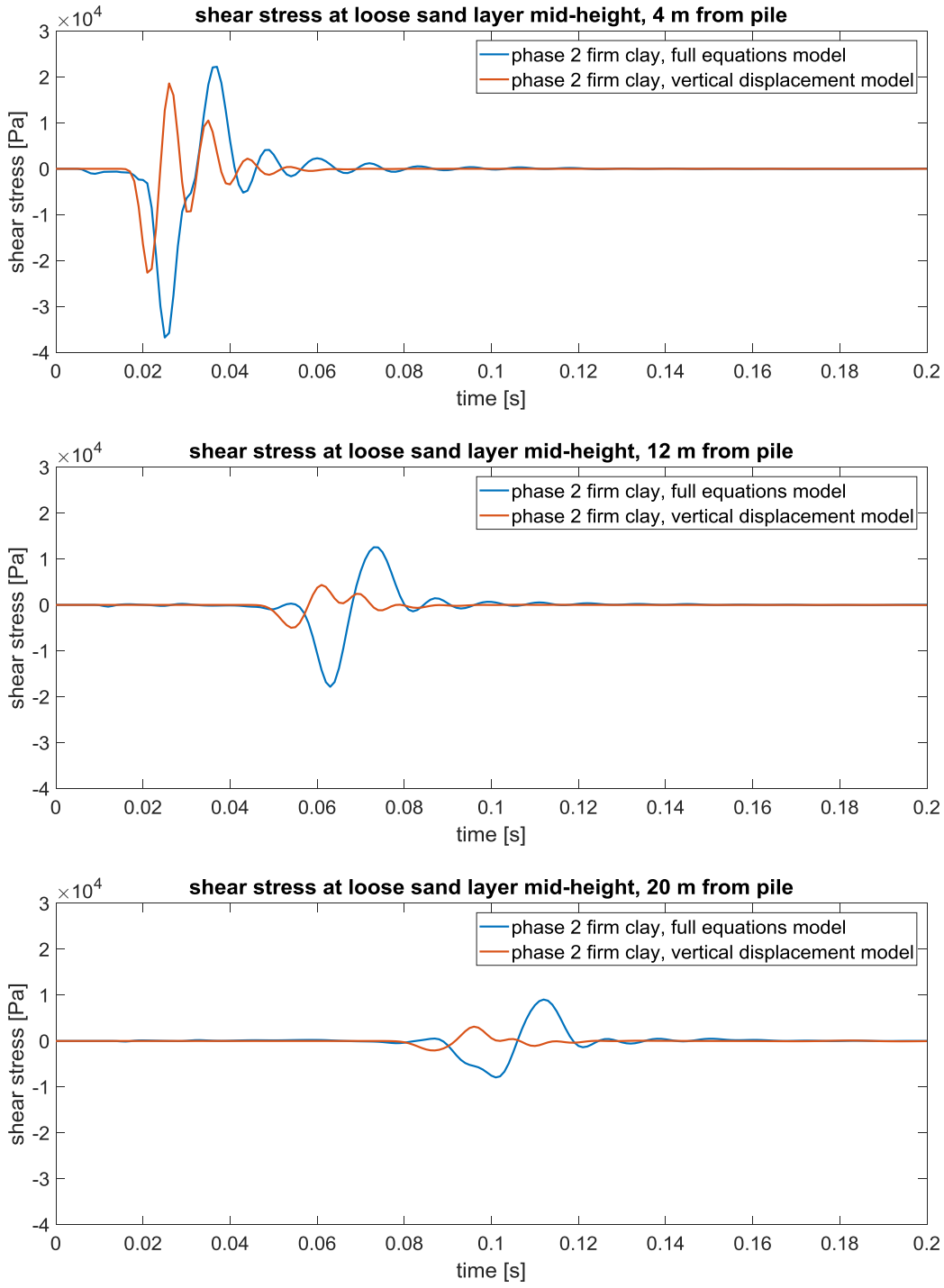

Figure 5.9: Comparison between vertical displacement model and full equations model for the case of firm confining layers

Figure 5.10 confirms the assumption made in the previous page. The figure shows the case of soft confining layers. The lower shear wave propagation velocity in the soft confining clay layers causes the wave front to arrive later (compared to the full equations model) at a random point in the sand layer for the simplified model.

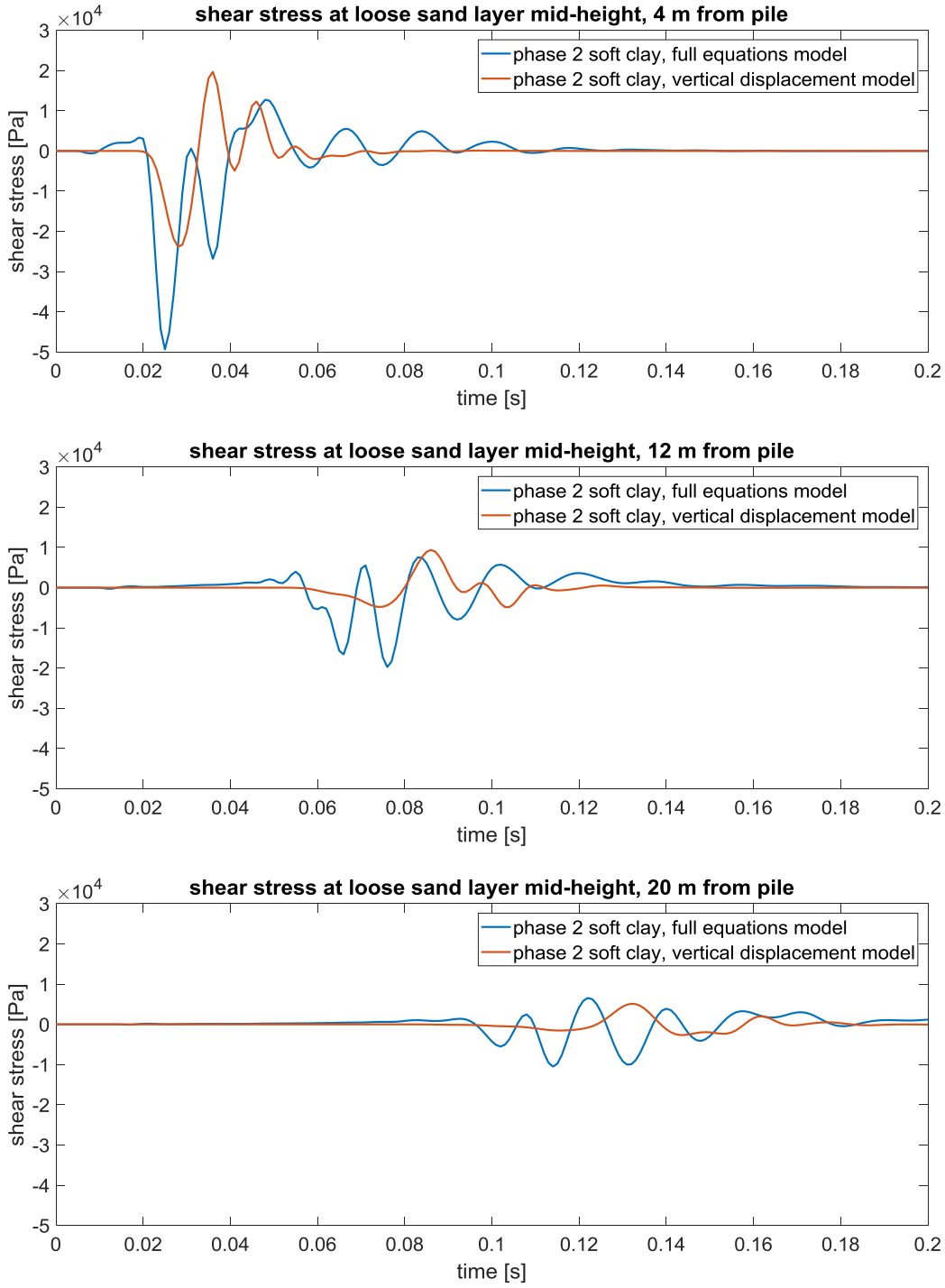

Figure 5.10: Comparison between vertical displacement model and full equations model for the case of soft confining layers

The results in figure 5.9 and 5.10 show that the simplified model in chapter 4 is fundamentally different from the full equations model presented in this chapter. The simplified model has stronger vertical interaction. This causes the shear stress amplitude to decay faster compared to the full equations model. The stiffness of the confining layers will also have a stronger influence on the arrival time of the wave front in the aquifer.

5.4 Slope modelling

The slope (figure 5.11 left) is modelled by an cylindrically symmetric model (figure 5.11 right). As was the case for the confined aquifer, the critical phase is when the pile tip is just embedded in the clay layer. The model consists of a loosely packed sand layer on top of either a soft or firm clay layer. The layering is given in table 5.2.

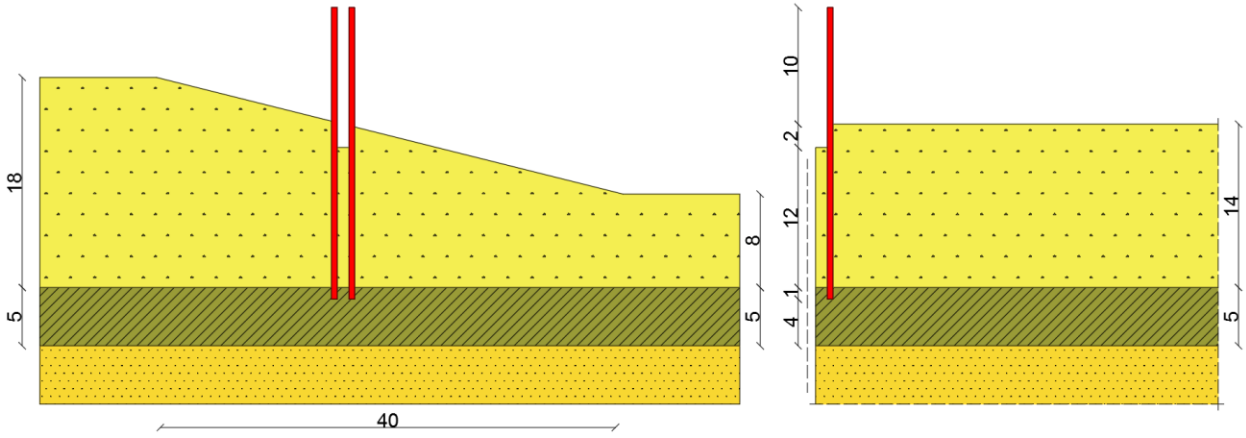

Figure 5.11: slope model

layer	start height	end height	soil type first calculation
1	0	14	loose sand
2	14	19	soft or firm clay
3	19	50	medium sand

Table 5.3: Layering of the slope model

The comparison of shear stresses for the case of a soft or firm undelying clay layer is shown in figure 5.12. The results are surprisingly similar. It appears that not the stiffness of the lower clay layer, but rather the stiffness of the upper clay layer is critical for the behaviour of the system.The slope model does not have an upper clay layer and the stiffness of the lower clay layer apperantly does not significantly influence the shear stresses in the sand layer.

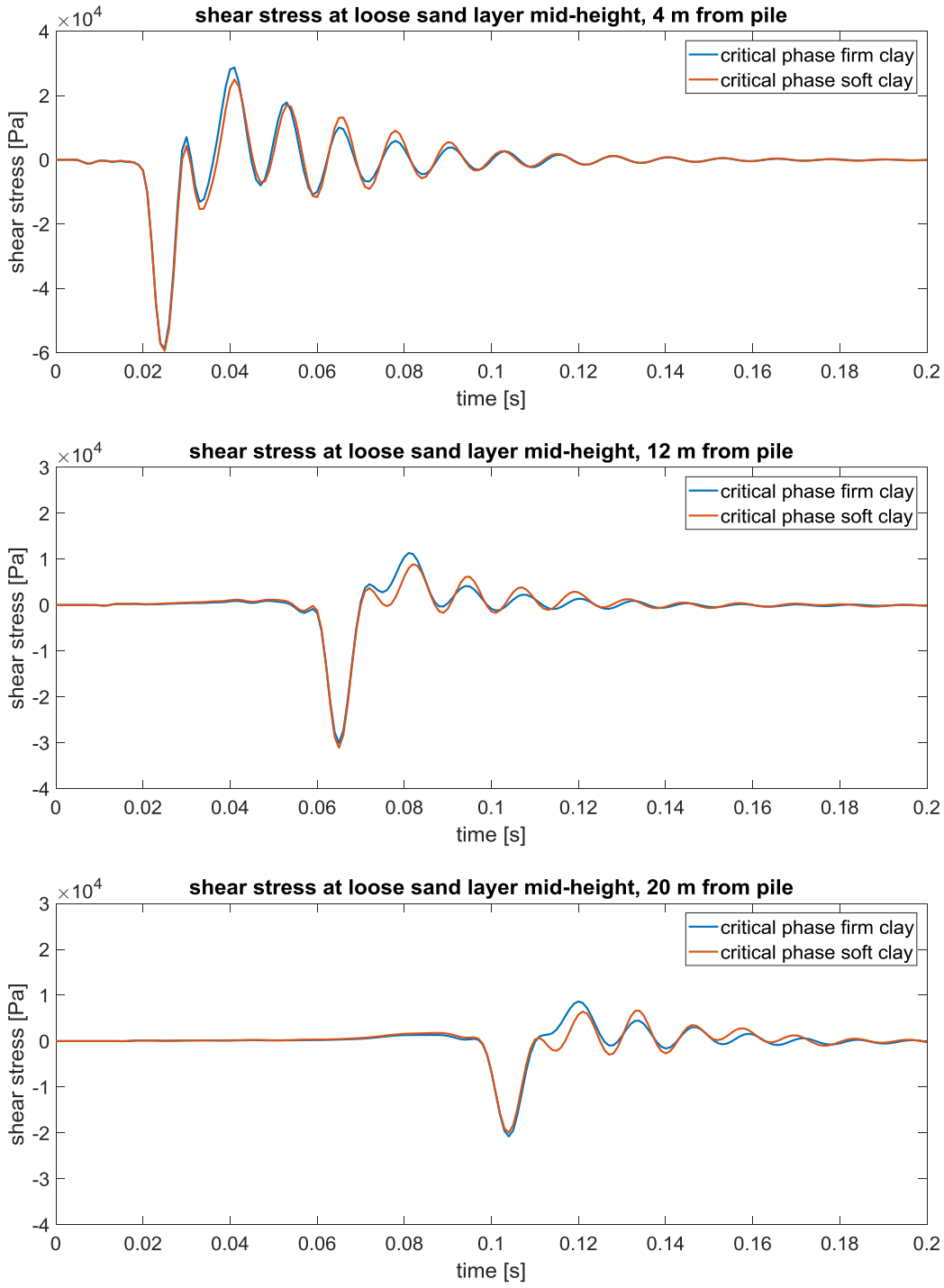

Figure 5.12: Comparison of the shear stresses for the slope model at various points in case of soft or firm clay layer underneath the sand layer

6 Liquefaction model

This chapter presents the liquefaction model and the coupling with the pile-soil-plug model. The sensitivity of the input and coupling variables will be analysed and discussed.

6.1 Model formulation

Impact pile driving is characterized by a dynamic phase following the hammer impact in which waves propagate into the soil domain. Once all energy has been transferred from the pile to the soil and the waves have propagated out of the soil domain, the consolidation phase starts. In this phase the excess pore pressures generated during the dynamic phase will dissipate. The consolidation phase lasts until the next blow occurs. This process is summarized in figure 6.1.

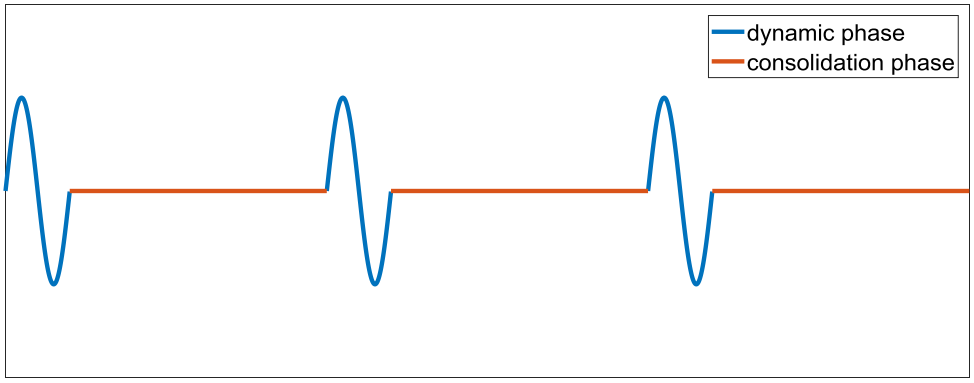

Figure 6.1: Typical shear loading for impact pile driving

The process of liquefaction can therefore be modelled by using the consolidation equation, with the addition of a excess pore pressure generation term for the dynamic phase. The cylindrically symmetric governing equation for soil consolidation reads (Verruit, 2013):

$$\frac{\partial p}{\partial t} = c_V \frac{\partial^2 p}{\partial z^2} + c_H \left(\frac{1}{r} \frac{\partial p}{\partial r} + \frac{\partial^2 p}{\partial r^2} \right) \tag{6.1}$$

p is the overpressure, c_V is the coefficient of vertical consolidation and c_H is the coefficient of horizontal consolidation. It is convenient to change p into the relative overpressure $r_u = \frac{p}{\sigma'_{v0}}$. σ'_{v0} is the initial effective stress. This gives the following set of equations:

$$\frac{\partial r_u}{\partial t} = r_{u,input}(t) + c_V \frac{\partial^2 r_u}{\partial z^2} + c_H \left(\frac{1}{r} \frac{\partial r_u}{\partial r} + \frac{\partial^2 r_u}{\partial r^2} \right) \quad @dynamic\ phase \tag{6.2}$$

$$\frac{\partial r_u}{\partial t} = c_V \frac{\partial^2 r_u}{\partial z^2} + c_H \left(\frac{1}{r} \frac{\partial r_u}{\partial r} + \frac{\partial^2 r_u}{\partial r^2} \right) \quad @consolidation\ phase \tag{6.3}$$

The input term requires an excess pore pressure generation model. An excellent overview of available models is found in the work of P. Meijers (Meijers, 2007). This overview is shown in figure 6.2. The Seed & Rahman model is the best fit for the purpose of the model presented in this chapter.

model / aspect	Barkan, standard	Barkan / Hergarden, advanced	C/L method	energy dissipation	Seed&Rahman
development in time	no	yes	yes	yes	yes
model originally for dry or saturated soil	dry	dry	dry	saturated	saturated
primary result	densification	densification	densification	excess pore pressure	excess pore pressure
driving parameter	acceleration	acceleration	shear strain	shear strain and shear stress	shear stress
preshearing accounted for?	probable implicitly	probable implicitly	probable implicitly	no	yes
loss of preshearing on liquefaction	no	no	no	no	no
stress rotation	no	no	no	no	no
threshold value for densification	yes	yes	no	no	no
upper limit densification	yes, $I_{D,final}=1$	yes	no	no	no

Figure 6.2: Overview of soil densification models (Meijers, 2007)

The Seed and Rahman model is based on experimental research studying the excess pore pressure development in sand specimen subjected to harmonic shear loading. The development curve of the relative overpressure was found to be very similar to that of an inverse sine function (figure 6.3).

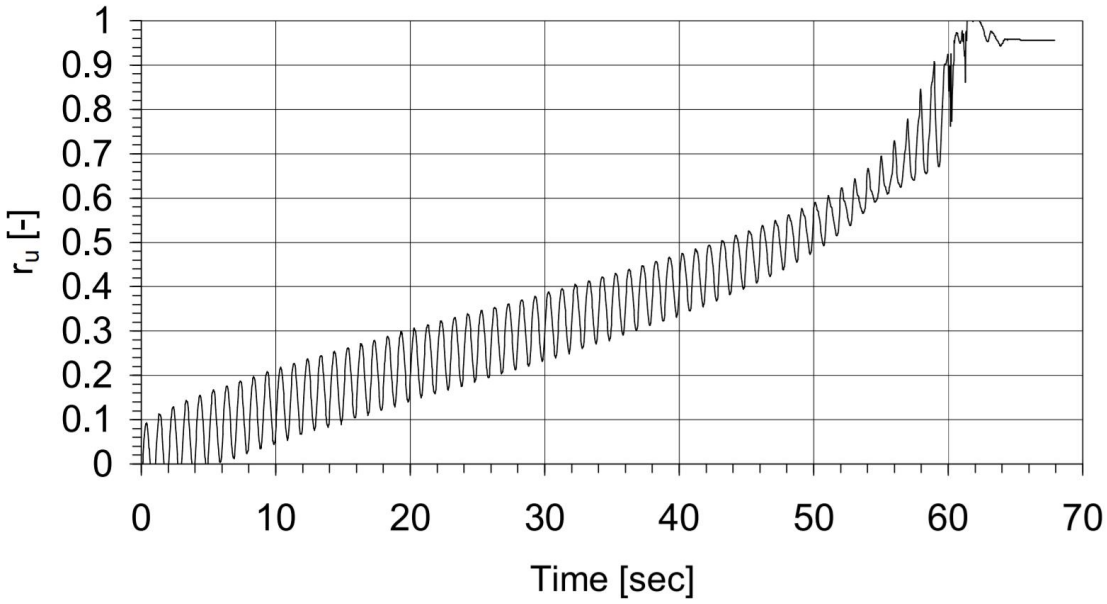

Figure 6.3: Observed development of excess pore pressures in a sand specimen subject to harmonic shear loading

According to this model, the relative overpressure is equal to:

$$r_u = \frac{2}{\pi} arcsin\left(\frac{N}{N_{liq}}\right)^{\frac{1}{2\theta}} \tag{6.4}$$

With:

$$N_{liq} = \left(\frac{a\sigma'_{v0} I_D}{\Delta\tau}\right)^b \tag{6.5}$$

N is the current amount of cycles, N_{liq} is the amount of cycles required to reach liquefaction. N_{liq} depends on the initial effective stress σ'_{v0}, the initial relative density of the sand I_D and the shear stress amplitude $\Delta\tau$. Commonly mentioned values in literature for the empirical constants θ, a and b are (Meijers, 2007):

$$a = 0.48 \tag{6.6}$$

$$b = 5 \tag{6.7}$$

$$\theta = 0.7 \tag{6.8}$$

The inverse sine function is plotted for theta equal to 0.7 (figure 6.4). The figure shows that the arcsin function can be approximated by a linear function $y = 0.8x$. The advantage of the linear function is that the relative overpressure can reach unity, while this is not the case for the arcsin function (the limit of this function is a relative overpressure of 0.88). The linear function can also be used to estimate the post liquefaction behavior. The adapted function used in this chapter is:

$$r_u = \frac{0.8 * 2}{\pi} \frac{N}{N_{liq}} = \frac{1.6}{\pi} \frac{N}{N_{liq}} \tag{6.9}$$

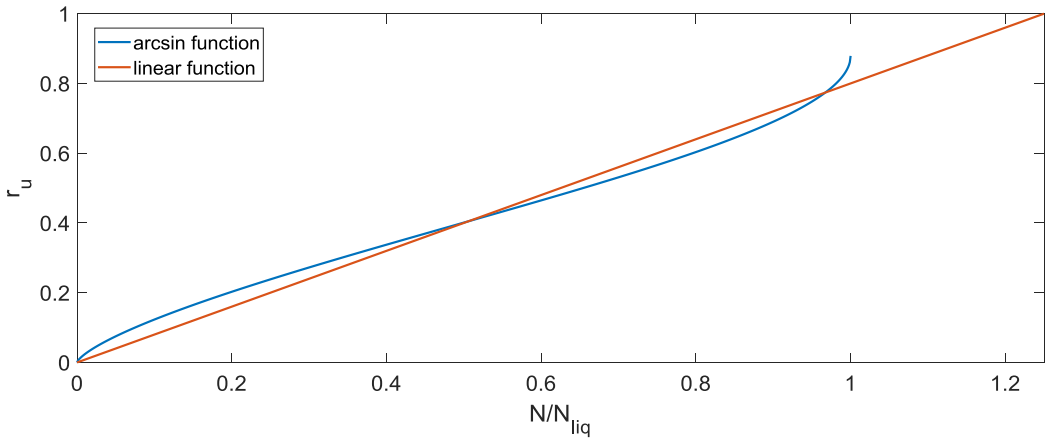

Figure 6.4: Comparison arcsin and linear function

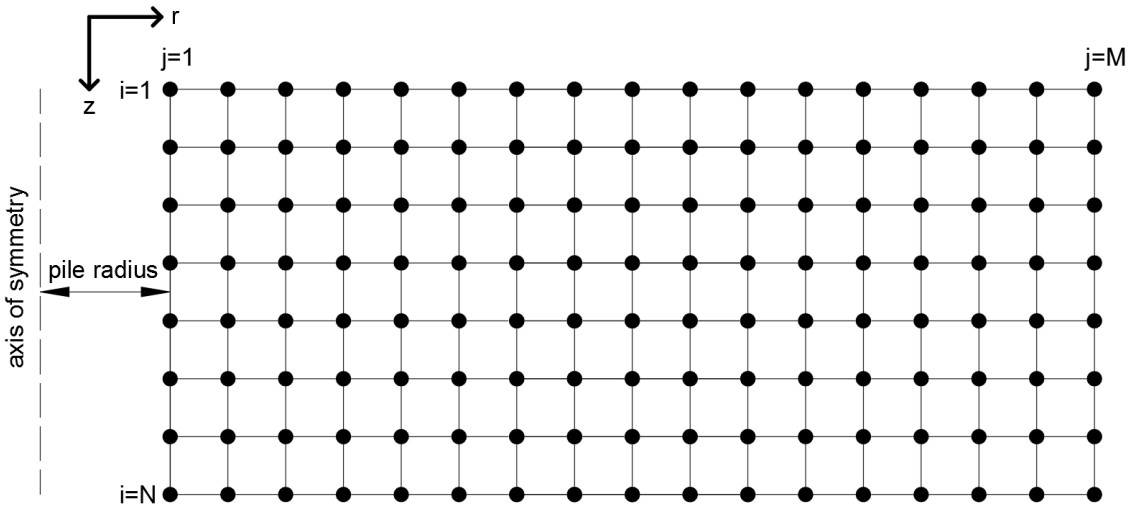

Figure 6.5: Liquefaction model

The increment of the relative overpressure at node (i,j) (figure 6.5) for one single blow exciting N^n cycles is now described by the following equations:

$$\Delta r_u^{i,j,n} = \frac{1.6N^n}{\pi N_{liq}^{i,j,n}} \tag{6.10}$$

$$N_{liq}^{i,j,n} = \left(\frac{a\sigma_{v0}'^{\,i} I_D}{\Delta\tau_{cycle}^{i,j,n}}\right)^b \tag{6.11}$$

i is the node position in vertical direction, j the node position in radial direction and n the blow count. The elastic model presented in chapter 5 and the liquefaction model are coupled in two steps. The first step is to represent the shear stresses obtained from the elastic model at each node by an equivalent cycle. Because $b = 5$, the relation between r_u and the shear cycle amplitude is power 5. A small drop in cycle amplitude is equal to a steep drop in generated r_u.Therefore, to increase the speed of the calculation, the primary shear cycle amplitude is taken as the average of the maximum and absolute value of the minimum shear stress at a certain node. All secondary cycles are described by an primary cycle equivalence factor, depending on the severity of the secondary cycles. Figure 6.6 shows two examples of shear loading patters. Pattern one has weak secondary cycles, while pattern two has severe secondary cycles. Table 6.1 shows that the generated relative overpressures drop quickly with decrease in cycle amplitude. Calculations show that the primary cycle equivalence factor is 1.1 for pattern 1 and 1.6 for pattern 2 (figure 6.7). Therefore:

$$c_1 = 1.1 \; up \; to \; 1.6 \tag{6.12}$$

$$\Delta r_u^{i,j,n} = \frac{1.6c_1N^n}{\pi N_{liq}^{i,j,n}} \tag{6.13}$$

N^n now only represents primary shear loading cycles.

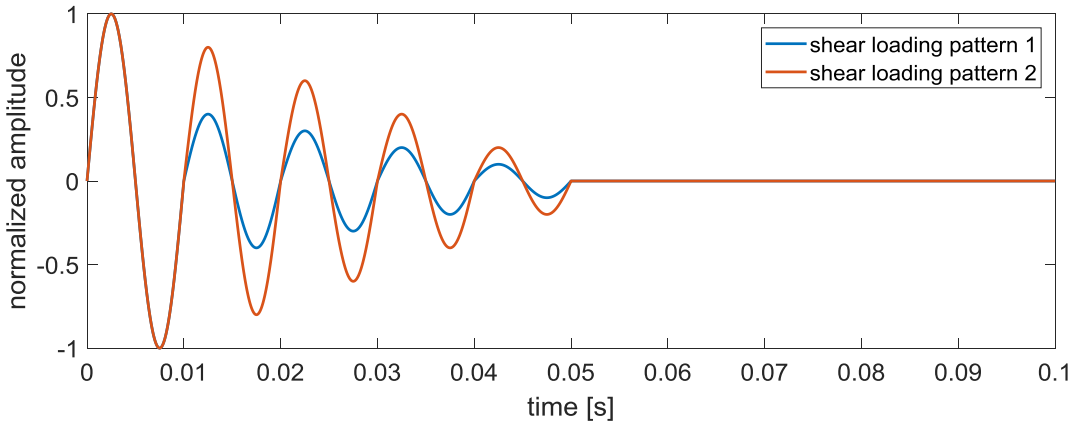

Figure 6.6: Two example shear loading patterns

cycle	cycle amplitude as percentage of the primary cycle amplitude pattern 1-2	overpressure generated by cycle as percentage of overpressure generated by primary cycle pattern 1-2
1	100-100	100-100
2	40-80	2-29
3	30-60	1-9
4	20-40	0-2
5	10-20	0-0
Equivalent cycle with an amplitude of the primary cycle has a duration of between 1.1-1.6 times the duration of the primary cycle		

Table 6.1: Cycle equivalence comparison

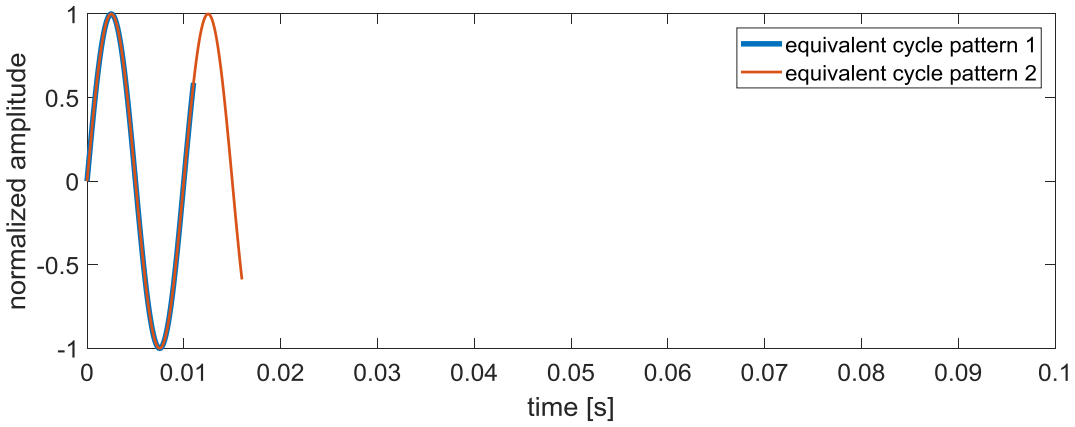

Figure 6.7: Equivalent cycles for the two shear loading patterns

The primary shear cycle amplitude is calculated for all nodes. Subsequently, the ratio is calculated between the primary shear cycle amplitude of a random node and the primary shear cycle amplitude at the interface with the same vertical height (figure 6.8). The ratio at each node is the primary output of the elastic model in chapter 5.

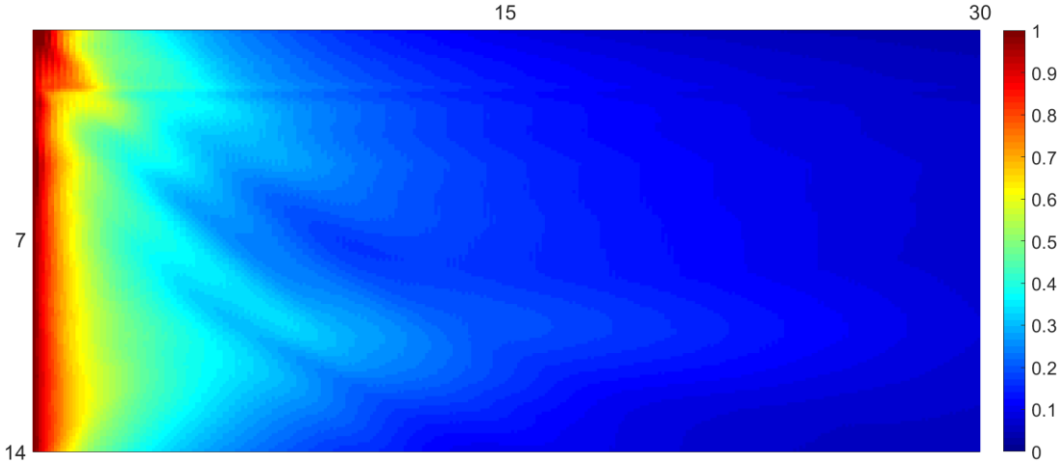

Figure 6.8: Ratio between primary shear cycle amplitude at random point and the primary shear cycle amplitude at interface with same vertical height

Realistic shear stresses are obtained by multiplying the ratios obtained from the elastic model by the yield shear stress at the interface:

$$\tau_{yield}^{i,1,n} = \left(\beta + \left(1 - r_u^{i,1,n}\right)(\alpha - \beta)\right) {\sigma'_{v0}}^{i} \tag{6.14}$$

$$\alpha = K_0 tan\delta = (1 - sin\varphi)\tan\left(\frac{2}{3}\varphi\right) \tag{6.15}$$

α is the ratio between yield shear stress and initial effective stress for zero relative overpressure. It can be approximated from the angle of internal friction φ. For example $\varphi = 30°$ gives $\alpha = 0.18$. β is the ratio between yield shear stress and initial effective stress for unity relative overpressure. Meijers (2007) recommends $\beta = 0.1$, though this may be considered a conservative value. The shear cycle at each node is now obtained by multiplying the ratio obtained from the elastic model with the yield shear stress:

$$\Delta\tau_{cycle}^{i,j,n} = \tau_{yield}^{i,1,n}\frac{\Delta\tau_{cycle,elastic}^{i,j}}{\Delta\tau_{cycle,elastic}^{i,1}} = \left(\beta + \left(1 - r_u^{i,1,n}\right)(\alpha - \beta)\right) {\sigma'_{v0}}^{i}\frac{\Delta\tau_{cycle,elastic}^{i,j}}{\Delta\tau_{cycle,elastic}^{i,1}} \tag{6.16}$$

From the previous chapters, it is well known that vertical shear waves are the main transfer mechanism of energy from the pile into the soil. The shear stresses at the interface obtained from the elastic model are too high because slip is neglected (the pile and soil are assumed to be rigidly connected). The previous equation solves this by correcting for yield shear stress $\left(cor = \frac{\left(\beta+\left(1-r_u^{i,1,n}\right)(\alpha-\beta)\right){\sigma'_{v0}}^{i}}{\Delta\tau_{cycle,elastic}^{i,1}}\right)$. This however implies that the resistance added to the pile in the elastic model is also too high. The previous chapters show that smaller resistance results in more cycles. A conservative approach is to assume that the cycles increase proportionally with the decrease in resistance at the interface:

$$increase\ in\ cycles = mean\left(\frac{\Delta\tau_{cycle,elastic}^{i,1}}{\left(\beta + \left(1 - r_u^{i,1,n}\right)(\alpha - \beta)\right)\sigma_{v0}'^{\,i}}\right) \tag{6.17}$$

The mean of the correction is taken, because $\sigma_{v0}'^{\,i,1}$ strongly varies with vertical position. This would result in strong variation of cycle increase, which is not realistic. Assuming that the cycles increase proportionally with the decrease in resistance at the interface is conservative, because increase in friction and toe resistance will take over some of the energy originally transferred by vertical shear waves, therefore a control parameter γ is added:

$$N^n = 1 + \left(\gamma * \left(mean\left(\frac{\Delta\tau_{cycle,elastic}^{i,1}}{\left(\beta + \left(1 - r_u^{i,1,n}\right)(\alpha - \beta)\right)\sigma_{v0}'^{\,i}}\right) - 1\right)\right) \tag{6.18}$$

γ ratio between the increase in amount of shear cycles and the decrease of resistance at the pile-soil interface. Two extreme cases of γ can be distinguished:

- The energy that cannot be carried anymore by a single vertical shear wave cycle is fully taken over by increased friction and toe resistance, $\gamma = 0$.
- There will not be any increase in friction and toe resistance. The energy that cannot be carried anymore by a single vertical shear wave cycle is still transferred by vertical shear waves, but by an increased amount of cycles, $\gamma = 1$.

Practical values of γ will be in-between 0 and 1. N^n now represents the total amount of primary cycles for each blow.

The final form of the excess pore pressure generation model is obtained by substituting the expressions for $\Delta\tau_{cycle}^{i,j,n}$ (equation 6.16) and N^n (equation 6.18) into equations 6.11 and 6.13:

$$\Delta r_u^{i,j,n} = \frac{1.6c_1}{\pi N_{liq}^{i,j,n}} * \left(1 + \left(\gamma * \left(mean\left(\frac{\Delta\tau_{cycle,elastic}^{i,1}}{\left(\beta + \left(1 - r_u^{i,1,n}\right)(\alpha - \beta)\right)\sigma_{v0}'^{\,i}}\right) - 1\right)\right)\right) \tag{6.19}$$

$$N_{liq}^{i,j,n} = \left(\frac{aI_D\Delta\tau_{cycle,elastic}^{i,1}}{\left(\beta + \left(1 - r_u^{i,1,n}\right)(\alpha - \beta)\right)\Delta\tau_{cycle,elastic}^{i,j}}\right)^b \tag{6.20}$$

The governing equation for the dynamic phase is therefore:

$$\frac{\partial r_u^{i,j,n}}{\partial t} = \frac{1.6c_1}{\pi T_{dyn}} * \frac{\left(1+\left(\gamma * \left(mean\left(\frac{\Delta\tau_{cycle,elastic}^{i,1}}{\left(\beta+\left(1-r_u^{i,1,n}\right)(\alpha-\beta)\right)\sigma_{v0}'^{\,i}}\right)-1\right)\right)\right)}{\left(\frac{aI_D\Delta\tau_{cycle,elastic}^{i,1}}{\left(\beta+\left(1-r_u^{i,1,n}\right)(\alpha-\beta)\right)\Delta\tau_{cycle,elastic}^{i,j}}\right)^b} + c_v\frac{\partial^2 r_u^{i,j,n}}{\partial z^2} + c_H\left(\frac{1}{r}\frac{\partial r_u^{i,j,n}}{\partial r} + \frac{\partial^2 r_u^{i,j,n}}{\partial r^2}\right) \tag{6.21}$$

T_{dyn} is the duration of the dynamic phase. The governing equation for the consolidation phase reads:

$$\frac{\partial r_u^{i,j,n}}{\partial t} = c_V\frac{\partial^2 r_u^{i,j,n}}{\partial z^2} + c_H\left(\frac{1}{r}\frac{\partial r_u^{i,j,n}}{\partial r} + \frac{\partial^2 r_u^{i,j,n}}{\partial r^2}\right) \tag{6.22}$$

Figure 6.9 gives the model scheme of the liquefaction model and shows the coupling with the elastic model.

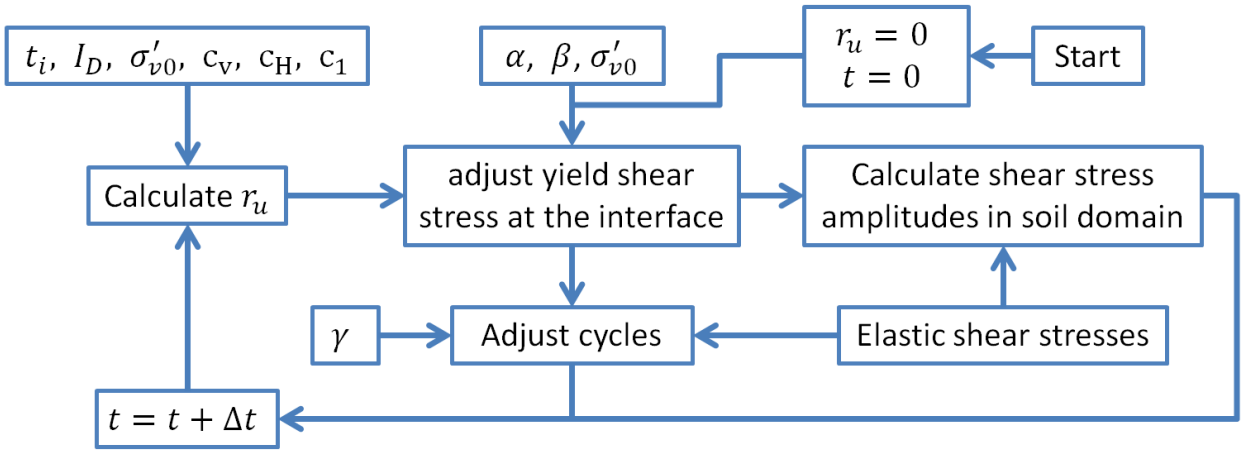

Figure 6.9: liquefaction model scheme

6.2 Slope liquefaction modelling

The liquefaction model only considers the upper loosely packed sand layer, with the boundary conditions shown in figure 6.10. Default input parameters can be found in input table 1.5. Based on the results in section 5.4, a cycle equivalence factor $c_1 = 1.4$ is chosen (medium severity secondary cycles).

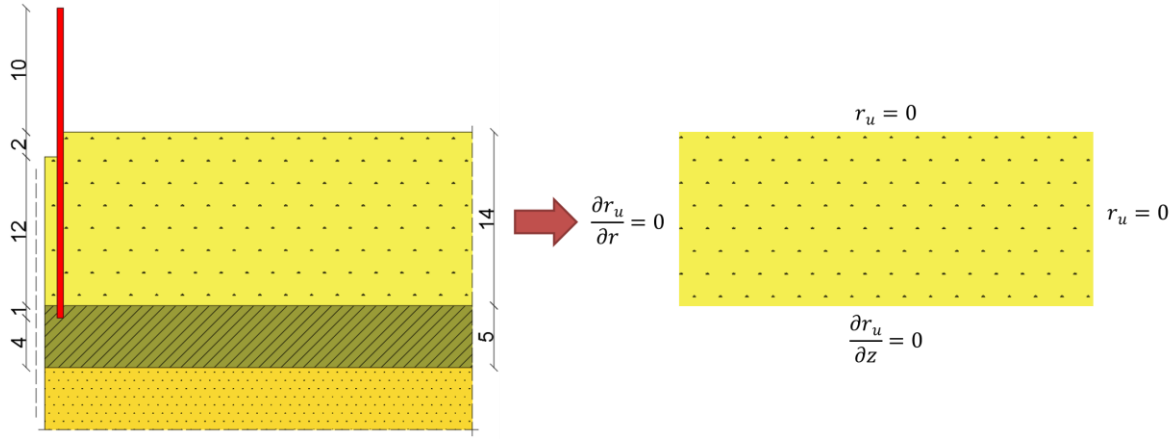

Figure 6.10: Slope liquefaction modelling

Figure 6.11 shows the steady state relative overpressure in the case the post liquefaction behaviour is neglected (relative overpressure cannot exceed unity). Figure 6.12 shows the case of approximating the post liquefaction behaviour by the linear function and figure 6.13 shows the development of the layer averaged relative overpressure as a function of time for both cases. Figure 6.13 indicates that the relative overpressures in the sand layer reach a steady state at around 2000 seconds for both cases. The layer averaged steady state relative overpressure is slightly higher for the case of neglecting post liquefaction behaviour. This is also clear from comparing figures 6.11 and 6.12: in figure 6.11 high relative overpressures seem to extend slightly further from the pile. Neglecting post liquefaction behaviour yields a conservative (on the safe side) solution, and is therefore used as default setting for further analysis.

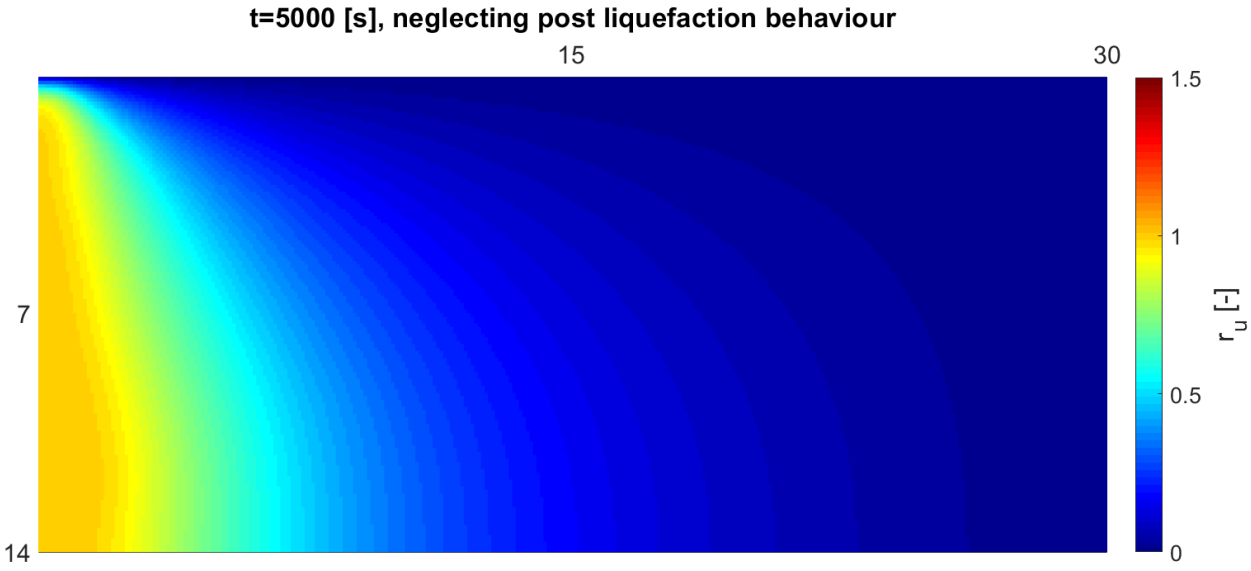

Figure 6.11: Steady state relative overpressure for default control parameters and neglecting post liquefaction behaviour

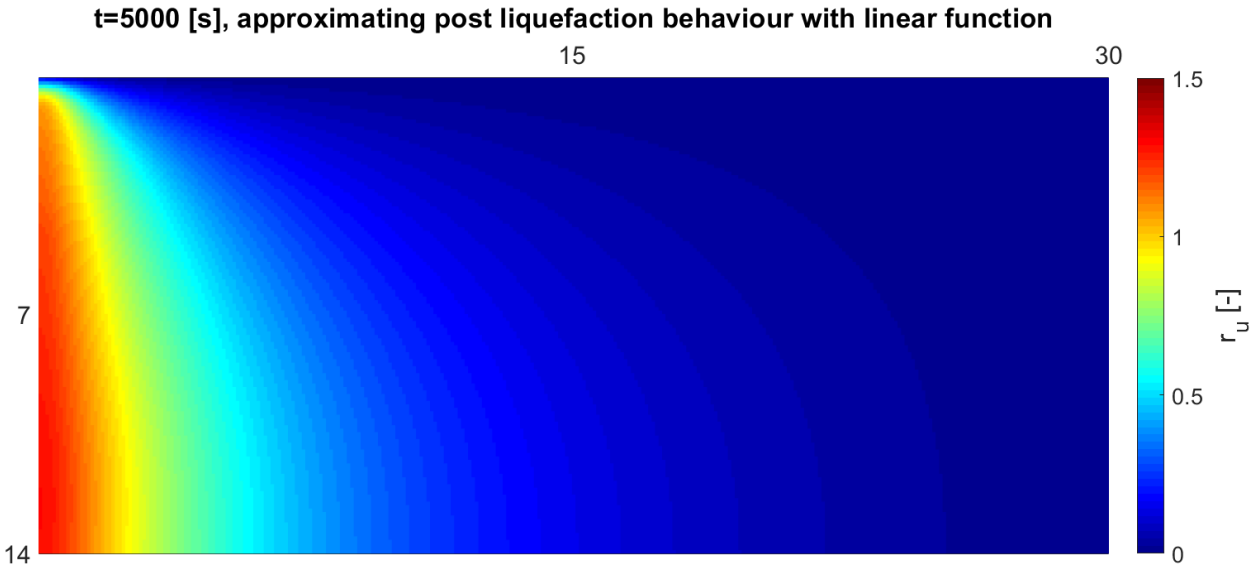

Figure 6.12: Steady state relative overpressure for default control parameters and approximating post liquefaction behaviour with a linear function

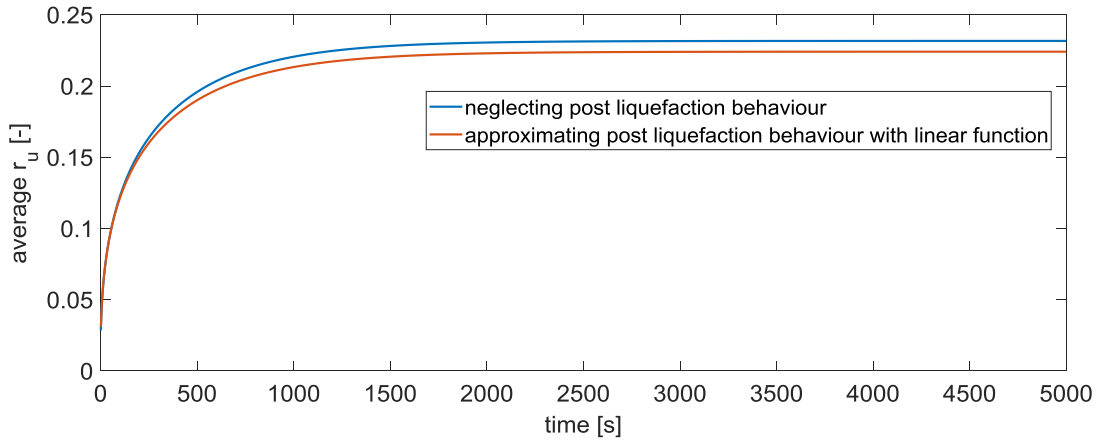

Figure 6.13: Comparison of the layer averaged relative overpressure development as a function of time for the two mentioned cases

Figures 6.14 and 6.15 show the sensitivity of β and γ. 0.01 and 0.16 can be considered theoretical limits of β. This is because the main transfer mechanism of shear stress in a viscous fluid is assumed to be locking between the soil particles. In case of smooth particles with poor sorting, β will approach zero. In case of angular particles with good sorting, β will approach α. Practical values of β and γ will be between the theoretical limits. In this range, β is significantly more sensitive compared to γ. The biggest uncertainty in the model is therefore β. Experimental validation of β is recommended to reduce this uncertainty.

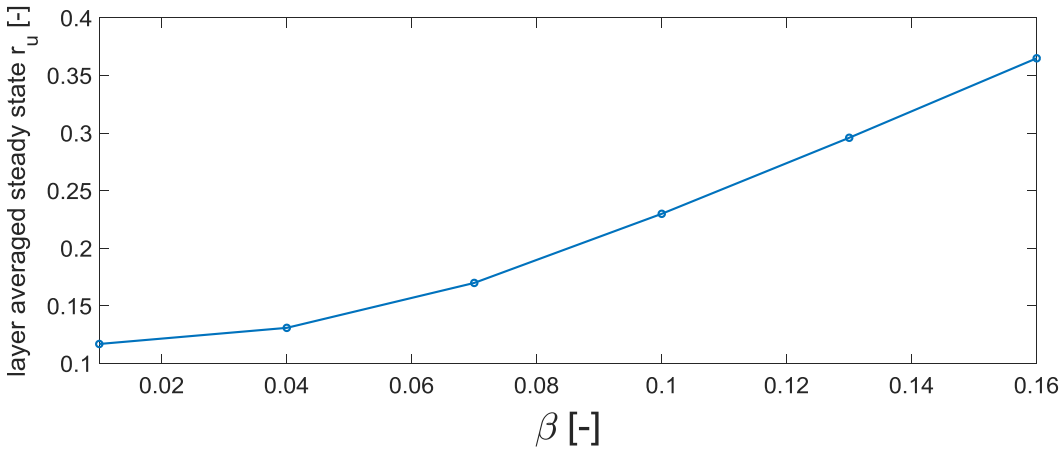

Figure 6.14: Sensitivity of β

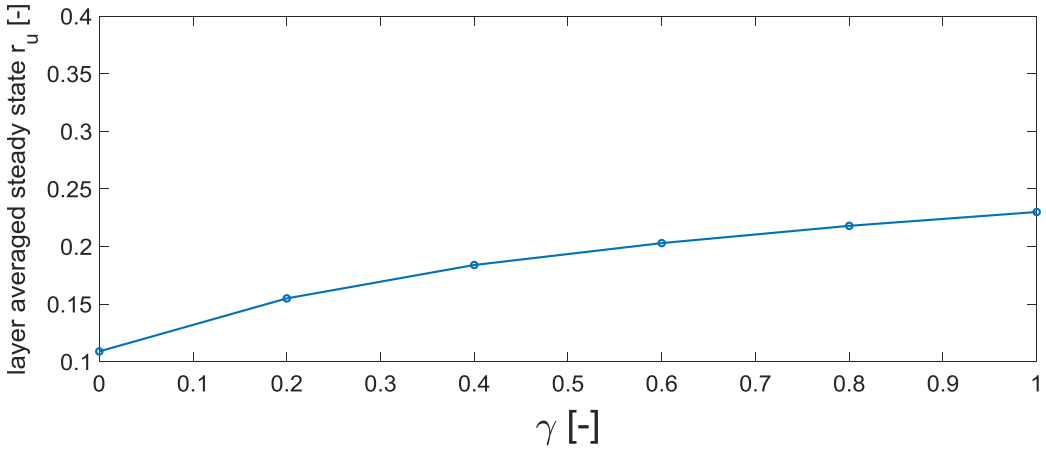

Figure 6.15: Sensitivity of γ

Figures 6.16, 6.17 and 6.18 show the sensitivity of the input variables: the time interval between each blow, the consolidation coefficient and the initial relative density. The initial relative density is clearly the most sensitive variable. This variable describes the initial packing of the sand and is therefore a strong measure for liquefaction potential. The time interval between each blow is the least sensitive variable. This is the only variable that can be altered during design.

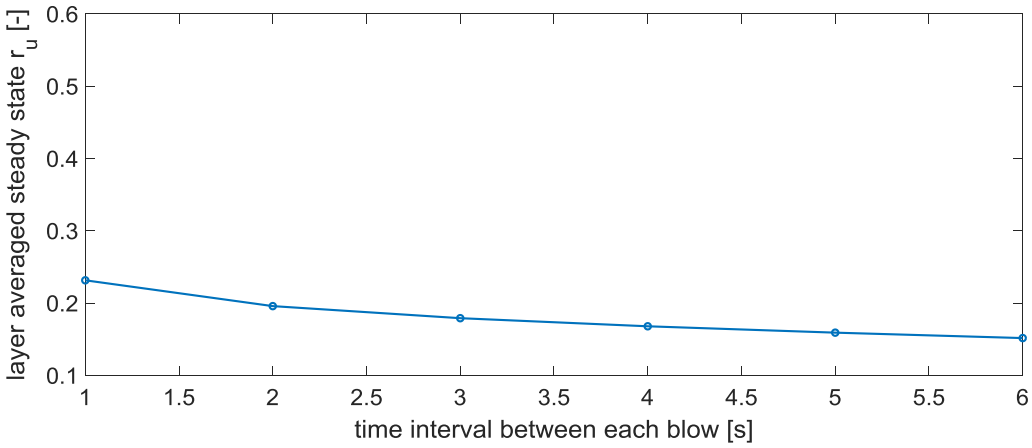

Figure 6.16: Sensitivity of the time interval between each blow

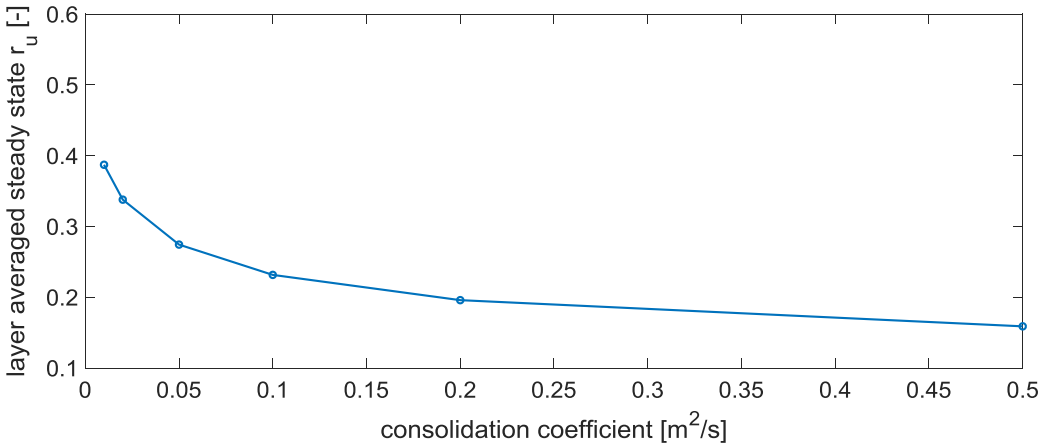

Figure 6.17: Sensitivity of the consolidation coefficient

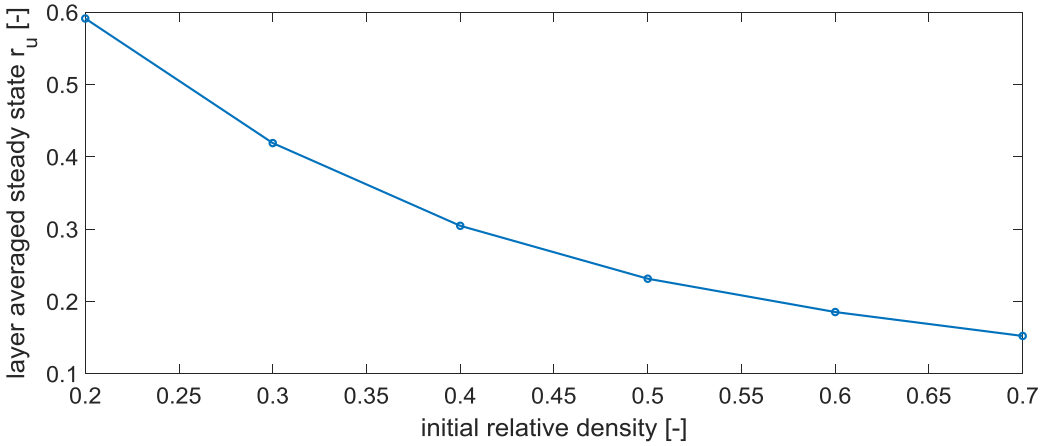

Figure 6.18: Sensitivity of the initial relative density

6.3 Confined aquifer liquefaction modelling

For the case of the confined aquifer, only the aquifer is considered for the liquefaction model. The boundary conditions are shown in figure 6.20. The default input variables can be found in input table 1.5. Elastic shear stresses derived from the case of two firm confining layers turn out to give the most severe results. Based on the results in section 5.3 for this case, a cycle equivalence factor $c_1 = 1.2$ is chosen (limited severity of the secondary cycles).

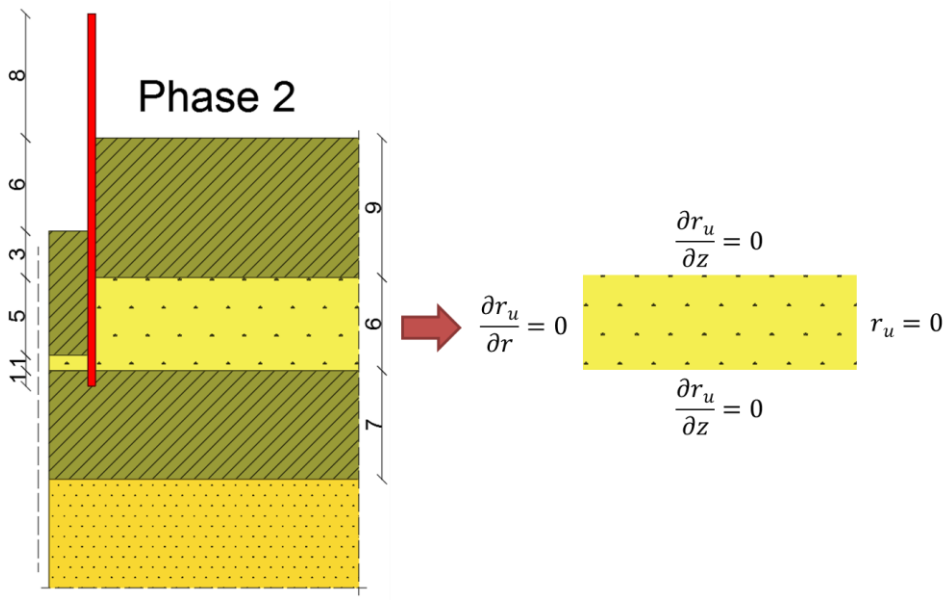

Figure 6.19: Confined aquifer liquefaction model

Figures 6.20, 6.21 and 6.22 show the steady state relative overpressure for the case of default values, $\beta = 0.05$ and $\gamma = 0.5$. The results are very similar to the confined aquifer model: β shows a higher sensitivity compared to γ. The biggest difference can be found in figure 6.23, which shows the layer averaged relative overpressure development in time for the three different cases. The aquifer only has one outflow boundary (compared to two for the slope model). Steady state is reached after 5000 seconds (compared to 2000 seconds for the slope model). Because of weaker drainage capacity, the steady state layer averaged relative overpressures are significantly higher compared to those shown in figure 6.13 for the slope model.

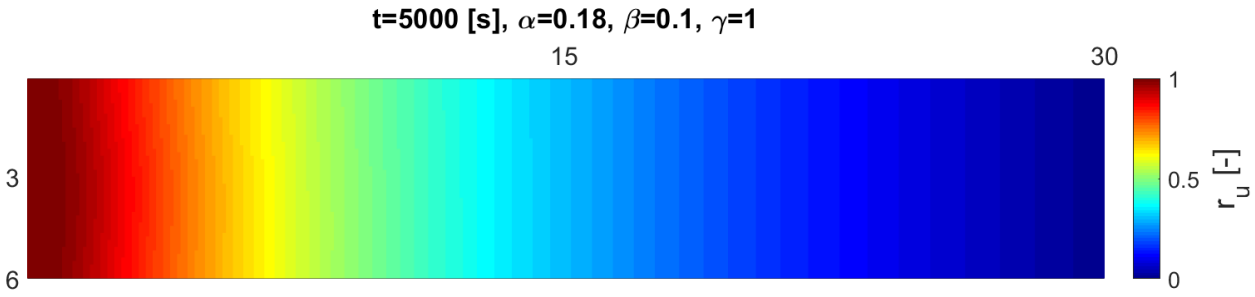

Figure 6.20: Steady state relative overpressure for default values

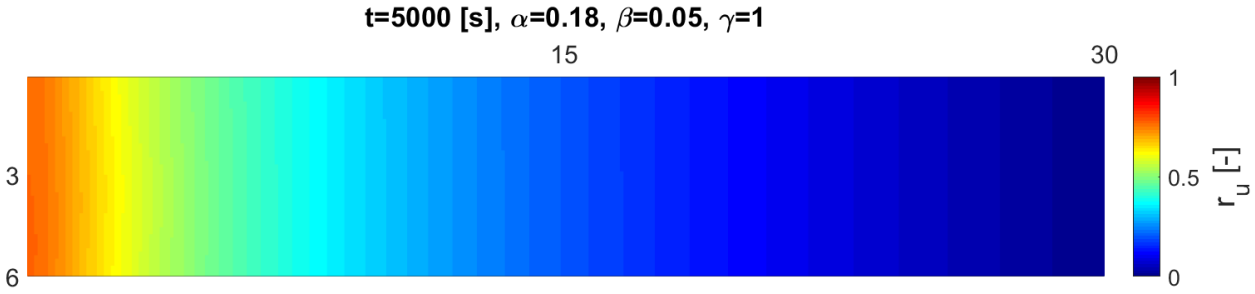

Figure 6.21: Steady state relative overpressure for beta = 0.05

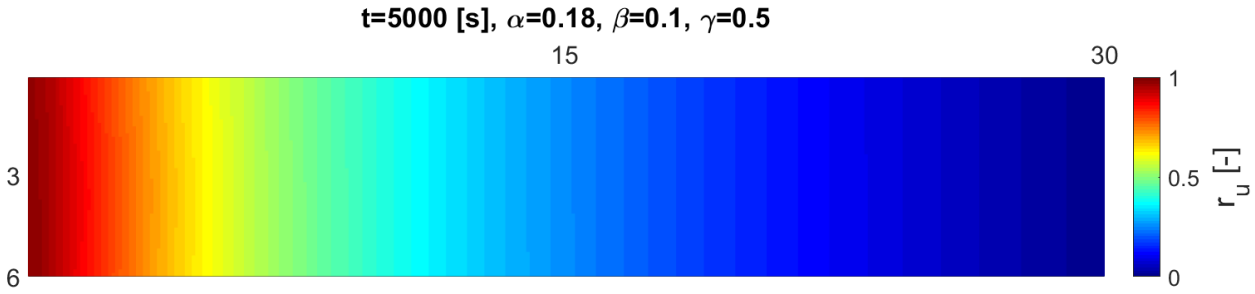

Figure 6.22: Steady state relative overpressure for gamma = 0.5

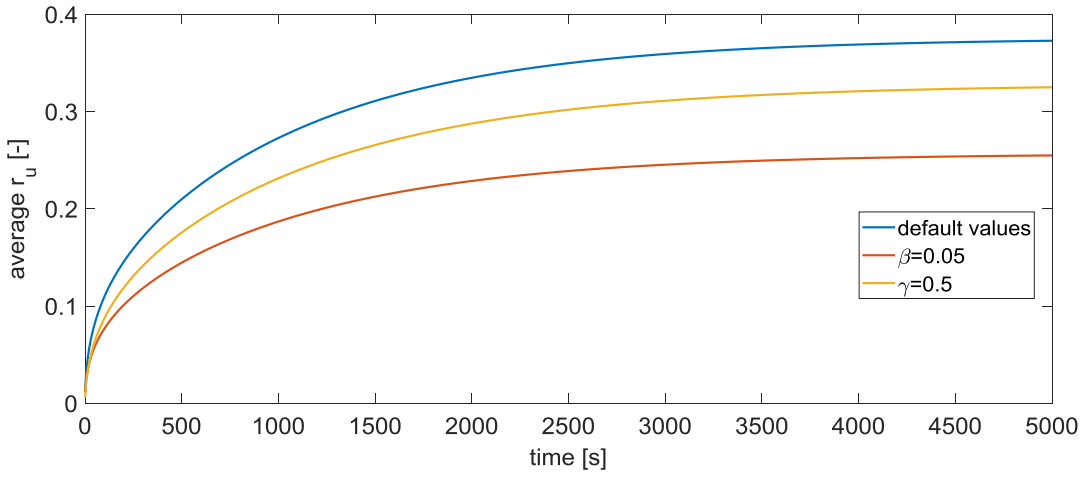

Figure 6.23: Comparison of the layer averaged relative overpressure development as a function of time for the three mentioned cases

7 Conclusion and recommendations

7.1 Conclusions

Some interesting conclusions can be drawn from each chapter. The Smith pile driving model, presented in chapter 3, is the basis of many modern pile driving software packages. This model is not suitable for describing wave propagation in the soil domain, since the soil is represented by rheological models. The model reveals some interesting aspects of pile driving, for example the linear relation between pile set and toe resistance and the quadratic relation between pile set and shaft resistance. Excess pore pressure accumulation at the interface reduces the shaft resistance and is therefore essential in achieving pile set.

Two existing simplified pile-soil models are presented in chapter 3. The van den Berghe and Holeyman model simplifies the pile to a rigid mass and the soil to concentric rigid cylinders. The Salgado et all. Model adds vertical discretization, simplifying the soil to thin ring slices without vertical interaction. Results show that these models achieve good results for homogenous soil. The models are inadequate for modelling layered soil.

Chapter 4 and 5 try to overcome the disadvantages of the existing pile driving models, by introducing coupled pile-soil-plug models that take vertical interaction into account. The simplified model in chapter 4 neglects radial displacement, while the model in chapter 5 solves the full equations. Results show that both models are fundamentally different. The simplified model shows much stronger vertical interaction, causing shear stress amplitudes to attenuate faster with radial distance from the pile. Additionally, wave front arrival at a certain position in a certain layer shows stronger dependence on stiffness of the surrounding layers in the simplified model.

The liquefaction model presented in chapter 6 is a combination of the differential equation governing cylindrically symmetric soil consolidation and the empirical Seed and Rahman model describing generation of relative overpressures as a function of shear stress amplitudes. Coupling with the pile-soil-plug model is achieved by introducing three coupling variables: α (ratio between yield shear stress and initial effective stress for zero relative overpressure), β (ratio between yield shear stress and initial effective stress for unity relative overpressure) and γ (ratio between the increase in amount of shear cycles and the decrease of resistance at the pile-soil interface). α is a well-defined variable in geotechnical engineering. β and γ are uncertain variables. Results show that β is the most sensitive and therefore the most uncertain variable in the model.

7.2 Recommendations

This thesis has investigated the pile-soil-plug interaction, the emission, propagation and attenuation of waves into the soil domain and resulting generation of excess pore pressures. The objective of the thesis was to develop a comprehensive framework, capable of estimating pile driving induced liquefaction instability. This objective has been achieved, although uncertainties remain regarding variables β and γ. Recommended values for these variables to obtain a conservative upper bound solution are 0.1 and 1. Further research may contribute to increasing the accuracy of this framework.

Numerical improvements are not recommended. This is because of the incompatibility of the timescales and critical time steps of liquefaction on the one hand (timescale $\sim$ 1000 s and critical time step $\sim$ 0.1 s) and wave propagation on the other hand (timescale $\sim$ 0.1 s and critical time step $\sim 10^{-5}$ s). A fully coupled model will therefore have a timescale of $\sim$ 1000 s and a critical time step of $\sim 10^{-5}$ s, which

results in unrealistic calculation times. Another issue is that the concept of yield shear stress at the interface is critical for pile driving induced liquefaction instability. No matter the followed modelling approach, the yield shear stress at the interface has to be included for the model to be realistic. This implies that it is impossible to set up a model without α and β being included as variables. The sensitivity of the variable γ (the only variable that can be improved numerically) is not considered significant enough to compensate for a sharp increase in calculation time.

Experimental validation of β is recommended instead. Increasing the certainty of predicting this variable will increase the accuracy of the model in general. Locking between particles is assumed to be the most important mechanism of shear transfer through a liquefied interface. β should therefore be verified for sand specimen with different sorting and angularity. A probabilistic model may be set up to couple results of the liquefaction model with slope stability analysis software. If all these steps are carried out successfully, it might be possible to formulate an empirical formula which predicts liquefaction instability risk as a function of three variables: the β (a measure for the peak shear stress amplitude that can be transferred into the soil domain), the initial relative density I_D (a measure for the liquefaction potential of the soil) and the consolidation coefficient c_v (a measure for the drainage capacity of the soil). These are the three critical (most sensitive) variables which can be used to make a first estimation of the full problem.

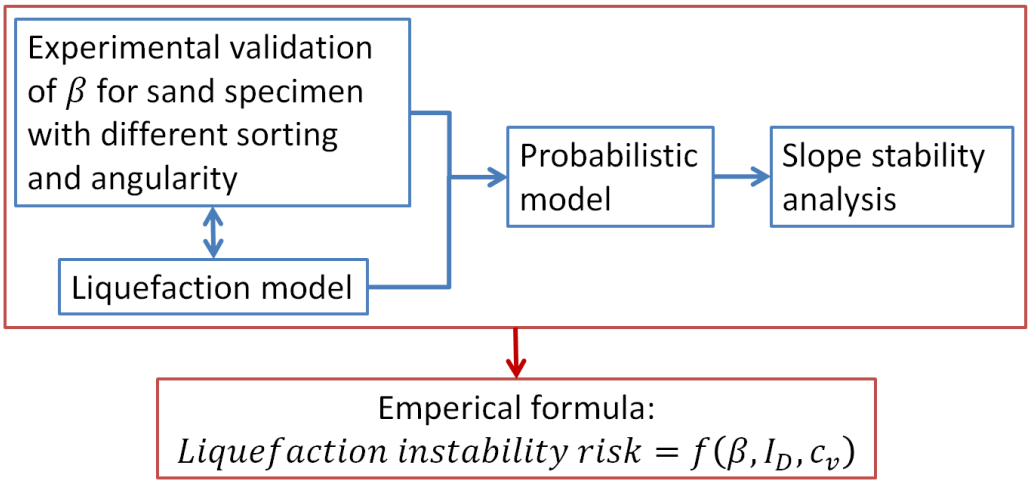

Figure 7.1: Recommendation for further research

8 Bibliography

Baks, H.T., Smith, R.C., Wang, Y. (1995). The modelling of piezoceramic patch interactions with shells, plates and beams. *Quarterly of Applied Mathematics*, Vol. 53, No. 2, pp. 353-381.

Banerjee, P.K., Butterfield, R. (1990). Advanced Geotechnical Analyses: Developments in Soil Mechanics and Foundation Engineering, Vol. 4, CRC Press, Boca Raton, USA.

Berghe, van den, J.F. (2001). *Sand Strength Degradation within the Framework of Vibratory Pile Driving.* PhD thesis, Katholieke Universiteit Leuven, Leuven, Belgium.

Bolt, B. A. (1993). Earthquakes. W.H. Freeman, New York, USA.

Dalen, van, K. (2015). *Lecture notes: MSc course CIE5340 Soil dynamics – Part B.* Delft University of Technology, Delft, the Netherlands.

Das, B.M., Ramana, G.V. (2011). Principles of Soil Dynamics (second edition). Cengage Learning, Boston, USA.

Deckner, F. (2013). *Ground vibrations due to pile and sheet pile driving – influencing factors, predictions and measurements*. Licentiate Thesis, Royal Institute of Technology Stockholm, Stockholm, Sweden.

Deeks, A.J., Randolph, M.F. (1993). Analytical modelling of hammer impact for pile driving. *International Journal for Numerical and Analytical methods in Geomechanics,* Vol. 17, pp. 279-302.

Gavin, H.P. (2016). *Lecture notes: MSc course CEE 541 Structural Dynamics - Numerical Integration in Structural Dynamics.* Duke University, Durham, U.S.A.

Head, J.M. & Jardine, F.M. (1992). *Ground-borne vibrations arising from piling*. CIRIA Technical Note 142, CIRIA, London, U.K.

Hicks, M.A. (2017). *PowerPoint slides : BSc course CTB2310 Soil mechanics*. Delft University of Technology, Delft, the Netherlands.

Holeyman, A. (1993) HYPERVIBIIa, An detailed numerical model proposed for Future Computer Implementation to evaluate the penetration speed of vibratory driven sheet Piles. *BBRI*, September, 54p.

Holeyman, A. (2000). Vibratory Driving Analysis – Keynote Lecture. *Proceedings of the 5th International Conference on the Application of Stress-Wave Theory to Piles,* Sao Paulo, Brazil.

Holscher, P. (2016). *Lecture notes: MSc course CIE5340 Soil dynamics – Part A Soil dynamics in urban areas.* Delft University of Technology, Delft, the Netherlands.

Kramer, S.L. (1996). Geotechnical Earthquake Engineering. Prentice-Hall, New Jersey, USA.

Massarsch, K.R., Fellenius, B.H. (2008). Ground Vibrations Induced by Impact Pile Driving. *Proceedings 6th Conference on Case Histories in Geotechnical Engineering*, Arlington.

Mazumder, S. (2016). Numerical Methods for Partial Differential Equations. Elsevier, London, U.K.

Meijers, P. (2007). *Settlement during vibratory sheet piling*. PhD thesis, Delft University of Technology, Delft, the Netherlands.

Metrikine, A.V. (2006). *Lecture notes: MSc course CT4140 Dynamics of Structures - Part 2 Wave Dynamics*. Delft University of Technology, Delft, the Netherlands.

Middendorp, P. (2004).Thirty years of experience with the wave equation solution based on method of characteristics. *Proceedings 7th International Conference on the Application of Stress Wave Theory to Piles*, Kuala Lumpur, Malaysia.

Naggar, M.H., Novak, M. (1994). Non-Linear Model for Dynamic Axial Pile Response. *Journal Geotechnical Engineering,* Vol. 120(2), pp. 308-329.

Raj, M. (2016). *Introduction to Matlab.* https://www.slideshare.net/profmohan1/introduction-to-matlab-59971000 , downloaded: 01-2018.

Randolph, M.F. (1987). Modelling of the soil plug response during pile driving. *Proceedings 9th Southeast Asian Geotechnical Conference,* Bangkok, Thailand.

Randolph, M.F. (2003). Science and empiricism in pile foundation design. *Geotechnique,* Vol. 10, pp. 847-875.

Salgado, R., Loukidis, D., Abou-Jaoude, G., Zhang,Y. (2015). The role of soil stiffness non-linearity in 1D pile driving simulations. *Geotechnique*, Vol. 65, No. 3, pp. 169–187.

Salgado, R., Zhang, Y., Abou-Jaoude, G., Loukidis, D., Bisht, V. (2017). Pile driving formulas based on pile wave equation analyses. *Computers and Geotechnics,* Vol. 81, pp. 307-321.

Simons, H.A., Randolph, M.F. (1985). A new approach to one-dimensional pile driving analysis. *Proceedings 5th International Conference on Numerical Methods in Geomechanics,* Nagoya, Japan.

Smith, E.A.L. (1960). Pile driving analysis by the wave equation. *Journal Soil Mechanics Foundation Engineering Division ASCE,* Vol. 86, pp. 35-61.

Tol, van, A.F. (2006). *Lecture notes: BSc course CTB1410 Foundation engineering*. Delft University of Technology, Delft, the Netherlands.

Verruijt, A. (2010). An introduction to soil dynamics. Springer, Dordrecht, Netherlands.

Verruijt, A. (2012). An introduction to soil mechanics. http://geo.verruijt.net/ , downloaded: 12-2017.

Verruijt, A. (2013). Theory and problems of poroelasticity. http://geo.verruijt.net/ , downloaded: 12-2017.

Wood, M., Humphrey, V. (2016). *Modelling and prediction of acoustic disturbances from off-shore piling.* PhD thesis, University of Southampton, Southampton, United Kingdom.

List of figures

List of tables

Appendix A1: Derivation of the Salgado pile driving model

Soil grid:

$$\rho \frac{\partial^2 w}{\partial t^2} = G\left(\frac{\partial^2 w}{\partial r^2} + \frac{1}{r}\frac{\partial w}{\partial r}\right) \tag{1}$$

First the equation is discretized:

$$\rho \frac{\partial^2}{\partial t^2} w_{i,j} = G\left(\frac{w_{i,j+1} - 2w_{i,j} + w_{i,j-1}}{\Delta r^2} + \frac{1}{r_j}\frac{w_{i,j+1} - w_{i,j-1}}{2\Delta r}\right) \tag{2}$$

After some algebraic manipulations:

$$\frac{\partial^2}{\partial t^2} w_{i,j} = C_1\left(w_{i,j+1} - 2w_{i,j} + w_{i,j-1}\right) + C_2\frac{1}{r_j}\left(w_{i,j+1} - w_{i,j-1}\right) \tag{3}$$

With:

$$C_1 = \frac{\Delta G}{\Delta r^2 \rho} \tag{4}$$

$$C_2 = \frac{G}{2\Delta r \rho} \tag{5}$$

Non-reflective boundary:

$$\frac{\partial w}{\partial r} = -\sqrt{\frac{\rho}{G}}\frac{\partial w}{\partial t} \tag{6}$$

The equation is discretized:

$$\frac{w_{i,j+1} - w_{i,j-1}}{2\Delta r} = -\sqrt{\frac{\rho}{G}}\frac{\partial}{\partial t} w_{i,j} \tag{7}$$

Which is equivalent to:

$$w_{i,j+1} = -C_3\frac{\partial}{\partial t} w_{i,j} + w_{i,j-1} \tag{8}$$

With:

$$C_3 = 2\Delta r\sqrt{\frac{\rho}{G}} \tag{9}$$

Equation 8 is substituted into equation 3 obtaining:

$$\frac{\partial^2}{\partial t^2} w_{i,j} = 2C_1 w_{i,j-1} - 2C_1 w_{i,j} - C_3\left(C_1 + C_2\frac{1}{r_j}\right)\frac{\partial}{\partial t} w_{i,j} \tag{10}$$

Pile:

$$\rho_p A_p \frac{\partial^2 w}{\partial t^2} = \pi d_P G\frac{\partial w}{\partial r} + E_p A_p \frac{\partial^2 w}{\partial z^2} \tag{11}$$

The equation is discretized:

$$\rho_p A_p \frac{\partial^2}{\partial t^2} w_{i,j} = \pi d_P G\frac{\left(w_{i,j+1} - w_{i,j}\right)}{\Delta r} + E_p A_p \frac{\left(w_{i+1,j} - 2w_{i,j} + w_{i-1,j}\right)}{\Delta z^2} \tag{12}$$

And after some algebraic manipulations:

$$\frac{\partial^2}{\partial t^2} w_{i,j} = C_4 w_{i,j+1} - (C_4 + 2C_5) w_{i,j} + C_5 w_{i+1,j} + C_5 w_{i-1,j} \tag{13}$$

With:

$$C_4 = \frac{\pi d_P G}{2\Delta r \rho_p A_p} \tag{14}$$

$$C_5 = \frac{E_p}{\Delta z^2 \rho_p} \tag{15}$$

Pile head:

$$E_p A_p \frac{\partial w}{\partial z} = -F_{imp}(t) \tag{16}$$

Discretization gives the following result:

$$E_p A_p \frac{w_{i+1,j} - w_{i-1,j}}{2\Delta z} = -F_{imp}(t) \tag{17}$$

Therefore:

$$w_{i-1,j} = C_6 F_{imp} + w_{i+1,j} \tag{18}$$

With:

$$C_6 = \frac{2\Delta z}{E_p A_p} \tag{19}$$

Substituting equation 18 into equation 13 gives the following result:

$$\frac{\partial^2}{\partial t^2} w_{i,j} = C_4 w_{i,j+1} - (C_4 + 2C_5) w_{i,j} + 2C_5 w_{i+1,j} + C_5 C_6 F_{imp} \tag{20}$$

Pile toe:

$$E_p A_p \frac{\partial w}{\partial z} = -\frac{A_p p_{lim}}{Q_{toe}} w - A_p p_{lim} J_{toe} \frac{\partial w}{\partial t} \tag{21}$$

The equation is discretized:

$$E_p A_p \frac{w_{i+1,j} - w_{i-1,j}}{2\Delta z} = -\frac{A_p p_{lim}}{Q_{toe}} w_{i,j} - A_p p_{lim} J_{toe} \frac{\partial}{\partial t} w_{i,j} \tag{22}$$

Which is equivalent to:

$$w_{i+1,j} = -C_7 w_{i,j} - C_8 \frac{\partial}{\partial t} w_{i,j} + w_{i-1,j} \tag{23}$$

With:

$$C_7 = \frac{2\Delta z p_{lim}}{Q_{toe} E_p} \tag{24}$$

$$C_8 = \frac{2\Delta z p_{lim} J_{toe}}{E_p} \tag{25}$$

Substituting equation 23 into equation 13 gives the following expression:

$$\frac{\partial^2}{\partial t^2} w_{i,j} = C_4 w_{i,j+1} - (C_4 + 2C_5 + C_5 C_7) w_{i,j} + 2C_5 w_{i-1,j} - C_5 C_8 \frac{\partial}{\partial t} w_{i,j} \quad (26)$$

Appendix A2: Derivation of the simplified cylindrically symmetric model

Grid:

$$\rho\frac{\partial^2 w}{\partial t^2}=\left(1+\alpha\frac{\partial}{\partial t}\right)\left(\left(K+\frac{4}{3}G\right)\frac{\partial^2 w}{\partial z^2}+G\left(\frac{\partial^2 w}{\partial r^2}+\frac{1}{r}\frac{\partial w}{\partial r}\right)\right) \tag{1}$$

The equation is discretized:

$$\rho\frac{\partial^2}{\partial t^2}w_{i,j}=\left(1+\alpha\frac{\partial}{\partial t}\right)\left(\left(K+\frac{4}{3}G\right)\frac{w_{i+1,j}-2w_{i,j}+w_{i-1,j}}{\Delta z^2}+G\left(\frac{w_{i,j+1}-2w_{i,j}+w_{i,j-1}}{\Delta r^2}+\frac{1}{r_j}\frac{w_{i,j+1}-w_{i,j-1}}{2\Delta r}\right)\right) \tag{2}$$

After performing some algebraic manipulations:

$$\frac{\partial^2}{\partial t^2}w_{i,j}=\left(1+\alpha\frac{\partial}{\partial t}\right)\left(-2(C_1+C_2)w_{i,j}+C_1w_{i+1,j}+C_1w_{i-1,j}+\left(C_2+C_3\frac{1}{r_j}\right)w_{i,j+1}+\left(C_2-C_3\frac{1}{r_j}\right)w_{i,j-1}\right) \tag{3}$$

With:

$$C_1=\frac{\left(K+\frac{4}{3}G\right)}{\Delta z^2\rho} \tag{4}$$

$$C_2=\frac{G}{\Delta r^2\rho} \tag{5}$$

$$C_3=\frac{G}{2\Delta r\rho} \tag{6}$$

Axis of symmetry:

$$\sigma_{rz}=G\frac{\partial w}{\partial r}=0 \tag{7}$$

Discretizing the equation:

$$w_{i,j-1}=w_{i,j+1} \tag{8}$$

Substituting equation 8 into equation 3 (please note no damping is used for boundary nodes):

$$\frac{\partial^2}{\partial t^2}w_{i,j}=-(2C_1+4C_2)w_{i,j}+C_1w_{i+1,j}+C_1w_{i-1,j}+4C_2w_{i,j+1} \tag{9}$$

Free surface:

$$\sigma_{zz}=\left(K+\frac{4}{3}G\right)\frac{\partial w}{\partial z}=0 \tag{10}$$

The equation is discretized:

$$w_{i-1,j} = w_{i+1,j} \tag{11}$$

Substituting equation 11 into equation 3 yields the following result:

$$\frac{\partial^2}{\partial t^2} w_{i,j} = -2(C_1 + C_2) w_{i,j} + 2C_1 w_{i+1,j} + \left(C_2 + C_3 \frac{1}{r_j}\right) w_{i,j+1} + \left(C_2 - C_3 \frac{1}{r_j}\right) w_{i,j-1} \tag{12}$$

Vertical continuous boundary:

$$\sigma_{rz} = G \frac{\partial w}{\partial r} = -\sqrt{G\rho} \frac{\partial w}{\partial t} \tag{13}$$

The equation is discretized:

$$G \frac{w_{i,j+1} - w_{i,j-1}}{2\Delta r} = -\sqrt{G\rho} \frac{\partial}{\partial t} w_{i,j} \tag{14}$$

This is equivalent to:

$$w_{i,j+1} = -C_4 \frac{\partial}{\partial t} w_{i,j} + w_{i,j-1} \tag{15}$$

With:

$$C_4 = 2\Delta r \sqrt{\frac{\rho}{G}} \tag{16}$$

Substituting equation 15 into equation 3 yields:

$$\begin{aligned} \frac{\partial^2}{\partial t^2} w_{i,j} = {} & -2(C_1 + C_2) w_{i,j} + C_1 w_{i+1,j} + C_1 w_{i-1,j} + 2C_2 w_{i,j-1} \\ & - C_4 \left(C_2 + C_3 \frac{1}{r_j}\right) \frac{\partial}{\partial t} w_{i,j} \end{aligned} \tag{17}$$

Horizontal continuous boundary:

$$\sigma_{zz} = \left(K + \frac{4}{3} G\right) \frac{\partial w}{\partial z} = -\sqrt{\left(K + \frac{4}{3} G\right) \rho} \frac{\partial w}{\partial t} \tag{18}$$

Discretize the equation:

$$\left(K + \frac{4}{3} G\right) \frac{w_{i+1,j} - w_{i-1,j}}{2\Delta z} = -\sqrt{\left(K + \frac{4}{3} G\right) \rho} \frac{\partial}{\partial t} w_{i,j} \tag{19}$$

Or:

$$w_{i+1,j} = -C_5 \frac{\partial}{\partial t} w_{i,j} + w_{i-1,j} \tag{20}$$

With:

$$C_5 = 2\Delta z \sqrt{\frac{\rho}{\left(K + \frac{4}{3} G\right)}} \tag{21}$$

Substituting equation 20 into equation 3 yields:

$$\frac{\partial^2}{\partial t^2} w_{i,j} = -2(C_1 + C_2) w_{i,j} + 2C_1 w_{i-1,j} + \left(C_2 + C_3 \frac{1}{r_j}\right) w_{i,j+1} + \left(C_2 - C_3 \frac{1}{r_j}\right) w_{i,j-1} - C_1 C_5 \frac{\partial}{\partial t} w_{i,j} \tag{22}$$

Pile:

$$\rho_p A_p \frac{\partial^2 w}{\partial t^2} = \pi d_e G \frac{\partial w}{\partial r}|_{outer} - \pi d_i G \frac{\partial w}{\partial r}|_{plug} + \frac{\partial^2 w}{\partial z^2} \tag{23}$$

The equation is discretized:

$$\rho_p A_p \frac{\partial^2}{\partial t^2} w_{i,j} = \pi d_e G \frac{w_{i,j+1} - w_{i,j}}{\Delta r} - \pi d_i G \frac{w_{i,j} - w_{i,j-1}}{\Delta r} + E_p A_p \frac{w_{i+1,j} - 2w_{i,j} + w_{i-1,j}}{\Delta z^2} \tag{24}$$

After some algebraic manipulations:

$$\frac{\partial^2}{\partial t^2} w_{i,j} = C_6 w_{i,j+1} + C_{6p} w_{i,j-1} + C_7 w_{i+1,j} + C_7 w_{i-1,j} + \left(-2C_7 - C_6 - C_{6p}\right) w_{i,j} \tag{25}$$

With:

$$C_6 = \frac{\pi d_e G}{\Delta r \rho_p A_p} \tag{26}$$

$$C_{6p} = \frac{\pi d_i G}{\Delta r \rho_p A_p} \tag{27}$$

$$C_7 = \frac{E_p}{\Delta z^2 \rho_p} \tag{28}$$

Pile head:

$$E_p A_p \frac{\partial w}{\partial z} = -F_{imp}(t) \tag{29}$$

Discretizing the equation:

$$E_p A_p \frac{w_{i+1,j} - w_{i-1,j}}{2\Delta z} = -F_{imp}(t) \tag{30}$$

This is equivalent to:

$$w_{i-1,j} = C_8 F_{imp}(t) + w_{i+1,j} \tag{31}$$

With:

$$C_8 = \frac{2\Delta z}{E_p A_p} \tag{32}$$

Substituting equation 31 into equation 25 yields:

$$\frac{\partial^2}{\partial t^2} w_{i,j} = C_6 w_{i,j+1} + C_{6p} w_{i,j-1} + 2C_7 w_{i+1,j} + \left(-2C_7 - C_6 - C_{6p}\right) w_{i,j} + C_7 C_8 F_{imp}(t) \tag{33}$$

Pile base:

$$E_p A_p \frac{\partial w}{\partial z} = \frac{1}{4}\pi \left(\left(d_n + \frac{\Delta z}{2} \right)^2 - \left(d_n - \frac{\Delta z}{2} \right)^2 \right) \left(K + \frac{4}{3} G \right) \frac{\partial w}{\partial z} \tag{34}$$

The equation is discretized:

$$E_p A_p \frac{w_{i+1,j} - w_{i-1,j}}{2\Delta z} = \frac{1}{2}\pi d_n \Delta r \left(K + \frac{4}{3} G \right) \frac{w_{i+1,j} - w_{i,j}}{\Delta z} \tag{35}$$

This is equivalent to:

$$w_{i+1,j} = C_9 \left(w_{i+1,j} - w_{i,j} \right) + w_{i-1,j} \tag{36}$$

With:

$$C_9 = \frac{\pi d_n \Delta r \left(K + \frac{4}{3} G \right)}{E_p A_p} \tag{37}$$

Substituting equation 36 into equation 25 yields:

$$\frac{\partial^2}{\partial t^2} w_{i,j} = C_6 w_{i,j+1} + C_{6p} w_{i,j-1} + C_7 C_9 w_{i+1,j} + 2C_7 w_{i-1,j} + \left(-2C_7 - C_6 - C_{6p} - C_7 C_9\right) w_{i,j} \tag{38}$$

Appendix A3: Derivation of the cylindrically symmetric model

Grid U:

Governing equation:

$$\rho\frac{\partial^2 u}{\partial t^2}=\left(1+\alpha\frac{\partial}{\partial t}\right)\left(\left(K+\frac{4}{3}G\right)\left(\frac{\partial^2 u}{\partial r^2}+\frac{1}{r}\frac{\partial u}{\partial r}-\frac{u}{r^2}\right)+\left(K+\frac{1}{3}G\right)\frac{\partial^2 w}{\partial r\partial z}+G\frac{\partial^2 u}{\partial z^2}\right) \tag{1}$$

Discretization of the governing equation:

$$\begin{aligned}\rho\frac{\partial^2}{\partial t^2}u_{i,j}=\left(1+\alpha\frac{\partial}{\partial t}\right)\Bigg(&\left(K+\frac{4}{3}G\right)\left(\frac{u_{i,j+1}-2u_{i,j}+u_{i,j-1}}{\Delta r^2}+\frac{1}{r_j}\frac{u_{i,j+1}-u_{i,j-1}}{2\Delta r}\right.\\&\left.-\frac{u_{i,j}}{r_j^2}\right)+\left(K+\frac{1}{3}G\right)\frac{w_{i+1,j+1}-w_{i+1,j-1}-w_{i-1,j+1}+w_{i-1,j-1}}{4\Delta z\Delta r}\\&+G\frac{u_{i+1,j}-2u_{i,j}+u_{i-1,j}}{\Delta z^2}\Bigg)\end{aligned} \tag{2}$$

This is equivalent to:

$$\begin{aligned}\frac{\partial^2}{\partial t^2}u_{i,j}=\left(1+\alpha\frac{\partial}{\partial t}\right)\Bigg(&\left(C_1+C_2\frac{1}{r_j}\right)u_{i,j+1}+\left(C_1-C_2\frac{1}{r_j}\right)u_{i,j-1}\\&-\left(2C_1+2C_5+C_3\frac{1}{r_j^2}\right)u_{i,j}+C_5u_{i+1,j}+C_5u_{i-1,j}+C_4w_{i+1,j+1}\\&-C_4w_{i+1,j-1}-C_4w_{i-1,j+1}+C_4w_{i-1,j-1}\Bigg)\end{aligned} \tag{3}$$

With:

$$C_1=\frac{\left(K+\frac{4}{3}G\right)}{\Delta r^2\rho} \tag{4}$$

$$C_2=\frac{\left(K+\frac{4}{3}G\right)}{2\Delta r\rho} \tag{5}$$

$$C_3=\frac{\left(K+\frac{4}{3}G\right)}{\rho} \tag{6}$$

$$C_4=\frac{\left(K+\frac{1}{3}G\right)}{4\Delta z\Delta r\rho} \tag{7}$$

$$C_5 = \frac{G}{\Delta z^2 \rho} \tag{8}$$

Grid W:

Governing equation:

$$\rho \frac{\partial^2 w}{\partial t^2} = \left(1 + \alpha \frac{\partial}{\partial t}\right)\left(\left(K + \frac{4}{3}G\right)\frac{\partial^2 w}{\partial z^2} + \left(K + \frac{1}{3}G\right)\left(\frac{\partial^2 u}{\partial r \partial z} + \frac{1}{r}\frac{\partial u}{\partial z}\right) + G\left(\frac{\partial^2 w}{\partial r^2} + \frac{1}{r}\frac{\partial w}{\partial r}\right)\right) \tag{9}$$

Discretization of the governing equation:

$$\begin{aligned}\rho \frac{\partial^2}{\partial t^2} w_{i,j} = \left(1 + \alpha \frac{\partial}{\partial t}\right)\Bigg(&\left(K + \frac{4}{3}G\right)\frac{w_{i+1,j} - 2w_{i,j} + w_{i-1,j}}{\Delta z^2} \\ &+ \left(K + \frac{1}{3}G\right)\Bigg(\frac{u_{i+1,j+1} - u_{i+1,j-1} - u_{i-1,j+1} + u_{i-1,j-1}}{4\Delta z \Delta r} \\ &+ \frac{1}{r_j}\frac{u_{i+1,j} - u_{i-1,j}}{2\Delta z}\Bigg) \\ &+ G\left(\frac{w_{i,j+1} - 2w_{i,j} + w_{i,j-1}}{\Delta r^2} + \frac{1}{r_j}\frac{w_{i,j+1} - w_{i,j-1}}{2\Delta r}\right)\Bigg)\end{aligned} \tag{10}$$

This is equivalent to:

$$\begin{aligned}\frac{\partial^2}{\partial t^2} w_{i,j} = \left(1 + \alpha \frac{\partial}{\partial t}\right)\Bigg(&C_6 w_{i+1,j} + C_6 w_{i-1,j} - (2C_6 + 2C_8) w_{i,j} + \left(C_8 + C_9 \frac{1}{r_j}\right) w_{i,j+1} \\ &+ \left(C_8 - C_9 \frac{1}{r_j}\right) w_{i,j-1} + C_4 u_{i+1,j+1} - C_4 u_{i+1,j-1} - C_4 u_{i-1,j+1} \\ &+ C_4 u_{i-1,j-1} + C_7 \frac{1}{r_j} u_{i+1,j} - C_7 \frac{1}{r_j} u_{i-1,j}\Bigg)\end{aligned} \tag{11}$$

With:

$$C_6 = \frac{\left(K + \frac{4}{3}G\right)}{\Delta z^2 \rho} \tag{12}$$

$$C_7 = \frac{\left(K + \frac{1}{3}G\right)}{2\Delta z \rho} \tag{13}$$

$$C_8 = \frac{G}{\Delta r^2 \rho} \tag{14}$$

$$C_9 = \frac{G}{2\Delta r \rho} \tag{15}$$

Free surface:

Boundary conditions:

$$\sigma_{zz} = \left(K + \frac{4}{3}G\right)\frac{\partial w}{\partial z} + \left(K - \frac{2}{3}G\right)\left(\frac{u}{r} + \frac{\partial u}{\partial r}\right) = 0 \tag{16}$$

$$\sigma_{rz} = G\left(\frac{\partial u}{\partial z} + \frac{\partial w}{\partial r}\right) = 0 \tag{17}$$

Discretization of the boundary conditions:

$$\left(K + \frac{4}{3}G\right)\frac{w_{i+1,j} - w_{i-1,j}}{2\Delta z} + \left(K - \frac{2}{3}G\right)\left(\frac{1}{r_j}u_{i,j} + \frac{u_{i,j+1} - u_{i,j-1}}{2\Delta r}\right) = 0 \tag{18}$$

$$\frac{u_{i+1,j} - u_{i-1,j}}{2\Delta z} + \frac{w_{i,j+1} - w_{i,j-1}}{2\Delta r} = 0 \tag{19}$$

This is equivalent to:

$$w_{i-1,j} = C_{10}\frac{1}{r_j}u_{i,j} + C_{11}u_{i,j+1} - C_{11}u_{i,j-1} + w_{i+1,j} \tag{20}$$

$$u_{i-1,j} = C_{12}w_{i,j+1} - C_{12}w_{i,j-1} + u_{i+1,j} \tag{21}$$

With:

$$C_{10} = \frac{2\Delta z\left(K - \frac{2}{3}G\right)}{\left(K + \frac{4}{3}G\right)} \tag{22}$$

$$C_{11} = \frac{\Delta z\left(K - \frac{2}{3}G\right)}{\Delta r\left(K + \frac{4}{3}G\right)} \tag{23}$$

$$C_{12} = \frac{\Delta z}{\Delta r} \tag{24}$$

Equations 3 and 11 with modified mixed derivative and without damping (damping only applied for internal nodes):

$$\begin{aligned}\frac{\partial^2}{\partial t^2}u_{i,j} = &\left(C_1 + C_2\frac{1}{r_j}\right)u_{i,j+1} + \left(C_1 - C_2\frac{1}{r_j}\right)u_{i,j-1} - \left(2C_1 + 2C_5 + C_3\frac{1}{r_j^2}\right)u_{i,j} \\ &+ C_5u_{i+1,j} + C_5u_{i-1,j} + C_{4m}w_{i+1,j+1} - C_{4m}w_{i+1,j-1} - C_{4m}w_{i,j+1} \\ &+ C_{4m}w_{i,j-1}\end{aligned} \tag{25}$$

$$\begin{aligned}\frac{\partial^2}{\partial t^2}w_{i,j} = &C_6w_{i+1,j} + C_6w_{i-1,j} - (2C_6 + 2C_8)w_{i,j} + \left(C_8 + C_9\frac{1}{r_j}\right)w_{i,j+1} \\ &+ \left(C_8 - C_9\frac{1}{r_j}\right)w_{i,j-1} + C_{4m}u_{i+1,j+1} - C_{4m}u_{i+1,j-1} - C_{4m}u_{i,j+1} \\ &+ C_{4m}u_{i,j-1} + C_7\frac{1}{r_j}u_{i+1,j} - C_7\frac{1}{r_j}u_{i-1,j}\end{aligned} \tag{26}$$

With:

$$C_{4m} = \frac{\left(K + \frac{1}{3}G\right)}{2\Delta z\Delta r\rho} \tag{27}$$

Substituting boundary condition expressions 20 and 21 into equations 25 and 26 yields the final result:

$$\begin{aligned}\frac{\partial^2}{\partial t^2}u_{i,j} = &\left(C_1 + C_2\frac{1}{r_j}\right)u_{i,j+1} + \left(C_1 - C_2\frac{1}{r_j}\right)u_{i,j-1} - \left(2C_1 + 2C_5 + C_3\frac{1}{r_j^2}\right)u_{i,j} \\ &+ 2C_5u_{i+1,j} + (C_5C_{12} - C_{4m})w_{i,j+1} + (C_{4m} - C_5C_{12})w_{i,j-1} \\ &+ C_{4m}w_{i+1,j+1} - C_{4m}w_{i+1,j-1}\end{aligned} \tag{28}$$

$$\begin{aligned}\frac{\partial^2}{\partial t^2}w_{i,j} = &2C_6w_{i+1,j} - (2C_6 + 2C_8)w_{i,j} + \left(C_8 + (C_9 - C_7C_{12})\frac{1}{r_j}\right)w_{i,j+1} \\ &+ \left(C_8 + (C_7C_{12} - C_9)\frac{1}{r_j}\right)w_{i,j-1} + C_6C_{10}\frac{1}{r_j}u_{i,j} + C_{4m}u_{i+1,j+1} \\ &- C_{4m}u_{i+1,j-1} + (C_6C_{11} - C_{4m})u_{i,j+1} + (C_{4m} - C_6C_{11})u_{i,j-1}\end{aligned} \tag{29}$$

Vertical non-reflective boundary:

Boundary conditions:

$$\sigma_{rr} = \left(K + \frac{4}{3}G\right)\frac{\partial u}{\partial r} + \left(K - \frac{2}{3}G\right)\left(\frac{u}{r} + \frac{\partial w}{\partial z}\right) = -\sqrt{\rho\left(K + \frac{4}{3}G\right)}\frac{\partial u}{\partial t} \tag{30}$$

$$\sigma_{rz} = G\left(\frac{\partial u}{\partial z} + \frac{\partial w}{\partial r}\right) = -\sqrt{\rho G}\frac{\partial w}{\partial t} \tag{31}$$

Discretization of the boundary conditions:

$$\begin{aligned}\left(K + \frac{4}{3}G\right)\frac{u_{i,j+1} - u_{i,j-1}}{2\Delta r} + \left(K - \frac{2}{3}G\right)\left(\frac{1}{r_j}u_{i,j} + \frac{w_{i+1,j} - w_{i-1,j}}{2\Delta z}\right) \\ = -\sqrt{\rho\left(K + \frac{4}{3}G\right)}\frac{\partial}{\partial t}u_{i,j}\end{aligned} \tag{32}$$

$$G\left(\frac{u_{i+1,j} - u_{i-1,j}}{2\Delta z} + \frac{w_{i,j+1} - w_{i,j-1}}{2\Delta r}\right) = -\sqrt{\rho G}\frac{\partial}{\partial t}w_{i,j} \tag{33}$$

This is equivalent to:

$$u_{i,j+1} = -C_{14}\frac{1}{r_j}u_{i,j} - C_{15}w_{i+1,j} + C_{15}w_{i-1,j} + u_{i,j-1} - C_{13}\frac{\partial}{\partial t}u_{i,j} \tag{34}$$

$$w_{i,j+1} = -C_{17}u_{i+1,j} + C_{17}u_{i-1,j} + w_{i,j-1} - C_{16}\frac{\partial}{\partial t}w_{i,j} \tag{35}$$

With:

$$C_{13} = 2\Delta r\sqrt{\frac{\rho}{\left(K + \frac{4}{3}G\right)}} \tag{36}$$

$$C_{14} = \frac{2\Delta r\left(K - \frac{2}{3}G\right)}{\left(K + \frac{4}{3}G\right)} \tag{37}$$

$$C_{15} = \frac{\Delta r\left(K - \frac{2}{3}G\right)}{\Delta z\left(K + \frac{4}{3}G\right)} \tag{38}$$

$$C_{16} = 2\Delta r\sqrt{\frac{\rho}{G}} \tag{39}$$

$$C_{17} = \frac{\Delta r}{\Delta z} \tag{40}$$

Equations 3 and 11 with modified mixed derivative and without damping:

$$\begin{aligned}\frac{\partial^2}{\partial t^2}u_{i,j} = {} & \left(C_1 + C_2\frac{1}{r_j}\right)u_{i,j+1} + \left(C_1 - C_2\frac{1}{r_j}\right)u_{i,j-1} - \left(2C_1 + 2C_5 + C_3\frac{1}{r_j^2}\right)u_{i,j} \\ & + C_5u_{i+1,j} + C_5u_{i-1,j} + C_{4m}w_{i+1,j} - C_{4m}w_{i+1,j-1} - C_{4m}w_{i-1,j} \\ & + C_{4m}w_{i-1,j-1}\end{aligned} \tag{41}$$

$$\begin{aligned}\frac{\partial^2}{\partial t^2}w_{i,j} = {} & C_6w_{i+1,j} + C_6w_{i-1,j} - (2C_6 + 2C_8)w_{i,j} + \left(C_8 + C_9\frac{1}{r_j}\right)w_{i,j+1} \\ & + \left(C_8 - C_9\frac{1}{r_j}\right)w_{i,j-1} + C_{4m}u_{i+1,j} - C_{4m}u_{i+1,j-1} - C_{4m}u_{i-1,j} \\ & + C_{4m}u_{i-1,j-1} + C_7\frac{1}{r_j}u_{i+1,j} - C_7\frac{1}{r_j}u_{i-1,j}\end{aligned} \tag{42}$$

Substituting boundary condition expressions 34 and 35 into equations 41 and 42 yields the final result:

$$\begin{aligned}\frac{\partial^2}{\partial t^2}u_{i,j} = {} & 2C_1u_{i,j-1} - \left(2C_1 + 2C_5 + C_1C_{14}\frac{1}{r_j} + (C_3 + C_2C_{14})\frac{1}{r_j^2}\right)u_{i,j} + C_5u_{i+1,j} \\ & + C_5u_{i-1,j} + \left(C_{4m} - C_{15}\left(C_1 + C_2\frac{1}{r_j}\right)\right)w_{i+1,j} - C_{4m}w_{i+1,j-1} \\ & + \left(C_{15}\left(C_1 + C_2\frac{1}{r_j}\right) - C_{4m}\right)w_{i-1,j} + C_{4m}w_{i-1,j-1} \\ & - C_{13}\left(C_1 + C_2\frac{1}{r_j}\right)\frac{\partial}{\partial t}u_{i,j}\end{aligned} \tag{43}$$

$$\begin{aligned}\frac{\partial^2}{\partial t^2}w_{i,j} = {} & C_6w_{i+1,j} + C_6w_{i-1,j} - (2C_6 + 2C_8)w_{i,j} + 2C_8w_{i,j-1} \\ & + \left(C_{4m} - C_{17}C_8 + (C_7 - C_{17}C_9)\frac{1}{r_j}\right)u_{i+1,j} - C_{4m}u_{i+1,j-1} \\ & + \left(C_{17}C_8 - C_{4m} + (C_{17}C_9 - C_7)\frac{1}{r_j}\right)u_{i-1,j} + C_{4m}u_{i-1,j-1} \\ & - C_{16}\left(C_8 + C_9\frac{1}{r_j}\right)\frac{\partial}{\partial t}w_{i,j}\end{aligned} \tag{44}$$

Horizontal non-reflective boundary:

Boundary conditions:

$$\sigma_{zz} = \left(K + \frac{4}{3}G\right)\frac{\partial w}{\partial z} + \left(K - \frac{2}{3}G\right)\left(\frac{u}{r} + \frac{\partial u}{\partial r}\right) = -\sqrt{\rho\left(K + \frac{4}{3}G\right)}\frac{\partial w}{\partial t} \tag{45}$$

$$\sigma_{rz} = G\left(\frac{\partial u}{\partial z} + \frac{\partial w}{\partial r}\right) = -\sqrt{\rho G}\frac{\partial u}{\partial t} \tag{46}$$

Discretization of the boundary conditions:

$$\left(K + \frac{4}{3}G\right)\frac{w_{i+1,j} - w_{i-1,j}}{2\Delta z} + \left(K - \frac{2}{3}G\right)\left(\frac{1}{r_j}u_{i,j} + \frac{u_{i,j+1} - u_{i,j-1}}{2\Delta r}\right) = -\sqrt{\rho\left(K + \frac{4}{3}G\right)}\frac{\partial}{\partial t}w_{i,j} \tag{47}$$

$$G\left(\frac{u_{i+1,j} - u_{i-1,j}}{2\Delta z} + \frac{w_{i,j+1} - w_{i,j-1}}{2\Delta r}\right) = -\sqrt{\rho G}\frac{\partial}{\partial t}u_{i,j} \tag{48}$$

This is equivalent to:

$$w_{i+1,j} = -C_{10}\frac{1}{r_j}u_{i,j} - C_{11}u_{i,j+1} + C_{11}u_{i,j-1} + w_{i-1,j} - C_{18}\frac{\partial}{\partial t}w_{i,j} \tag{49}$$

$$u_{i+1,j} = -C_{12}w_{i,j+1} + C_{12}w_{i,j-1} + u_{i-1,j} - C_{19}\frac{\partial}{\partial t}u_{i,j} \tag{50}$$

With:

$$C_{18} = 2\Delta z\sqrt{\frac{\rho}{\left(K + \frac{4}{3}G\right)}} \tag{51}$$

$$C_{19} = 2\Delta z\sqrt{\frac{\rho}{G}} \tag{52}$$

Equations 3 and 11 with modified mixed derivative and without damping:

$$\begin{aligned}\frac{\partial^2}{\partial t^2}u_{i,j} = &\left(C_1 + C_2\frac{1}{r_j}\right)u_{i,j+1} + \left(C_1 - C_2\frac{1}{r_j}\right)u_{i,j-1} - \left(2C_1 + 2C_5 + C_3\frac{1}{r_j^2}\right)u_{i,j} \\ &+ C_5u_{i+1,j} + C_5u_{i-1,j} + C_{4m}w_{i,j+1} - C_{4m}w_{i,j-1} - C_{4m}w_{i-1,j+1} \\ &+ C_{4m}w_{i-1,j-1}\end{aligned} \tag{53}$$

$$\begin{aligned}\frac{\partial^2}{\partial t^2}w_{i,j} = &C_6w_{i+1,j} + C_6w_{i-1,j} - (2C_6 + 2C_8)w_{i,j} + \left(C_8 + C_9\frac{1}{r_j}\right)w_{i,j+1} \\ &+ \left(C_8 - C_9\frac{1}{r_j}\right)w_{i,j-1} + C_{4m}u_{i,j+1} - C_{4m}u_{i,j-1} - C_{4m}u_{i-1,j+1} \\ &+ C_{4m}u_{i-1,j-1} + C_7\frac{1}{r_j}u_{i+1,j} - C_7\frac{1}{r_j}u_{i-1,j}\end{aligned} \tag{54}$$

Substituting boundary condition expressions 49 and 50 into equations 53 and 54 yields the final result:

$$\begin{aligned}\frac{\partial^2}{\partial t^2}u_{i,j} = &\left(C_1 + C_2\frac{1}{r_j}\right)u_{i,j+1} + \left(C_1 - C_2\frac{1}{r_j}\right)u_{i,j-1} - \left(2C_1 + 2C_5 + C_3\frac{1}{r_j^2}\right)u_{i,j} \\ &+ 2C_5u_{i-1,j} + (C_{4m} - C_5C_{12})w_{i,j+1} + (C_5C_{12} - C_{4m})w_{i,j-1} \\ &- C_{4m}w_{i-1,j+1} + C_{4m}w_{i-1,j-1} - C_5C_{19}\frac{\partial}{\partial t}u_{i,j}\end{aligned} \tag{55}$$

$$\begin{aligned}\frac{\partial^2}{\partial t^2}w_{i,j} = &2C_6w_{i-1,j} - (2C_6 + 2C_8)w_{i,j} + \left(C_8 + (C_9 - C_7C_{12})\frac{1}{r_j}\right)w_{i,j+1} \\ &+ \left(C_8 + (C_7C_{12} - C_9)\frac{1}{r_j}\right)w_{i,j-1} - C_6C_{10}\frac{1}{r_j}u_{i,j} \\ &+ (C_{4m} - C_6C_{11})u_{i,j+1} + (C_6C_{11} - C_{4m})u_{i,j-1} - C_{4m}u_{i-1,j+1} \\ &+ C_{4m}u_{i-1,j-1} - C_6C_{18}\frac{\partial}{\partial t}w_{i,j} - C_7C_{19}\frac{1}{r_j}\frac{\partial}{\partial t}u_{i,j}\end{aligned} \tag{56}$$

Axis of symmetry:

Modified governing equation (section 5.1):

$$\rho\frac{\partial^2 w}{\partial t^2} = \left(K + \frac{4}{3}G\right)\frac{\partial^2 w}{\partial z^2} + \left(K + \frac{1}{3}G\right)\left(\frac{\partial^2 u}{\partial r\partial z}\right) + 2G\frac{\partial^2 w}{\partial r^2} \tag{57}$$

Discretization of the governing equation:

$$\frac{\partial^2}{\partial t^2}w_{i,j} = \frac{\left(K+\frac{4}{3}G\right)}{\Delta z^2\rho}\left(w_{i+1,j} - 2w_{i,j} + w_{i-1,j}\right) + \frac{\left(K+\frac{1}{3}G\right)}{4\Delta z\Delta r\rho}\left(u_{i+1,j+1} - u_{i+1,j-1} - u_{i-1,j+1} + u_{i-1,j-1}\right) + \frac{2G}{\Delta r^2\rho}\left(w_{i,j+1} - 2w_{i,j} + w_{i,j-1}\right) \quad (58)$$

Since the following relations hold for the axis of symmetry:

$$w_{i,j-1} = w_{i,j+1} \quad and \quad u_{i+1,j-1} = -u_{i+1,j+1} \quad and \quad u_{i-1,j-1} = -u_{i-1,j+1} \quad (59)$$

The final expression is:

$$\frac{\partial^2}{\partial t^2}w_{i,j} = C_6 w_{i+1,j} + C_6 w_{i-1,j} - (2C_6 + 4C_8)w_{i,j} + 4C_8 w_{i,j+1} + C_{4m}u_{i+1,j+1} - C_{4m}u_{i-1,j+1} \quad (60)$$

Pile W:

Governing equation:

$$\frac{\partial^2 w}{\partial t^2} = \frac{E_P}{\rho_P(1-v_P^2)}\frac{\partial^2 w}{\partial z^2} + \frac{E_P v_P}{\rho_P(1-v_P^2)}\frac{1}{r}\frac{\partial u}{\partial z} + \frac{G}{\rho_P t_P}\frac{\partial w}{\partial r}|_{soil} - \frac{G}{\rho_P t_P}|_{plug}\frac{\partial w}{\partial r}|_{plug} + \frac{G}{\rho_P t_P}|_{soil}\frac{\partial u}{\partial z}|_{soil} \quad (61)$$

Discretization of the governing:

$$\frac{\partial^2}{\partial t^2}w_{i,j} = \frac{E_P}{\Delta z^2\rho_P(1-v_P^2)}\left(w_{i+1,j} - 2w_{i,j} + w_{i-1,j}\right) + \frac{E_P v_P}{2\Delta z\rho_P(1-v_P^2)}\frac{1}{r_j}\left(u_{i+1,j} - u_{i-1,j}\right) + \frac{G}{\Delta r\rho_P t_P}\left(w_{i,j+1} - w_{i,j}\right) - \frac{G}{\Delta r\rho_P t_P}|_{plug}\left(w_{i,j} - w_{i,j-1}\right) + \frac{G}{\Delta z\rho_P t_P}|_{soil}\left(u_{i+1,j} - u_{i,j}\right) \quad (62)$$

This is equivalent to:

$$\frac{\partial^2}{\partial t^2}w_{i,j} = C_{20}w_{i+1,j} + C_{20}w_{i-1,j} - \left(2C_{20} + C_{22} + C_{22p}\right)w_{i,j} + C_{22}w_{i,j+1} + C_{22p}w_{i,j-1} + \left(C_{21}\frac{1}{r_j} + C_{23s}\right)u_{i+1,j} - C_{21}\frac{1}{r_j}u_{i-1,j} - C_{23s}u_{i,j} \quad (63)$$

With

$$C_{20} = \frac{E_P}{\Delta z^2 \rho_P (1 - v_P^2)} \tag{64}$$

$$C_{21} = \frac{E_P v_P}{2\Delta z \rho_P (1 - v_P^2)} \tag{65}$$

$$C_{22} = \frac{G}{\Delta r \rho_P t_P} \tag{66}$$

$$C_{22p} = \frac{G}{\Delta r \rho_P t_P} \tag{67}$$

$$C_{23s} = \frac{G}{\Delta z \rho_P t_P} \tag{68}$$

Pile U:

Governing equation:

$$\begin{aligned} \frac{\partial^2 u}{\partial t^2} = & -\frac{v_P E_P}{\rho_P (1 - v_P^2)} \frac{1}{r} \frac{\partial w}{\partial z} - \frac{E_P}{\rho_P (1 - v_P^2)} \frac{1}{r^2} u - \frac{E_P t_P^2}{12 \rho_P (1 - v_P^2)} \frac{\partial^4 u}{\partial z^4} \\ & + \frac{\left(K + \frac{4}{3} G\right)}{\rho_P t_P} \frac{\partial u}{\partial r}\Big|_{soil} - \frac{\left(K + \frac{4}{3} G\right)}{\rho_P t_P}\Big|_{plug} \frac{\partial u}{\partial r}\Big|_{plug} \\ & + \frac{\left(K - \frac{2}{3} G\right)}{\rho_P t_P}\Big|_{soil} \left(\frac{u}{r} + \frac{\partial w}{\partial z}\right)\Big|_{soil} \end{aligned} \tag{69}$$

Discretization of the governing equation:

$$\begin{aligned} \rho \frac{\partial^2}{\partial t^2} u_{i,j} = & -\frac{v_P E_P}{2\Delta z \rho_P (1 - v_P^2)} \frac{1}{r_j} \left(w_{i+1,j} - w_{i-1,j}\right) - \frac{E_P}{\rho_P (1 - v_P^2)} \frac{1}{r_j^2} u_{i,j} \\ & - \frac{E_P t_P^2}{12 \Delta z^4 \rho_P (1 - v_P^2)} \left(u_{i-2,j} - 4u_{i-1,j} + 6u_{i,j} - 4u_{i+1,j} + u_{i+2,j}\right) \\ & + \frac{\left(K + \frac{4}{3} G\right)}{\Delta r \rho_P t_P} \left(u_{i,j+1} - u_{i,j}\right) - \frac{\left(K + \frac{4}{3} G\right)}{\Delta r \rho_P t_P}\Big|_{plug} \left(u_{i,j} - u_{i,j-1}\right) \\ & + \frac{\left(K - \frac{2}{3} G\right)}{\rho_P t_P}\Big|_{soil} \frac{1}{r_j} u_{i,j} + \frac{\left(K - \frac{2}{3} G\right)}{\Delta z \rho_P t_P}\Big|_{soil} \left(w_{i+1,j} - w_{i,j}\right) \end{aligned} \tag{70}$$

This is equivalent to:

$$\rho\frac{\partial^2}{\partial t^2}u_{i,j} = \left(C_{29s} - C_{24}\frac{1}{r_j}\right)w_{i+1,j} + C_{24}\frac{1}{r_j}w_{i-1,j} - C_{29s}w_{i,j} + \left(-C_{27} - 6C_{26} - C_{27p} + C_{28s}\frac{1}{r_j} - C_{25}\frac{1}{r_j^2}\right)u_{i,j} - C_{26}u_{i-2,j} + 4C_{26}u_{i-1,j} + 4C_{26}u_{i+1,j} - C_{26}u_{i+2,j} + C_{27}u_{i,j+1} + C_{27p}u_{i,j-1} \quad (71)$$

With:

$$C_{24} = \frac{v_P E_P}{2\Delta z\rho_P(1-v_P^2)} \quad (72)$$

$$C_{25} = \frac{E_P}{\rho_P(1-v_P^2)} \quad (73)$$

$$C_{26} = \frac{E_P t_P^2}{12\Delta z^4\rho_P(1-v_P^2)} \quad (74)$$

$$C_{27} = \frac{\left(K+\frac{4}{3}G\right)}{\Delta r\rho_P t_P} \quad (75)$$

$$C_{27p} = \frac{\left(K+\frac{4}{3}G\right)}{\Delta r\rho_P t_P} \quad (76)$$

$$C_{28s} = \frac{\left(K-\frac{2}{3}G\right)}{\rho_P t_P} \quad (77)$$

$$C_{29s} = \frac{\left(K-\frac{2}{3}G\right)}{\Delta z\rho_P t_P} \quad (78)$$

Pile head:

Boundary conditions:

$$\left(\frac{\partial w}{\partial z} + v_P\frac{u}{r}\right) = -\frac{1-v_P^2}{E_p A_p}F_{imp}(t) \quad (79)$$

$$\frac{\partial^2 u}{\partial z^2} = 0 \quad (80)$$

$$\frac{\partial^3 u}{\partial z^3} = 0 \quad (81)$$

Discretization of the boundary conditions:

$$w_{i-1,j} = \frac{2\Delta z(1-v_P^2)}{E_p A_p} F_{imp}(t) + 2\Delta z v_P \frac{1}{r_j} u_{i,j} + w_{i+1,j} \tag{82}$$

$$\frac{u_{i+1,j} - 2u_{i,j} + u_{i-1,j}}{\Delta z^2} = 0 \tag{83}$$

$$\frac{\frac{1}{2}u_{i+2,j} - u_{i+1,j} + u_{i-1,j} - \frac{1}{2}u_{i-2,j}}{\Delta z^3} = 0 \tag{84}$$

This is equivalent to:

$$w_{i-1,j} = w_{i+1,j} + C_{31}\frac{1}{r_j}u_{i,j} + C_{30}F_{imp}(t) \tag{85}$$

$$u_{i-2,j} = 6u_{i,j} - 8u_{i+1,j} + 3u_{i+2,j} \tag{86}$$

$$u_{i-1,j} = 3u_{i,j} - 3u_{i+1,j} + u_{i+2,j} \tag{87}$$

With:

$$C_{30} = \frac{2\Delta z(1-v_P^2)}{E_p A_p} \tag{88}$$

$$C_{31} = 2\Delta z v_P \tag{89}$$

Substituting boundary condition expressions 85, 86 and 87 into equations 63 and 71 yields the final result:

$$\begin{aligned}\frac{\partial^2}{\partial t^2}w_{i,j} = {} & 2C_{20}w_{i+1,j} - \left(2C_{20} + C_{22} + C_{22p}\right)w_{i,j} + C_{22}w_{i,j+1} + C_{22p}w_{i,j-1} \\ & + \left((C_{20}C_{31} - 3C_{21})\frac{1}{r_j} - C_{23s}\right)u_{i,j} + \left(4C_{21}\frac{1}{r_j} + C_{23s}\right)u_{i+1,j} \\ & - C_{21}\frac{1}{r_j}u_{i+2,j} + C_{20}C_{30}F_{imp}(t)\end{aligned} \tag{90}$$

$$\begin{aligned}\frac{\partial^2}{\partial t^2}u_{i,j} = {} & C_{29s}w_{i+1,j} - w_{i,j}C_{29s} + \left(-C_{27} - C_{27p} + C_{28s}\frac{1}{r_j} + (C_{24}C_{31} - C_{25})\frac{1}{r_j^2}\right)u_{i,j} \\ & + C_{27}u_{i,j+1} + C_{27p}u_{i,j-1} + C_{24}C_{30}\frac{1}{r_j}F_{imp}(t)\end{aligned} \tag{91}$$

Pile toe:

Boundary conditions:

$$\left(\frac{\partial w}{\partial z}+v_P\frac{u}{r}\right)=\frac{\pi d_p\Delta r(1-v_P^2)}{E_pA_p}\left(\left(K+\frac{4}{3}G\right)\frac{\partial w}{\partial z}|_{soil}+\left(K-\frac{2}{3}G\right)\left(\frac{u}{r}+\frac{\partial u}{\partial r}|_{soil}\right)\right) \tag{92}$$

$$\frac{\partial^2 u}{\partial z^2}=0 \tag{93}$$

$$\frac{\partial^3 u}{\partial z^3}=0 \tag{94}$$

Discretization of the boundary conditions:

$$\begin{aligned} w_{i+1,j}=&\frac{2\pi d_p\Delta r(1-v_P^2)\left(K+\frac{4}{3}G\right)}{E_pA_p}\left(w_{i+1,j}-w_{i,j}\right)\\ &+\frac{2\Delta z\left(\pi d_p\Delta r(1-v_P^2)\left(K-\frac{2}{3}G\right)-v_PE_pA_p\right)}{E_pA_p}\frac{1}{r_j}u_{i,j}\\ &+\frac{2\Delta z\pi d_p(1-v_P^2)\left(K-\frac{2}{3}G\right)}{E_pA_p}\left(u_{i,j+1}-u_{i,j}\right)+w_{i-1,j}\end{aligned} \tag{95}$$

$$\frac{u_{i+1,j}-2u_{i,j}+u_{i-1,j}}{\Delta z^2}=0 \tag{96}$$

$$\frac{\frac{1}{2}u_{i+2,j}-u_{i+1,j}+u_{i-1,j}-\frac{1}{2}u_{i-2,j}}{\Delta z^3}=0 \tag{97}$$

This is equivalent to:

$$w_{i+1,j}=C_{32}w_{i+1,j}+w_{i-1,j}-C_{32}w_{i,j}+\left(C_{33}\frac{1}{r_j}-C_{34}\right)u_{i,j}+C_{34}u_{i,j+1} \tag{98}$$

$$u_{i+2,j}=6u_{i,j}-8u_{i-1,j}+3u_{i-2,j} \tag{99}$$

$$u_{i+1,j}=3u_{i,j}-3u_{i-1,j}+u_{i-2,j} \tag{100}$$

With:

$$C_{32}=\frac{2\pi d_p\Delta r(1-v_P^2)\left(K+\frac{4}{3}G\right)}{E_pA_p} \tag{101}$$

$$C_{33}=\frac{2\Delta z\left(\pi d_p\Delta r(1-v_P^2)\left(K-\frac{2}{3}G\right)-v_PE_pA_p\right)}{E_pA_p} \tag{102}$$

$$C_{34} = \frac{2\Delta z \pi d_p (1 - v_P^2)\left(K - \frac{2}{3}G\right)}{E_p A_p} \tag{103}$$

Substituting boundary condition expressions 85, 86 and 87 into equations 63 and 71 yields the final result:

$$\begin{aligned}\frac{\partial^2}{\partial t^2} w_{i,j} = {} & C_{20}C_{32}w_{i+1,j} + 2C_{20}w_{i-1,j} - \left(2C_{20} + C_{20}C_{32} + C_{22} + C_{22p}\right)w_{i,j} \\ & + C_{22}w_{i,j+1} + C_{22p}w_{i,j-1} \\ & + \left(2C_{23s} - C_{20}C_{34} + (C_{20}C_{33} + 3C_{21})\frac{1}{r_j}\right)u_{i,j} \\ & + \left(-3C_{23s} - 4C_{21}\frac{1}{r_j}\right)u_{i-1,j} + \left(C_{21}\frac{1}{r_j} + C_{23s}\right)u_{i-2,j} + C_{20}C_{34}u_{i,j+1}\end{aligned} \tag{104}$$

$$\begin{aligned}\frac{\partial^2}{\partial t^2} u_{i,j} = {} & \left(C_{29s}C_{32} - C_{24}C_{32}\frac{1}{r_j}\right)w_{i+1,j} + C_{29s}w_{i-1,j} \\ & + \left(-C_{29s}C_{32} - C_{29s} + C_{24}C_{32}\frac{1}{r_j}\right)w_{i,j} \\ & + \left(-C_{27} - C_{27p} - C_{29s}C_{34} + (C_{28s} + C_{29s}C_{33} + C_{24}C_{34})\frac{1}{r_j}\right. \\ & \left. + (-C_{24}C_{33} - C_{25})\frac{1}{r_j^2}\right)u_{i,j} + \left(C_{29s}C_{34} + C_{27} - C_{24}C_{34}\frac{1}{r_j}\right)u_{i,j+1} \\ & + C_{27p}u_{i,j-1}\end{aligned} \tag{105}$$

Second node from head:

Boundary condition:

$$u_{i-2} = 3u_{i-1} - 3u_i + u_{i+1} \tag{106}$$

Substituting boundary condition 106 into equation 63:

$$\begin{aligned}\rho\frac{\partial^2}{\partial t^2} u_{i,j} = {} & \left(C_{29s} - C_{24}\frac{1}{r_j}\right)w_{i+1,j} + C_{24}\frac{1}{r_j}w_{i-1,j} - w_{i,j}C_{29s} \\ & + \left(-C_{27} - 3C_{26} - C_{27p} + C_{28s}\frac{1}{r_j} - C_{25}\frac{1}{r_j^2}\right)u_{i,j} + C_{26}u_{i-1,j} \\ & + 3C_{26}u_{i+1,j} - C_{26}u_{i+2,j} + C_{27}u_{i,j+1} + C_{27p}u_{i,j-1}\end{aligned} \tag{107}$$

Second node from toe:

Boundary condition:

$$u_{i+2} = 3u_{i+1} - 3u_i + u_{i-1} \tag{108}$$

Substituting boundary condition 108 into equation 63:

$$\begin{aligned}\rho \frac{\partial^2}{\partial t^2} u_{i,j} = &\left(C_{29s} - C_{24}\frac{1}{r_j}\right) w_{i+1,j} + C_{24}\frac{1}{r_j} w_{i-1,j} - w_{i,j} C_{29s} \\ &+ \left(-C_{27} - 3C_{26} - C_{27p} + C_{28s}\frac{1}{r_j} - C_{25}\frac{1}{r_j^2}\right) u_{i,j} - C_{26} u_{i-2,j} \\ &+ 3C_{26} u_{i-1,j} + C_{26} u_{i+1,j} + C_{27} u_{i,j+1} + C_{27p} u_{i,j-1}\end{aligned} \tag{109}$$

Appendix B1: Matlab code Smith pile driving model

```
clearvars
close all
clc

beta=0.25; %Newmark scheme variable
gamma=0.5; %Newmark scheme variable
E=200*(10^9); %Young's modulus pile [N/m^2]
l=30; %pile length [m]
dof=301; %amount of discrete pile elements
di=1.96; %pile internal diameter [m]
de=2; %pile external diameter [m]
rho=7850; %pile volumetric weight [kg/m^3]
quake=2.5*(10^-3); %quake [m]
Jb=0.5; %damping ratio pile base [s/m]
Js=0.16; % damping ratio pile shaft [s/m]
pub=8*(10^6); %static limit pile base [N/m^2]
pus=5*(10^4); %static limit pile shaft [N/m^2]
v0=5; %hammer impact velocity [m/s]
mh=20000; %hammer mass [kg]
kc=10^10; %cushion stiffness [N/m]
acc=2; %numerical accuracy (minimum value=1.1)

cp=sqrt(E/rho);
dt=(l/(dof-1))/(acc*cp);
Ar=(((de^2)-(di^2))*pi())/4;
ki=(E*Ar)/(l/(dof-1));
dm=Ar*(l/(dof-1))*rho;
Z=(E*Ar)/cp;
Rub=pub*Ar;
Rus=(l/(dof-1))*de*pi()*pus;
t=0:dt:0.25;
doft=size(t,2)+1;
alpha=kc/(2*Z);
omega=sqrt(kc/mh);
c1=1/(beta*(dt^2));
c2=1/(beta*dt);
c3=1-(1/(2*beta));
c4=gamma/(beta*dt);
c5=1-(gamma/beta);
c6=dt*(1-(gamma/(2*beta)));
K=diag((2*ki*ones(1,dof)))+diag((-ki*ones(1,dof-1)),-1)+diag((-ki*ones(1,dof-1)),1);
K(1,1)=ki;
K(dof,dof)=ki;
M=diag((dm*ones(1,dof)));
C(dof,dof)=0;
Ma=(c1*M)+(c4*C)+K;
Mai=inv(Ma);
Mb=(c1*M)+(c4*C);
Mc=(c2*M)-(c5*C);
Md=(c3*M)+(c6*C);
```

```
U(dof,doft)=0;
V(dof,doft)=0;
A(dof,doft)=0;
sum(dof)=0;
sumb=0;
F(dof,1)=0;
for a=1:size(t,2)
    Fh=Z*(((v0*alpha)/sqrt((omega^2)-(alpha^2)))*exp(-alpha*t(a))*sin(sqrt((omega^2)-
(alpha^2))*t(a)));
    for i=1:dof
        if a>1 && abs(U(i,a)-sum(i))>quake
            sum(i)=sum(i)+U(i,a)-U(i,(a-1));
            F(i,a)=-(Rus*((U(i,a)-sum(i))/abs(U(i,a)-sum(i))))-(Rus*Js*V(i,a));
        else
            F(i,a)=-(Rus*((U(i,a)-sum(i))/quake))-(Rus*Js*V(i,a));
        end
    end
    F(1,a)=F(1,a)+Fh;
    if a>1 && (U(dof,a)-sumb)>quake
        sumb=sumb+U(dof,a)-U(dof,(a-1));
        Fb=-Rub-(Rub*Jb*V(dof,a));
    elseif a>1 && (U(dof,a)-sumb)<0
        Fb=0;
    else
        Fb=-(Rub*((U(dof,a)-sumb)/quake))-(Rub*Jb*V(dof,a));
    end
    F(dof,a)=F(dof,a)+Fb;
    U(:,a+1)=Mai*(F(:,a)+(Mb*U(:,a))+(Mc*V(:,a))-(Md*A(:,a)));
    V(:,a+1)=(c4*(U(:,a+1)-U(:,a)))+(c5*V(:,a))+(c6*A(:,a));
    A(:,a+1)=(c1*(U(:,a+1)-U(:,a)))-(c2*V(:,a))+(c3*A(:,a));
    if t(a)<0.01
        clf
        plot(V(:,a+1))
        axis([0 dof -3 3])
        ylabel('velocity [m/s]','FontSize',14)
        xlabel('vertical position [m]','FontSize',14)
        set(gca,'XTick',[0 dof/2 dof])
        set(gca,'XTickLabel',[0 1/2 1] )
        title(['t = ' sprintf('%0.5f',t(a)) ' [s]'],'FontSize',14)
        drawnow
    end
end
close all
plot(t,(10^3).*U(dof,2:end))
ylabel('pile toe displacement [mm]','FontSize',14)
xlabel('time [s]','FontSize',14)
```

Appendix B2: Matlab code Salgado pile driving model

```
clearvars
close all
clc

dz=0.1; %vertical grid size
dr=0.1; %radia grid size
Z=20; %pile length
R=20; %radial domain length
dp=2; %pile diameter
t=40*(10^-3); %pile shell thickness
rhop=7850; %pile volumetric wieght
Ep=200*(10^9); %pile Young's modulus
v0=5; %hammer impact velocity
mh=20000; %hammer mass
kc=10*(10^9); %cushion stiffness
quake=2.5*(10^-3); %quake
Jb=0.5; %damping ratio pile base
pub=8*(10^6); %static limit pile base
tend=0.1; %end time computation
tstep=0.001; %show plots at these intervals
acc=2; %numerical accuracy (minimum value = 1.1)
%Layering definition [startheight endheight shearmodulus density; nextlayer...]
layer=[1 5/dz 110*(10^6) 1800; (5/dz)+1 10/dz 70*(10^6) 1700; (10/dz)+1 15/dz 110*(10^6) 1800;
(15/dz)+1 (Z/dz)+1 150*(10^6) 2000];

dofz=(Z/dz)+1;
dofr=(R/dr)+1;
dof=dofz*dofr;
doft=tend/tstep;
Ap=0.25*pi()*(((dp+(t/2))^2)-((dp-(t/2))^2));
Imp=(Ep*Ap)/sqrt(Ep/rhop);
alpha=kc/(2*Imp);
omega=sqrt(kc/mh);
q1=((v0*alpha)/sqrt((omega^2)-(alpha^2)))*Imp;
q2=sqrt((omega^2)-(alpha^2));
tv=0:tstep:tend;
geo=zeros(dofz,dofr);
geo(:,2:dofr-1)=1;
geov=zeros(dofz,dofr);
geov(:,dofr)=1;
geop1=zeros(dofz,dofr);
geop1(1,1)=1;
geop2=zeros(dofz,dofr);
geop2(2:dofz-1,1)=1;
geop3=zeros(dofz,dofr);
geop3(dofz,1)=1;
r=zeros(dofr,1);
geor=zeros(dofz,dofr);
geovr=zeros(dofz,dofr);
for i=1:dofr
```

```
    r(i,1)=(dr*(i+(dp/(2*dr))-1));
    geor(:,i)=(1/r(i,1)).*geo(:,i);
    geovr(:,i)=(1/r(i,1)).*geov(:,i);
end
c1=zeros(dofz,dofr);
c2=zeros(dofz,dofr);
c3=zeros(dofz,dofr);
c4=zeros(dofz,dofr);
c5=zeros(dofz,dofr);
c6=zeros(dofz,dofr);
c7=zeros(dofz,dofr);
c8=zeros(dofz,dofr);
for i=1:size(layer,1)
    c1(layer(i,1):layer(i,2),:)=layer(i,3)/((dr^2)*layer(i,4));
    c2(layer(i,1):layer(i,2),:)=layer(i,3)/(2*dr*layer(i,4));
    c3(layer(i,1):layer(i,2),:)=2*dr*sqrt(layer(i,4)/layer(i,3));
    c4(layer(i,1):layer(i,2),:)=(pi()*dp*layer(i,3))/(dr*rhop*Ap);
    c5(layer(i,1):layer(i,2),:)=Ep/((dz^2)*rhop);
    c6(layer(i,1):layer(i,2),:)=(2*dz)/(Ep*Ap);
    c7(layer(i,1):layer(i,2),:)=(2*dz*pub)/(quake*Ep);
    c8(layer(i,1):layer(i,2),:)=(2*dz*pub*Jb)/Ep;
end
M1=sparse(dof,dof);
M2=sparse(dof,dof);
M22=-(2.*c1).*geo;
M1=M1+sparse(1:dof,1:dof,M22(:),dof,dof);
M21=(c1.*geo)-(c2.*geor);
M1=M1+sparse(dofz+1:dof,1:dof-dofz,M21(dofz+1:dof)',dof,dof);
M23=(c1.*geo)+(c2.*geor);
M1=M1+sparse(1:dof-dofz,dofz+1:dof,M23(1:dof-dofz)',dof,dof);
M22=-(2.*c1).*geov;
M1=M1+sparse(1:dof,1:dof,M22(:),dof,dof);
M21=(2.*c1).*geov;
M1=M1+sparse(dofz+1:dof,1:dof-dofz,M21(dofz+1:dof)',dof,dof);
M22=-((c3.*c1).*geov)-((c3.*c2).*geovr);
M2=M2+sparse(1:dof,1:dof,M22(:),dof,dof);
M22=-((2.*c5).*geop1)-(c4.*geop1);
M1=M1+sparse(1:dof,1:dof,M22(:),dof,dof);
M32=(2.*c5).*geop1;
M1=M1+sparse(1:dof-1,2:dof,M32(1:dof-1)',dof,dof);
M23=c4.*geop1;
M1=M1+sparse(1:dof-dofz,dofz+1:dof,M23(1:dof-dofz)',dof,dof);
M22=-((2.*c5).*geop2)-(c4.*geop2);
M1=M1+sparse(1:dof,1:dof,M22(:),dof,dof);
M12=c5.*geop2;
M1=M1+sparse(2:dof,1:dof-1,M12(2:dof)',dof,dof);
M32=c5.*geop2;
M1=M1+sparse(1:dof-1,2:dof,M32(1:dof-1)',dof,dof);
M23=c4.*geop2;
M1=M1+sparse(1:dof-dofz,dofz+1:dof,M23(1:dof-dofz)',dof,dof);
M22=-((2.*c5).*geop3)-(c4.*geop3)-((c5.*c7).*geop3);
M1=M1+sparse(1:dof,1:dof,M22(:),dof,dof);
M12=(2.*c5).*geop3;
```

```
M1=M1+sparse(2:dof,1:dof-1,M12(2:dof)',dof,dof);
M23=c4.*geop3;
M1=M1+sparse(1:dof-dofz,dofz+1:dof,M23(1:dof-dofz)',dof,dof);
M22=-(c5.*c8).*geop3;
M2=M2+sparse(1:dof,1:dof,M22(:),dof,dof);
Mi=speye(dof,dof);
Mz=sparse(dof,dof);
M=[Mz Mi; M1 M2];
F=zeros(2*dof,1);
F(dof+1)=c5(dofz,1)*c6(dofz,1);
w0=zeros(2*dof,1);
figure('units','normalized','outerposition',[0 0 1 1])
for n=1:doft
    tspan=((n-1)*tstep):(tstep/2):(n*tstep);
    [t,w]=ode45(@(t,w) M*w+((q1*exp(-alpha*t)*sin(q2*t)).*F),tspan,w0);
    w0=w(3,:)';
    W=w(3,1:dof)';
    WW=reshape(W,[dofz,dofr]);
    pcolor(WW)
    colormap(jet)
    set(gca,'XAxisLocation','top','YAxisLocation','left','ydir','reverse')
    colorbar
    caxis([-(10^-3) (10^-3)])
    xticks([0 dofr])
    xticklabels([0  R])
    yticks([0 dofz])
    yticklabels([0 Z])
    set(gca,'FontSize',15);
    axis equal
    axis tight
    set(gcf,'color','w');
    shading flat
    title(['t = ' sprintf('%0.5f',tv(n+1))],'FontSize',20)
    drawnow;
end
```

Appendix B3: Matlab code simplified cylindrically symmetric model

```
clearvars
close all
clc

dz=0.1; %vertical grid size
dr=0.1; %horizontal grid size
Z=16; %pile length below surface
Zt=8; %pile length above surface
R=20; %radial domain size
Zf=35; %vertical domain size
dn=2; %nominal pile diameter
th=40*(10^-3); %pile thickness
plug=10; %plug height
damp=0.00001; %damping
tend=0.1; %end time calculation
tstep=0.001; %intervals at which plot is shown
rhop=7850; %volumetric wieght pile
Ep=200*(10^9); %Young's modulus pile
v0=5; %impact velocity hammer
mh=20000; %mass hammer
kc=10*(10^9); %cushion stiffness
%soil and plug layering definition [startheight endheight shearmodulus bulkmodulus density;
nextlayer...]
layer=[1 9/dz 110*(10^6) 5000*(10^6) 1800; (9/dz)+1 15/dz 70*(10^6) 3800*(10^6) 1700; (15/dz)+1
22/dz 110*(10^6) 5000*(10^6) 1800; (22/dz)+1 (Zf/dz)+1 150*(10^6) 5900*(10^6) 2000];
layerp=[1 8/dz 110*(10^6) 5000*(10^6) 1800; (8/dz)+1 9/dz 70*(10^6) 3800*(10^6) 1700; (9/dz)+1
plug/dz 110*(10^6) 5000*(10^6) 1800];

dofz=((Zt+Zf)/dz)+1;
dofzz=((Zt+Z)/dz)+1;
dofzt=Zt/dz;
dofp=(((Zt+Z)-plug)/dz)+1;
dofr=((R+(dn/2))/dr)+1;
dofrr=((dn/2)/dr)+1;
dof=dofz*dofr;
Ap=0.25*pi()*(((dn+(th/2))^2)-((dn-(th/2))^2));
Imp=(Ep*Ap)/sqrt(Ep/rhop);
alpha=kc/(2*Imp);
omega=sqrt(kc/mh);
Imp=(Ep*Ap)/sqrt(Ep/rhop);
q1=((v0*alpha)/sqrt((omega^2)-(alpha^2)))*Imp;
q2=sqrt((omega^2)-(alpha^2));
doft=tend/tstep;
tv=0:tstep:tend;
geo=zeros(dofz,dofr);
geo(dofzt+2:dofz-1,2:dofr-1)=1;
geo(dofzt+2:dofp,2:dofrr)=0;
geo(dofzt+1:dofzz,dofrr)=0;
geo(dofzz,dofrr)=1;
geos=zeros(dofz,dofr);
```

```
geos(dofp:dofz-1,1)=1;
geof=zeros(dofz,dofr);
geof(dofzt+1,dofrr+1:dofr-1)=1;
geof(dofp,2:dofrr-1)=1;
geov=zeros(dofz,dofr);
geov(dofzt+2:dofz-1,dofr)=1;
geoh=zeros(dofz,dofr);
geoh(dofz,2:dofr-1)=1;
geop1=zeros(dofz,dofr);
geop1(1,dofrr)=1;
geop2=zeros(dofz,dofr);
geop2(2:dofzz-2,dofrr)=1;
geop3=zeros(dofz,dofr);
geop3(dofzz-1,dofrr)=1;
r=zeros(dofr,1);
geor=zeros(dofz,dofr);
geofr=zeros(dofz,dofr);
geovr=zeros(dofz,dofr);
geohr=zeros(dofz,dofr);
gs=geo+geof+geov+geoh+geos+geop1+geop2+geop3;
gs(gs==0)=NaN;
for i=1:dofr
    r(i,1)=(dr*(i-1));
    if i>1
        geor(:,i)=(1/r(i,1)).*geo(:,i);
        geofr(:,i)=(1/r(i,1)).*geof(:,i);
        geovr(:,i)=(1/r(i,1)).*geov(:,i);
        geohr(:,i)=(1/r(i,1)).*geoh(:,i);
    end
end
c1=zeros(dofz,dofr);
c2=zeros(dofz,dofr);
c3=zeros(dofz,dofr);
c4=zeros(dofz,dofr);
c5=zeros(dofz,dofr);
c6=zeros(dofz,dofr);
c6p=zeros(dofz,dofr);
c7=zeros(dofz,dofr);
c9=zeros(dofz,dofr);
c7(1:dofzz-1,dofrr)=Ep/((dz^2)*rhop);
c8=(2*dz)/(Ep*Ap);
for i=1:size(layer,1)
    c1(dofzt+layer(i,1):dofzt+layer(i,2),:)=(layer(i,4)+((4/3)*layer(i,3)))/((dz^2)*layer(i,5));
    c2(dofzt+layer(i,1):dofzt+layer(i,2),:)=layer(i,3)/((dr^2)*layer(i,5));
    c3(dofzt+layer(i,1):dofzt+layer(i,2),:)=layer(i,3)/(2*dr*layer(i,5));
    c4(dofzt+layer(i,1):dofzt+layer(i,2),:)=2*dr*sqrt(layer(i,5)/layer(i,3));

c5(dofzt+layer(i,1):dofzt+layer(i,2),:)=2*dz*sqrt(layer(i,5)/(layer(i,4)+((4/3)*layer(i,3))));
    c6(dofzt+layer(i,1):dofzt+layer(i,2),:)=(pi()*(dn+(th/2))*layer(i,3))/(dr*rhop*Ap);

c9(dofzt+layer(i,1):dofzt+layer(i,2),:)=(2*pi()*dn*dr*(layer(i,4)+((4/3)*layer(i,3))))/(Ep*Ap);
end
for i=1:size(layerp,1)
```

```
    c1(dofp-1+layerp(i,1):dofp-1+layerp(i,2),1:dofrr-
1)=(layerp(i,4)+((4/3)*layerp(i,3)))/((dz^2)*layerp(i,5));
    c2(dofp-1+layerp(i,1):dofp-1+layerp(i,2),1:dofrr-1)=layerp(i,3)/((dr^2)*layerp(i,5));
    c3(dofp-1+layerp(i,1):dofp-1+layerp(i,2),1:dofrr-1)=layerp(i,3)/(2*dr*layerp(i,5));
    c4(dofp-1+layerp(i,1):dofp-1+layerp(i,2),1:dofrr-1)=2*dr*sqrt(layerp(i,5)/layerp(i,3));
    c5(dofp-1+layerp(i,1):dofp-1+layerp(i,2),1:dofrr-
1)=2*dz*sqrt(layerp(i,5)/(layerp(i,4)+((4/3)*layerp(i,3))));
    c9(dofp-1+layerp(i,1):dofp-1+layerp(i,2),1:dofrr-
1)=(2*pi()*dn*dr*(layerp(i,4)+((4/3)*layerp(i,3))))/(Ep*Ap);
end
for i=1:size(layerp,1)
    c6p(dofp-1+layerp(i,1):dofp-1+layerp(i,2),dofrr)=(pi()*(dn-(th/2))*layerp(i,3))/(dr*rhop*Ap);
end
M1=sparse(dof,dof);
M22=(-2.*(c1+c2)).*geo;
M1=M1+sparse(1:dof,1:dof,M22(:),dof,dof);
M12=c1.*geo;
M1=M1+sparse(2:dof,1:dof-1,M12(2:dof)',dof,dof);
M32=c1.*geo;
M1=M1+sparse(1:dof-1,2:dof,M32(1:dof-1)',dof,dof);
M21=(c2.*geo)-(c3.*geor);
M1=M1+sparse(dofz+1:dof,1:dof-dofz,M21(dofz+1:dof)',dof,dof);
M23=(c2.*geo)+(c3.*geor);
M1=M1+sparse(1:dof-dofz,dofz+1:dof,M23(1:dof-dofz)',dof,dof);
M22=((-2.*c1)+(-4.*c2)).*geos;
M1=M1+sparse(1:dof,1:dof,M22(:),dof,dof);
M12=c1.*geos;
M12(dofp,1)=0;
M1=M1+sparse(2:dof,1:dof-1,M12(2:dof)',dof,dof);
M32=c1.*geos;
M32(dofp,1)=2*c1(dofp,1);
M1=M1+sparse(1:dof-1,2:dof,M32(1:dof-1)',dof,dof);
M23=(4.*c2).*geos;
M1=M1+sparse(1:dof-dofz,dofz+1:dof,M23(1:dof-dofz)',dof,dof);
M22=(-2.*(c1+c2)).*geof;
M1=M1+sparse(1:dof,1:dof,M22(:),dof,dof);
M32=(2.*c1).*geof;
M1=M1+sparse(1:dof-1,2:dof,M32(1:dof-1)',dof,dof);
M21=(c2.*geof)-(c3.*geofr);
M1=M1+sparse(dofz+1:dof,1:dof-dofz,M21(dofz+1:dof)',dof,dof);
M23=(c2.*geof)+(c3.*geofr);
M1=M1+sparse(1:dof-dofz,dofz+1:dof,M23(1:dof-dofz)',dof,dof);
M2=damp.*M1;
M22=(-2.*(c1+c2)).*geov;
M1=M1+sparse(1:dof,1:dof,M22(:),dof,dof);
M12=c1.*geov;
M1=M1+sparse(2:dof,1:dof-1,M12(2:dof)',dof,dof);
M32=c1.*geov;
M1=M1+sparse(1:dof-1,2:dof,M32(1:dof-1)',dof,dof);
M21=(2.*c2).*geov;
M1=M1+sparse(dofz+1:dof,1:dof-dofz,M21(dofz+1:dof)',dof,dof);
Md=-c4.*((c2.*geov)+(c3.*geovr));
M2=M2+sparse(1:dof,1:dof,Md(:),dof,dof);
```

```
M22=(-2.*(c1+c2)).*geoh;
M1=M1+sparse(1:dof,1:dof,M22(:),dof,dof);
M12=(2.*c1).*geoh;
M1=M1+sparse(2:dof,1:dof-1,M12(2:dof)',dof,dof);
M21=(c2.*geoh)-(c3.*geohr);
M1=M1+sparse(dofz+1:dof,1:dof-dofz,M21(dofz+1:dof)',dof,dof);
M23=(c2.*geoh)+(c3.*geohr);
M1=M1+sparse(1:dof-dofz,dofz+1:dof,M23(1:dof-dofz)',dof,dof);
Md=-c1.*(c5.*geoh);
M2=M2+sparse(1:dof,1:dof,Md(:),dof,dof);
M22=(-(2.*c7)-c6-c6p).*geop1;
M1=M1+sparse(1:dof,1:dof,M22(:),dof,dof);
M32=(2.*c7).*geop1;
M1=M1+sparse(1:dof-1,2:dof,M32(1:dof-1)',dof,dof);
M21=c6p.*geop1;
M1=M1+sparse(dofz+1:dof,1:dof-dofz,M21(dofz+1:dof)',dof,dof);
M23=c6.*geop1;
M1=M1+sparse(1:dof-dofz,dofz+1:dof,M23(1:dof-dofz)',dof,dof);
M22=(-(2.*c7)-c6-c6p).*geop2;
M1=M1+sparse(1:dof,1:dof,M22(:),dof,dof);
M12=c7.*geop2;
M1=M1+sparse(2:dof,1:dof-1,M12(2:dof)',dof,dof);
M32=c7.*geop2;
M1=M1+sparse(1:dof-1,2:dof,M32(1:dof-1)',dof,dof);
M21=c6p.*geop2;
M1=M1+sparse(dofz+1:dof,1:dof-dofz,M21(dofz+1:dof)',dof,dof);
M23=c6.*geop2;
M1=M1+sparse(1:dof-dofz,dofz+1:dof,M23(1:dof-dofz)',dof,dof);
M22=(-(2.*c7)-c6-c6p-(c7.*c9)).*geop3;
M1=M1+sparse(1:dof,1:dof,M22(:),dof,dof);
M12=(2.*c7).*geop3;
M1=M1+sparse(2:dof,1:dof-1,M12(2:dof)',dof,dof);
M32=(c7.*c9).*geop3;
M1=M1+sparse(1:dof-1,2:dof,M32(1:dof-1)',dof,dof);
M21=c6p.*geop3;
M1=M1+sparse(dofz+1:dof,1:dof-dofz,M21(dofz+1:dof)',dof,dof);
M23=c6.*geop3;
M1=M1+sparse(1:dof-dofz,dofz+1:dof,M23(1:dof-dofz)',dof,dof);
Mi=speye(dof,dof);
Mz=sparse(dof,dof);
M=[Mz Mi; M1 M2];
F=zeros(2*dof,1);
F(dof+((dofrr-1)*dofz)+1)=c7(1,dofrr)*c8;
w0=zeros(2*dof,1);
figure('units','normalized','outerposition',[0 0 1 1])
for n=1:doft
    tspan=((n-1)*tstep):(tstep/2):(n*tstep);
    [t,w]=ode45(@(t,w) M*w+(q1*exp(-alpha*t)*sin(q2*t)).*F,tspan,w0);
    w0=w(3,:)';
    W=reshape(w(3,1:dof)',[dofz,dofr]);
    pcolor(gs.*W)
    colormap(jet)
    set(gca,'XAxisLocation','top','YAxisLocation','left','ydir','reverse')
```

```
    colorbar
    caxis([-(10^-3) (10^-3)])
    xticks([0 dofrr dofr])
    xticklabels([0 (dn/2) R])
    yticks([dofp dofz])
    yticklabels([z-plug Zf])
    set(gca,'FontSize',15);
    axis equal
    axis tight
    set(gcf,'color','w');
    shading flat
    title(['t = ' sprintf('%0.5f',tv(n+1))],'FontSize',20)
    drawnow;
end
```

Appendix B4: Matlab code cylindrically symmetric model

```
clearvars
close all
clc

dz=0.1; %vertical grid size
dr=0.1; %radial grid size
Zt=8; %pile length above surface
Z=16; %pile length beneath surface
R=41; %radial domain size
plug=10; %plug height
Zf=50; %vertical domain size
dn=2; %nominal pile diameter
th=40*(10^-3);  %pile shell thickness
damp=0.0001; %soil damping
dampi=0.00002; %pile damping
tend=0.1; %end time calculation
tstep=0.001; %intervals at which plot is shown
rhop=7850;  %pile density
Ep=200*(10^9); %pile Young's modulus
vp=0.3; %pile Poisson ratio
v0=5; %impact velocity hammer
mh=20000; %mass hammer
kc=10^10; %cushion stiffness
%soil and plug layering definition [startheight endheight shearmodulus bulkmodulus density;
nextlayer...]
layer=[1 9/dz 110*(10^6) 5000*(10^6) 1800; (9/dz)+1 15/dz 70*(10^6) 3800*(10^6) 1700; (15/dz)+1
22/dz 110*(10^6) 5000*(10^6) 1800; (22/dz)+1 (Zf/dz)+1 150*(10^6) 5900*(10^6) 2000];
layerp=[1 8/dz 110*(10^6) 5000*(10^6) 1800; (8/dz)+1 9/dz 70*(10^6) 3800*(10^6) 1700; (9/dz)+1
plug/dz 110*(10^6) 5000*(10^6) 1800];

dofz=((Zt+Zf)/dz)+1;
dofzz=((Zt+Z)/dz)+1;
dofr=((R+(dn/2))/dr)+1;
dofrr=((dn/2)/dr)+1;
dof=dofz*dofr;
doff=2*dof;
doft=tend/tstep;
dofp=(((Z+Zt)-plug)/dz)+1;
dofpt=Zt/dz;
tv=0:tstep:tend;
Ap=0.25*pi()*(((dn+(th/2))^2)-((dn-(th/2))^2));
Imp=(Ep*Ap)/sqrt(Ep/rhop);
alpha=kc/(2*Imp);
omega=sqrt(kc/mh);
q1=((v0*alpha)/sqrt((omega^2)-(alpha^2)))*Imp;
q2=sqrt((omega^2)-(alpha^2));
layer(2:end,1)=layer(2:end,1)+(dofpt.*ones(size(layer,1)-1,1));
layer(:,2)=layer(:,2)+(dofpt.*ones(size(layer,1),1));
c1=zeros(dofz,dofr);
c2=zeros(dofz,dofr);
```

```
c3=zeros(dofz,dofr);
c4=zeros(dofz,dofr);
c4m=zeros(dofz,dofr);
c4mm=zeros(dofz,dofr);
c5=zeros(dofz,dofr);
c6=zeros(dofz,dofr);
c7=zeros(dofz,dofr);
c8=zeros(dofz,dofr);
c9=zeros(dofz,dofr);
c10=zeros(dofz,dofr);
c11=zeros(dofz,dofr);
c12=zeros(dofz,dofr);
c13=zeros(dofz,dofr);
c14=zeros(dofz,dofr);
c15=zeros(dofz,dofr);
c16=zeros(dofz,dofr);
c17=zeros(dofz,dofr);
c18=zeros(dofz,dofr);
c19=zeros(dofz,dofr);
c20=zeros(dofz,dofr);
c21=zeros(dofz,dofr);
c22=zeros(dofz,dofr);
c22p=zeros(dofz,dofr);
c23s=zeros(dofz,dofr);
c24=zeros(dofz,dofr);
c25=zeros(dofz,dofr);
c26=zeros(dofz,dofr);
c27=zeros(dofz,dofr);
c27p=zeros(dofz,dofr);
c28s=zeros(dofz,dofr);
c29s=zeros(dofz,dofr);
c30=zeros(dofz,dofr);
c31=zeros(dofz,dofr);
c32=zeros(dofz,dofr);
c33=zeros(dofz,dofr);
c34=zeros(dofz,dofr);
for i=1:size(layer,1)
c1(layer(i,1):layer(i,2),:)=(layer(i,4)+((4/3)*layer(i,3)))/((dr^2)*layer(i,5));
c2(layer(i,1):layer(i,2),:)=(layer(i,4)+((4/3)*layer(i,3)))/(2*dr*layer(i,5));
c3(layer(i,1):layer(i,2),:)=(layer(i,4)+((4/3)*layer(i,3)))/layer(i,5);
c4(layer(i,1):layer(i,2),:)=(layer(i,4)+((1/3)*layer(i,3)))/(4*dz*dr*layer(i,5));
c4m(layer(i,1):layer(i,2),:)=(layer(i,4)+((1/3)*layer(i,3)))/(2*dz*dr*layer(i,5));
c4mm(layer(i,1):layer(i,2),:)=(layer(i,4)+((1/3)*layer(i,3)))/(1*dz*dr*layer(i,5));
c5(layer(i,1):layer(i,2),:)=layer(i,3)/((dz^2)*layer(i,5));
c6(layer(i,1):layer(i,2),:)=(layer(i,4)+((4/3)*layer(i,3)))/((dz^2)*layer(i,5));
c7(layer(i,1):layer(i,2),:)=(layer(i,4)+((1/3)*layer(i,3)))/(2*dz*layer(i,5));
c8(layer(i,1):layer(i,2),:)=layer(i,3)/((dr^2)*layer(i,5));
c9(layer(i,1):layer(i,2),:)=layer(i,3)/(2*dr*layer(i,5));
c10(layer(i,1):layer(i,2),:)=(2*dz*(layer(i,4)-
((2/3)*layer(i,3))))/(layer(i,4)+((4/3)*layer(i,3)));
c11(layer(i,1):layer(i,2),:)=(dz*(layer(i,4)-
((2/3)*layer(i,3))))/(dr*(layer(i,4)+((4/3)*layer(i,3))));
c12(layer(i,1):layer(i,2),:)=dz/dr;
```

```
c13(layer(i,1):layer(i,2),:)=2*dr*sqrt(layer(i,5)/(layer(i,4)+((4/3)*layer(i,3))));
c14(layer(i,1):layer(i,2),:)=(2*dr*(layer(i,4)-
((2/3)*layer(i,3))))/(layer(i,4)+((4/3)*layer(i,3)));
c15(layer(i,1):layer(i,2),:)=(dr*(layer(i,4)-
((2/3)*layer(i,3))))/(dz*(layer(i,4)+((4/3)*layer(i,3))));
c16(layer(i,1):layer(i,2),:)=2*dr*sqrt(layer(i,5)/layer(i,3));
c17(layer(i,1):layer(i,2),:)=dr/dz;
c18(layer(i,1):layer(i,2),:)=2*dz*sqrt(layer(i,5)/(layer(i,4)+((4/3)*layer(i,3))));
c19(layer(i,1):layer(i,2),:)=2*dz*sqrt(layer(i,5)/layer(i,3));
c20(layer(i,1):layer(i,2),:)=Ep/((dz^2)*rhop*(1-(vp^2)));
c21(layer(i,1):layer(i,2),:)=(Ep*vp)/(2*dz*rhop*(1-(vp^2)));
c22(layer(i,1):layer(i,2),:)=layer(i,3)/(dr*rhop*th);
c23s(layer(i,1):layer(i,2),:)=layer(i,3)/(dz*rhop*th);
c24(layer(i,1):layer(i,2),:)=(vp*Ep)/(2*dz*rhop*(1-(vp^2)));
c25(layer(i,1):layer(i,2),:)=Ep/(rhop*(1-(vp^2)));
c26(layer(i,1):layer(i,2),:)=(Ep*(th^2))/(12*(dz^4)*rhop*(1-(vp^2)));
c27(layer(i,1):layer(i,2),:)=(layer(i,4)+((4/3)*layer(i,3)))/(dr*rhop*th);
c28s(layer(i,1):layer(i,2),:)=(layer(i,4)-((2/3)*layer(i,3)))/(rhop*th);
c29s(layer(i,1):layer(i,2),:)=(layer(i,4)-((2/3)*layer(i,3)))/(dz*rhop*th);
c30(layer(i,1):layer(i,2),:)=(2*dz*(1-(vp^2)))/(Ep*Ap);
c31(layer(i,1):layer(i,2),:)=2*dz*vp;
c32(layer(i,1):layer(i,2),:)=(2*pi()*dn*dr*(1-(vp^2))*(layer(i,4)+((4/3)*layer(i,3))))/(Ep*Ap);
c33(layer(i,1):layer(i,2),:)=(2*dz*((pi()*dn*dr*(1-(vp^2))*(layer(i,4)-((2/3)*layer(i,3))))-
(vp*Ep*Ap)))/(Ep*Ap);
c34(layer(i,1):layer(i,2),:)=(2*dz*pi()*dn*(1-(vp^2))*(layer(i,4)-((2/3)*layer(i,3))))/(Ep*Ap);
end
c22(1:dofpt,:)=0;
c23s(1:dofpt,:)=0;
c27(1:dofpt,:)=0;
c28s(1:dofpt,:)=0;
c29s(1:dofpt,:)=0;
c23s(dofp:dofz,:)=0;
c28s(dofp:dofz,:)=0;
c29s(dofp:dofz,:)=0;
if plug>0
for i=1:size(layerp,1)
c1(dofp-1+layerp(i,1):dofp-1+layerp(i,2),1:dofrr-
1)=(layerp(i,4)+((4/3)*layerp(i,3)))/((dr^2)*layerp(i,5));
c2(dofp-1+layerp(i,1):dofp-1+layerp(i,2),1:dofrr-
1)=(layerp(i,4)+((4/3)*layerp(i,3)))/(2*dr*layerp(i,5));
c3(dofp-1+layerp(i,1):dofp-1+layerp(i,2),1:dofrr-
1)=(layerp(i,4)+((4/3)*layerp(i,3)))/layerp(i,5);
c4(dofp-1+layerp(i,1):dofp-1+layerp(i,2),1:dofrr-
1)=(layerp(i,4)+((1/3)*layerp(i,3)))/(4*dz*dr*layerp(i,5));
c4m(dofp-1+layerp(i,1):dofp-1+layerp(i,2),1:dofrr-
1)=(layerp(i,4)+((1/3)*layerp(i,3)))/(2*dz*dr*layerp(i,5));
c4mm(dofp-1+layerp(i,1):dofp-1+layerp(i,2),1:dofrr-
1)=(layerp(i,4)+((1/3)*layerp(i,3)))/(1*dz*dr*layerp(i,5));
c5(dofp-1+layerp(i,1):dofp-1+layerp(i,2),1:dofrr-1)=layerp(i,3)/((dz^2)*layerp(i,5));
c6(dofp-1+layerp(i,1):dofp-1+layerp(i,2),1:dofrr-
1)=(layerp(i,4)+((4/3)*layerp(i,3)))/((dz^2)*layerp(i,5));
c7(dofp-1+layerp(i,1):dofp-1+layerp(i,2),1:dofrr-
1)=(layerp(i,4)+((1/3)*layerp(i,3)))/(2*dz*layerp(i,5));
```

```
c8(dofp-1+layerp(i,1):dofp-1+layerp(i,2),1:dofrr-1)=layerp(i,3)/((dr^2)*layerp(i,5));
c9(dofp-1+layerp(i,1):dofp-1+layerp(i,2),1:dofrr-1)=layerp(i,3)/(2*dr*layerp(i,5));
c10(dofp-1+layerp(i,1):dofp-1+layerp(i,2),1:dofrr-1)=(2*dz*(layerp(i,4)-
((2/3)*layerp(i,3))))/(layerp(i,4)+((4/3)*layerp(i,3)));
c11(dofp-1+layerp(i,1):dofp-1+layerp(i,2),1:dofrr-1)=(dz*(layerp(i,4)-
((2/3)*layerp(i,3))))/(dr*(layerp(i,4)+((4/3)*layerp(i,3))));
c13(dofp-1+layerp(i,1):dofp-1+layerp(i,2),1:dofrr-
1)=2*dr*sqrt(layerp(i,5)/(layerp(i,4)+((4/3)*layerp(i,3))));
c14(dofp-1+layerp(i,1):dofp-1+layerp(i,2),1:dofrr-1)=(2*dr*(layerp(i,4)-
((2/3)*layerp(i,3))))/(layerp(i,4)+((4/3)*layerp(i,3)));
c15(dofp-1+layerp(i,1):dofp-1+layerp(i,2),1:dofrr-1)=(dr*(layerp(i,4)-
((2/3)*layerp(i,3))))/(dz*(layerp(i,4)+((4/3)*layerp(i,3))));
c16(dofp-1+layerp(i,1):dofp-1+layerp(i,2),1:dofrr-1)=2*dr*sqrt(layerp(i,5)/layerp(i,3));
c18(dofp-1+layerp(i,1):dofp-1+layerp(i,2),1:dofrr-
1)=2*dz*sqrt(layerp(i,5)/(layerp(i,4)+((4/3)*layerp(i,3))));
c19(dofp-1+layerp(i,1):dofp-1+layerp(i,2),1:dofrr-1)=2*dz*sqrt(layerp(i,5)/layerp(i,3));
c22p(dofp-1+layerp(i,1):dofp-1+layerp(i,2),dofrr)=layerp(i,3)/(dr*rhop*th);
c27p(dofp-1+layerp(i,1):dofp-1+layerp(i,2),dofrr)=(layerp(i,4)+((4/3)*layerp(i,3)))/(dr*rhop*th);
end
end
geo=zeros(dofz,dofr);
geo(dofpt+2:dofz-1,2:dofr-1)=1;
geo(dofpt+2:dofp,2:dofrr)=0;
geo(dofpt+2:dofzz,dofrr)=0;
geos=zeros(dofz,dofr);
geos(dofp+1:dofz-1,1)=1;
geof=zeros(dofz,dofr);
geof(dofpt+1,dofrr+1:dofr-1)=1;
geof(dofp,2:dofrr-1)=1;
geoe=zeros(dofz,dofr);
geoe(dofp,1)=1;
geov=zeros(dofz,dofr);
geov(dofpt+2:dofz-1,dofr)=1;
geoh=zeros(dofz,dofr);
geoh(dofz,2:dofr-1)=1;
geop1=zeros(dofz,dofr);
geop1(1,dofrr)=1;
geop2=zeros(dofz,dofr);
geop2(2,dofrr)=1;
geop3=zeros(dofz,dofr);
geop3(3:dofzz-2,dofrr)=1;
geop4=zeros(dofz,dofr);
geop4(dofzz-1,dofrr)=1;
geop5=zeros(dofz,dofr);
geop5(dofzz,dofrr)=1;
r=zeros(dofr,1);
geor=zeros(dofz,dofr);
geofr=zeros(dofz,dofr);
geovr=zeros(dofz,dofr);
geohr=zeros(dofz,dofr);
geop1r=zeros(dofz,dofr);
geop2r=zeros(dofz,dofr);
geop3r=zeros(dofz,dofr);
```

```
geop4r=zeros(dofz,dofr);
geop5r=zeros(dofz,dofr);
geor2=zeros(dofz,dofr);
geofr2=zeros(dofz,dofr);
geovr2=zeros(dofz,dofr);
geohr2=zeros(dofz,dofr);
geop1r2=zeros(dofz,dofr);
geop2r2=zeros(dofz,dofr);
geop3r2=zeros(dofz,dofr);
geop4r2=zeros(dofz,dofr);
geop5r2=zeros(dofz,dofr);
gs=geo+geof+geov+geoh+geos+geoe+geop1+geop2+geop3+geop4+geop5;
gs(gs==0)=NaN;
for i=1:dofr
    r(i,1)=(dr*(i-1));
    if i>1
        geor(:,i)=(1/r(i,1)).*geo(:,i);
        geofr(:,i)=(1/r(i,1)).*geof(:,i);
        geovr(:,i)=(1/r(i,1)).*geov(:,i);
        geohr(:,i)=(1/r(i,1)).*geoh(:,i);
        geop1r(:,i)=(1/r(i,1)).*geop1(:,i);
        geop2r(:,i)=(1/r(i,1)).*geop2(:,i);
        geop3r(:,i)=(1/r(i,1)).*geop3(:,i);
        geop4r(:,i)=(1/r(i,1)).*geop4(:,i);
        geop5r(:,i)=(1/r(i,1)).*geop5(:,i);
        geor2(:,i)=(1/(r(i,1)^2)).*geo(:,i);
        geofr2(:,i)=(1/(r(i,1)^2)).*geof(:,i);
        geovr2(:,i)=(1/(r(i,1)^2)).*geov(:,i);
        geohr2(:,i)=(1/(r(i,1)^2)).*geoh(:,i);
        geop1r2(:,i)=(1/(r(i,1)^2)).*geop1(:,i);
        geop2r2(:,i)=(1/(r(i,1)^2)).*geop2(:,i);
        geop3r2(:,i)=(1/(r(i,1)^2)).*geop3(:,i);
        geop4r2(:,i)=(1/(r(i,1)^2)).*geop4(:,i);
        geop5r2(:,i)=(1/(r(i,1)^2)).*geop5(:,i);
    end
end
M1=sparse(doff,doff);
W22=(-2.*(c6+c8)).*geo;
M1=M1+sparse(1:dof,1:dof,W22(:),doff,doff);
W12=c6.*geo;
M1=M1+sparse(2:dof,1:dof-1,W12(2:dof)',doff,doff);
W32=c6.*geo;
M1=M1+sparse(1:dof-1,2:dof,W32(1:dof-1)',doff,doff);
W21=(c8.*geo)-(c9.*geor);
M1=M1+sparse(dofz+1:dof,1:dof-dofz,W21(dofz+1:dof)',doff,doff);
W23=(c8.*geo)+(c9.*geor);
M1=M1+sparse(1:dof-dofz,dofz+1:dof,W23(1:dof-dofz)',doff,doff);
U12=-c7.*geor;
M1=M1+sparse(2:dof,dof+1:doff-1,U12(2:dof)',doff,doff);
U32=c7.*geor;
M1=M1+sparse(1:dof-1,dof+2:doff,U32(1:dof-1)',doff,doff);
U33=c4.*geo;
M1=M1+sparse(1:dof-dofz-1,dof+dofz+2:doff,U33(1:dof-dofz-1)',doff,doff);
```

```
U31=-c4.*geo;
M1=M1+sparse(dofz:dof,dof+1:doff-dofz+1,U31(dofz:dof)',doff,doff);
U13=-c4.*geo;
M1=M1+sparse(1:dof-dofz+1,dof+dofz:doff,U13(1:dof-dofz+1)',doff,doff);
U11=c4.*geo;
M1=M1+sparse(dofz+2:dof,dof+1:doff-dofz-1,U11(dofz+2:dof)',doff,doff);
W33=c4.*geo;
M1=M1+sparse(dof+1:doff-dofz-1,dofz+2:dof,W33(1:dof-dofz-1)',doff,doff);
W31=-c4.*geo;
M1=M1+sparse(dof+dofz:doff,1:dof-dofz+1,W31(dofz:dof)',doff,doff);
W13=-c4.*geo;
M1=M1+sparse(dof+1:doff-dofz+1,dofz:dof,W13(1:dof-dofz+1)',doff,doff);
W11=c4.*geo;
M1=M1+sparse(dof+dofz+2:doff,1:dof-dofz-1,W11(dofz+2:dof)',doff,doff);
U22=((-2.*(c1+c5)).*geo)-(c3.*geor2);
M1=M1+sparse(dof+1:doff,dof+1:doff,U22(:),doff,doff);
U12=c5.*geo;
M1=M1+sparse(dof+2:doff,dof+1:doff-1,U12(2:dof)',doff,doff);
U32=c5.*geo;
M1=M1+sparse(dof+1:doff-1,dof+2:doff,U32(1:dof-1)',doff,doff);
U21=(c1.*geo)-(c2.*geor);
M1=M1+sparse(dof+dofz+1:doff,dof+1:doff-dofz,U21(dofz+1:dof)',doff,doff);
U23=(c1.*geo)+(c2.*geor);
M1=M1+sparse(dof+1:doff-dofz,dof+dofz+1:doff,U23(1:dof-dofz)',doff,doff);
M2=(damp.*M1);
W22=(-2.*(c6+c8)).*geof;
M1=M1+sparse(1:dof,1:dof,W22(:),doff,doff);
W32=(2.*c6).*geof;
M1=M1+sparse(1:dof-1,2:dof,W32(1:dof-1)',doff,doff);
W21=(c8.*geof)+(((c7.*c12)-c9).*geofr);
M1=M1+sparse(dofz+1:dof,1:dof-dofz,W21(dofz+1:dof)',doff,doff);
W23=(c8.*geof)+((c9-(c7.*c12)).*geofr);
M1=M1+sparse(1:dof-dofz,dofz+1:dof,W23(1:dof-dofz)',doff,doff);
U22=(c6.*c10).*geofr;
M1=M1+sparse(1:dof,dof+1:doff,U22(:),doff,doff);
U33=c4m.*geof;
M1=M1+sparse(1:dof-dofz-1,dof+dofz+2:doff,U33(1:dof-dofz-1)',doff,doff);
U31=-c4m.*geof;
M1=M1+sparse(dofz:dof,dof+1:doff-dofz+1,U31(dofz:dof)',doff,doff);
U23=((c6.*c11)-c4m).*geof;
M1=M1+sparse(1:dof-dofz,dof+dofz+1:doff,U23(1:dof-dofz)',doff,doff);
U21=(c4m-(c6.*c11)).*geof;
M1=M1+sparse(dofz+1:dof,dof+1:doff-dofz,U21(dofz+1:dof)',doff,doff);
W33=c4m.*geof;
M1=M1+sparse(dof+1:doff-dofz-1,dofz+2:dof,W33(1:dof-dofz-1)',doff,doff);
W31=-c4m.*geof;
M1=M1+sparse(dof+dofz:doff,1:dof-dofz+1,W31(dofz:dof)',doff,doff);
W23=((c5.*c12)-c4m).*geof;
M1=M1+sparse(dof+1:doff-dofz,dofz+1:dof,W23(1:dof-dofz)',doff,doff);
W21=(c4m-(c5.*c12)).*geof;
M1=M1+sparse(dof+dofz+1:doff,1:dof-dofz,W21(dofz+1:dof)',doff,doff);
U22=((-2.*(c1+c5)).*geof)-(c3.*geofr2);
M1=M1+sparse(dof+1:doff,dof+1:doff,U22(:),doff,doff);
```

```
U32=(2.*c5).*geof;
M1=M1+sparse(dof+1:doff-1,dof+2:doff,U32(1:dof-1)',doff,doff);
U21=(c1.*geof)-(c2.*geofr);
M1=M1+sparse(dof+dofz+1:doff,dof+1:doff-dofz,U21(dofz+1:dof)',doff,doff);
U23=(c1.*geof)+(c2.*geofr);
M1=M1+sparse(dof+1:doff-dofz,dof+dofz+1:doff,U23(1:dof-dofz)',doff,doff);
W22=(-2.*(c6+c8)).*geov;
M1=M1+sparse(1:dof,1:dof,W22(:),doff,doff);
W12=c6.*geov;
M1=M1+sparse(2:dof,1:dof-1,W12(2:dof)',doff,doff);
W32=c6.*geov;
M1=M1+sparse(1:dof-1,2:dof,W32(1:dof-1)',doff,doff);
W21=(2.*c8).*geov;
M1=M1+sparse(dofz+1:dof,1:dof-dofz,W21(dofz+1:dof)',doff,doff);
U12=(((c17.*c8)-c4m).*geov)+(((c17.*c9)-c7).*geovr);
M1=M1+sparse(2:dof,dof+1:doff-1,U12(2:dof)',doff,doff);
U32=((c4m-(c17.*c8)).*geov)+((c7-(c17.*c9)).*geovr);
M1=M1+sparse(1:dof-1,dof+2:doff,U32(1:dof-1)',doff,doff);
U31=-c4m.*geov;
M1=M1+sparse(dofz:dof,dof+1:doff-dofz+1,U31(dofz:dof)',doff,doff);
U11=c4m.*geov;
M1=M1+sparse(dofz+2:dof,dof+1:doff-dofz-1,U11(dofz+2:dof)',doff,doff);
Md=-((c16.*c8).*geov)-((c16.*c9).*geovr);
M2=M2+sparse(1:dof,1:dof,Md(:),doff,doff);
W12=(((c15.*c1)-c4m).*geov)+((c15.*c2).*geovr);
M1=M1+sparse(dof+2:doff,1:dof-1,W12(2:dof)',doff,doff);
W32=((c4m-(c15.*c1)).*geov)-((c15.*c2).*geovr);
M1=M1+sparse(dof+1:doff-1,2:dof,W32(1:dof-1)',doff,doff);
W31=-c4m.*geov;
M1=M1+sparse(dof+dofz:doff,1:dof-dofz+1,W31(dofz:dof)',doff,doff);
W11=c4m.*geov;
M1=M1+sparse(dof+dofz+2:doff,1:dof-dofz-1,W11(dofz+2:dof)',doff,doff);
U22=-((2.*(c1+c5)).*geov)-((c1.*c14).*geovr)-((c3+(c2.*c14)).*geovr2);
M1=M1+sparse(dof+1:doff,dof+1:doff,U22(:),doff,doff);
U12=c5.*geov;
M1=M1+sparse(dof+2:doff,dof+1:doff-1,U12(2:dof)',doff,doff);
U32=c5.*geov;
M1=M1+sparse(dof+1:doff-1,dof+2:doff,U32(1:dof-1)',doff,doff);
U21=(2.*c1).*geov;
M1=M1+sparse(dof+dofz+1:doff,dof+1:doff-dofz,U21(dofz+1:dof)',doff,doff);
Md=-((c13.*c1).*geov)-((c13.*c2).*geovr);
M2=M2+sparse(dof+1:doff,dof+1:doff,Md(:),doff,doff);
W22=(-2.*(c6+c8)).*geoh;
M1=M1+sparse(1:dof,1:dof,W22(:),doff,doff);
W12=(2.*c6).*geoh;
M1=M1+sparse(2:dof,1:dof-1,W12(2:dof)',doff,doff);
W21=(c8.*geoh)+(((c7.*c12)-c9).*geohr);
M1=M1+sparse(dofz+1:dof,1:dof-dofz,W21(dofz+1:dof)',doff,doff);
W23=(c8.*geoh)+((c9-(c7.*c12)).*geohr);
M1=M1+sparse(1:dof-dofz,dofz+1:dof,W23(1:dof-dofz)',doff,doff);
U22=-(c6.*c10).*geohr;
M1=M1+sparse(1:dof,dof+1:doff,U22(:),doff,doff);
U13=-c4m.*geoh;
```

```
M1=M1+sparse(1:dof-dofz+1,dof+dofz:doff,U13(1:dof-dofz+1)',doff,doff);
U11=c4m.*geoh;
M1=M1+sparse(dofz+2:dof,dof+1:doff-dofz-1,U11(dofz+2:dof)',doff,doff);
U23=(c4m-(c6.*c11)).*geoh;
M1=M1+sparse(1:dof-dofz,dof+dofz+1:doff,U23(1:dof-dofz)',doff,doff);
U21=((c6.*c11)-c4m).*geoh;
M1=M1+sparse(dofz+1:dof,dof+1:doff-dofz,U21(dofz+1:dof)',doff,doff);
Md=-(c6.*c18).*geoh;
M2=M2+sparse(1:dof,1:dof,Md(:),doff,doff);
Md=-(c7.*c19).*geohr;
M2=M2+sparse(1:dof,dof+1:doff,Md(:),doff,doff);
W13=-c4m.*geoh;
M1=M1+sparse(dof+1:doff-dofz+1,dofz:dof,W13(1:dof-dofz+1)',doff,doff);
W11=c4m.*geoh;
M1=M1+sparse(dof+dofz+2:doff,1:dof-dofz-1,W11(dofz+2:dof)',doff,doff);
W23=(c4m-(c5.*c12)).*geoh;
M1=M1+sparse(dof+1:doff-dofz,dofz+1:dof,W23(1:dof-dofz)',doff,doff);
W21=((c5.*c12)-c4m).*geoh;
M1=M1+sparse(dof+dofz+1:doff,1:dof-dofz,W21(dofz+1:dof)',doff,doff);
U22=((-2.*(c1+c5)).*geoh)-(c3.*geohr2);
M1=M1+sparse(dof+1:doff,dof+1:doff,U22(:),doff,doff);
U12=(2.*c5).*geoh;
M1=M1+sparse(dof+2:doff,dof+1:doff-1,U12(2:dof)',doff,doff);
U21=(c1.*geoh)-(c2.*geohr);
M1=M1+sparse(dof+dofz+1:doff,dof+1:doff-dofz,U21(dofz+1:dof)',doff,doff);
U23=(c1.*geoh)+(c2.*geohr);
M1=M1+sparse(dof+1:doff-dofz,dof+dofz+1:doff,U23(1:dof-dofz)',doff,doff);
Md=-(c5.*c19).*geoh;
M2=M2+sparse(dof+1:doff,dof+1:doff,Md(:),doff,doff);
W22=(-(2.*c6)-(4.*c8)).*geos;
M1=M1+sparse(1:dof,1:dof,W22(:),doff,doff);
W12=c6.*geos;
M1=M1+sparse(2:dof,1:dof-1,W12(2:dof)',doff,doff);
W32=c6.*geos;
M1=M1+sparse(1:dof-1,2:dof,W32(1:dof-1)',doff,doff);
W23=(4.*c8).*geos;
M1=M1+sparse(1:dof-dofz,dofz+1:dof,W23(1:dof-dofz)',doff,doff);
U33=c4m.*geos;
M1=M1+sparse(1:dof-dofz-1,dof+dofz+2:doff,U33(1:dof-dofz-1)',doff,doff);
U13=-c4m.*geos;
M1=M1+sparse(1:dof-dofz+1,dof+dofz:doff,U13(1:dof-dofz+1)',doff,doff);
W22=(-(2.*c6)-(4.*c8)).*geoe;
M1=M1+sparse(1:dof,1:dof,W22(:),doff,doff);
W32=(2.*c6).*geoe;
M1=M1+sparse(1:dof-1,2:dof,W32(1:dof-1)',doff,doff);
W23=(4.*c8).*geoe;
M1=M1+sparse(1:dof-dofz,dofz+1:dof,W23(1:dof-dofz)',doff,doff);
U33=c4mm.*geoe;
M1=M1+sparse(1:dof-dofz-1,dof+dofz+2:doff,U33(1:dof-dofz-1)',doff,doff);
U23=((2.*(c6.*c11))-c4mm).*geoe;
M1=M1+sparse(1:dof-dofz,dof+dofz+1:doff,U23(1:dof-dofz)',doff,doff);
M3=M1;
W22=-((2.*c20)+c22+c22p).*geop1;
```

```
M1=M1+sparse(1:dof,1:dof,W22(:),doff,doff);
W32=(2.*c20).*geop1;
M1=M1+sparse(1:dof-1,2:dof,W32(1:dof-1)',doff,doff);
W21=c22p.*geop1;
M1=M1+sparse(1+dofz:dof,1:dof-dofz,W21(1+dofz:dof)',doff,doff);
W23=c22.*geop1;
M1=M1+sparse(1:dof-dofz,dofz+1:dof,W23(1:dof-dofz)',doff,doff);
U22=(((c20.*c30)-(3.*c21)).*geop1r)-(c23s.*geop1);
M1=M1+sparse(1:dof,dof+1:doff,U22(:),doff,doff);
U32=((4.*c21).*geop1r)+(c23s.*geop1);
M1=M1+sparse(1:dof-1,dof+2:doff,U32(1:dof-1)',doff,doff);
U42=-c21.*geop1r;
M1=M1+sparse(1:dof-2,dof+3:doff,U42(1:dof-2)',doff,doff);
W22=-c29s.*geop1;
M1=M1+sparse(dof+1:doff,1:dof,W22(:),doff,doff);
W32=c29s.*geop1;
M1=M1+sparse(dof+1:doff-1,2:dof,W32(1:dof-1)',doff,doff);
U22=((-c27-c27p).*geop1)+(c28s.*geop1r)+(((c24.*c31)-c25).*geop1r2);
M1=M1+sparse(dof+1:doff,dof+1:doff,U22(:),doff,doff);
U21=c27p.*geop1;
M1=M1+sparse(dof+dofz+1:doff,dof+1:doff-dofz,U21(dofz+1:dof)',doff,doff);
U23=c27.*geop1;
M1=M1+sparse(dof+1:doff-dofz,dof+dofz+1:doff,U23(1:dof-dofz)',doff,doff);
W22=-((2.*c20)+c22+c22p).*geop2;
M1=M1+sparse(1:dof,1:dof,W22(:),doff,doff);
W12=c20.*geop2;
M1=M1+sparse(2:dof,1:dof-1,W12(2:dof)',doff,doff);
W32=c20.*geop2;
M1=M1+sparse(1:dof-1,2:dof,W32(1:dof-1)',doff,doff);
W21=c22p.*geop2;
M1=M1+sparse(dofz+1:dof,1:dof-dofz,W21(dofz+1:dof)',doff,doff);
W23=c22.*geop2;
M1=M1+sparse(1:dof-dofz,dofz+1:dof,W23(1:dof-dofz)',doff,doff);
U22=-c23s.*geop2;
M1=M1+sparse(1:dof,dof+1:doff,U22(:),doff,doff);
U12=-c21.*geop2r;
M1=M1+sparse(2:dof,dof+1:doff-1,U12(2:dof)',doff,doff);
U32=(c21.*geop2r)+(c23s.*geop2);
M1=M1+sparse(1:dof-1,dof+2:doff,U32(1:dof-1)',doff,doff);
W22=-c29s.*geop2;
M1=M1+sparse(dof+1:doff,1:dof,W22(:),doff,doff);
W12=c24.*geop2r;
M1=M1+sparse(dof+2:doff,1:dof-1,W12(2:dof)',doff,doff);
W32=(-c24.*geop2r)+(c29s.*geop2);
M1=M1+sparse(dof+1:doff-1,2:dof,W32(1:dof-1)',doff,doff);
U22=-(((3.*c26)+c27+c27p).*geop2)+(c28s.*geop2r)-(c25.*geop2r2);
M1=M1+sparse(dof+1:doff,dof+1:doff,U22(:),doff,doff);
U12=(1.*c26).*geop2;
M1=M1+sparse(dof+2:doff,dof+1:doff-1,U12(2:dof)',doff,doff);
U32=(3.*c26).*geop2;
M1=M1+sparse(dof+1:doff-1,dof+2:doff,U32(1:dof-1)',doff,doff);
U42=-c26.*geop2;
M1=M1+sparse(dof+1:doff-2,dof+3:doff,U42(1:dof-2)',doff,doff);
```

```
U21=c27p.*geop2;
M1=M1+sparse(dof+dofz+1:doff,dof+1:doff-dofz,U21(1+dofz:dof)',doff,doff);
U23=c27.*geop2;
M1=M1+sparse(dof+1:doff-dofz,dof+dofz+1:doff,U23(1:dof-dofz)',doff,doff);
W22=-((2.*c20)+c22+c22p).*geop3;
M1=M1+sparse(1:dof,1:dof,W22(:),doff,doff);
W12=c20.*geop3;
M1=M1+sparse(2:dof,1:dof-1,W12(2:dof)',doff,doff);
W32=c20.*geop3;
M1=M1+sparse(1:dof-1,2:dof,W32(1:dof-1)',doff,doff);
W21=c22p.*geop3;
M1=M1+sparse(dofz+1:dof,1:dof-dofz,W21(dofz+1:dof)',doff,doff);
W23=c22.*geop3;
M1=M1+sparse(1:dof-dofz,dofz+1:dof,W23(1:dof-dofz)',doff,doff);
U22=-c23s.*geop3;
M1=M1+sparse(1:dof,dof+1:doff,U22(:),doff,doff);
U12=-c21.*geop3r;
M1=M1+sparse(2:dof,dof+1:doff-1,U12(2:dof)',doff,doff);
U32=(c21.*geop3r)+(c23s.*geop3);
M1=M1+sparse(1:dof-1,dof+2:doff,U32(1:dof-1)',doff,doff);
W22=-c29s.*geop3;
M1=M1+sparse(dof+1:doff,1:dof,W22(:),doff,doff);
W12=c24.*geop3r;
M1=M1+sparse(dof+2:doff,1:dof-1,W12(2:dof)',doff,doff);
W32=(-c24.*geop3r)+(c29s.*geop3);
M1=M1+sparse(dof+1:doff-1,2:dof,W32(1:dof-1)',doff,doff);
U22=-(((6.*c26)+c27+c27p).*geop3)+(c28s.*geop3r)-(c25.*geop3r2);
M1=M1+sparse(dof+1:doff,dof+1:doff,U22(:),doff,doff);
U02=-c26.*geop3;
M1=M1+sparse(dof+3:doff,dof+1:doff-2,U02(3:dof)',doff,doff);
U12=(4.*c26).*geop3;
M1=M1+sparse(dof+2:doff,dof+1:doff-1,U12(2:dof)',doff,doff);
U32=(4.*c26).*geop3;
M1=M1+sparse(dof+1:doff-1,dof+2:doff,U32(1:dof-1)',doff,doff);
U42=-c26.*geop3;
M1=M1+sparse(dof+1:doff-2,dof+3:doff,U42(1:dof-2)',doff,doff);
U21=c27p.*geop3;
M1=M1+sparse(dof+dofz+1:doff,dof+1:doff-dofz,U21(1+dofz:dof)',doff,doff);
U23=c27.*geop3;
M1=M1+sparse(dof+1:doff-dofz,dof+dofz+1:doff,U23(1:dof-dofz)',doff,doff);
W22=-((2.*c20)+c22+c22p).*geop4;
M1=M1+sparse(1:dof,1:dof,W22(:),doff,doff);
W12=c20.*geop4;
M1=M1+sparse(2:dof,1:dof-1,W12(2:dof)',doff,doff);
W32=c20.*geop4;
M1=M1+sparse(1:dof-1,2:dof,W32(1:dof-1)',doff,doff);
W21=c22p.*geop4;
M1=M1+sparse(dofz+1:dof,1:dof-dofz,W21(dofz+1:dof)',doff,doff);
W23=c22.*geop4;
M1=M1+sparse(1:dof-dofz,dofz+1:dof,W23(1:dof-dofz)',doff,doff);
U22=-c23s.*geop4;
M1=M1+sparse(1:dof,dof+1:doff,U22(:),doff,doff);
U12=-c21.*geop4r;
```

```
M1=M1+sparse(2:dof,dof+1:doff-1,U12(2:dof)',doff,doff);
U32=(c21.*geop4r)+(c23s.*geop4);
M1=M1+sparse(1:dof-1,dof+2:doff,U32(1:dof-1)',doff,doff);
W22=-c29s.*geop4;
M1=M1+sparse(dof+1:doff,1:dof,W22(:),doff,doff);
W12=c24.*geop4r;
M1=M1+sparse(dof+2:doff,1:dof-1,W12(2:dof)',doff,doff);
W32=(-c24.*geop4r)+(c29s.*geop4);
M1=M1+sparse(dof+1:doff-1,2:dof,W32(1:dof-1)',doff,doff);
U22=-(((3.*c26)+c27+c27p).*geop4)+(c28s.*geop4r)-(c25.*geop4r2);
M1=M1+sparse(dof+1:doff,dof+1:doff,U22(:),doff,doff);
U02=-c26.*geop4;
M1=M1+sparse(dof+3:doff,dof+1:doff-2,U02(3:dof)',doff,doff);
U12=(3.*c26).*geop4;
M1=M1+sparse(dof+2:doff,dof+1:doff-1,U12(2:dof)',doff,doff);
U32=(1.*c26).*geop4;
M1=M1+sparse(dof+1:doff-1,dof+2:doff,U32(1:dof-1)',doff,doff);
U21=c27p.*geop4;
M1=M1+sparse(dof+dofz+1:doff,dof+1:doff-dofz,U21(1+dofz:dof)',doff,doff);
U23=c27.*geop4;
M1=M1+sparse(dof+1:doff-dofz,dof+dofz+1:doff,U23(1:dof-dofz)',doff,doff);
W22=-((2.*c20)+c22+c22p+(c20.*c32)).*geop5;
M1=M1+sparse(1:dof,1:dof,W22(:),doff,doff);
W12=(2.*c20).*geop5;
M1=M1+sparse(2:dof,1:dof-1,W12(2:dof)',doff,doff);
W32=(c20.*c32).*geop5;
M1=M1+sparse(1:dof-1,2:dof,W32(1:dof-1)',doff,doff);
W21=c22p.*geop5;
M1=M1+sparse(dofz+1:dof,1:dof-dofz,W21(dofz+1:dof)',doff,doff);
W23=c22.*geop5;
M1=M1+sparse(1:dof-dofz,dofz+1:dof,W23(1:dof-dofz)',doff,doff);
U22=(((2.*c23s)-(c20.*c34)).*geop5)+(((c20.*c33)+(3.*c21)).*geop5r);
M1=M1+sparse(1:dof,dof+1:doff,U22(:),doff,doff);
U02=(c23s.*geop5)+(c21.*geop5r);
M1=M1+sparse(3:dof,dof+1:doff-2,U02(3:dof)',doff,doff);
U12=-((3.*c23s).*geop5)-((4.*c21).*geop5r);
M1=M1+sparse(2:dof,dof+1:doff-1,U12(2:dof)',doff,doff);
U23=(c20.*c34).*geop5;
M1=M1+sparse(1:dof-dofz,dof+dofz+1:doff,U23(1:dof-dofz)',doff,doff);
W22=((-c29s-(c29s.*c32)).*geop5)+((c24.*c32).*geop5r);
M1=M1+sparse(dof+1:doff,1:dof,W22(:),doff,doff);
W12=c29s.*geop5;
M1=M1+sparse(dof+2:doff,1:dof-1,W12(2:dof)',doff,doff);
W32=((c29s.*c32).*geop5)-((c24.*c32).*geop5r);
M1=M1+sparse(dof+1:doff-1,2:dof,W32(1:dof-1)',doff,doff);
U22=((-c27-c27p-(c29s.*c34)).*geop5)+((c28s+(c29s.*c33)+(c24.*c34)).*geop5r)+((-c25-
(c24.*c33)).*geop5r2);
M1=M1+sparse(dof+1:doff,dof+1:doff,U22(:),doff,doff);
U21=c27p.*geop5;
M1=M1+sparse(dof+dofz+1:doff,dof+1:doff-dofz,U21(dofz+1:dof)',doff,doff);
U23=((c27+(c29s.*c34)).*geop5)-((c24.*c34).*geop5r);
M1=M1+sparse(dof+1:doff-dofz,dof+dofz+1:doff,U23(1:dof-dofz)',doff,doff);
M2=M2+((M1-M3).*dampi);
```

```
Mz=sparse(doff,doff);
Mi=speye(doff,doff);
M=[Mz Mi; M1 M2];
F=zeros(2*doff,1);
F(doff+((dofrr-1)*dofz)+1)=c20(1,dofrr)*c30(1,dofrr);
F(doff+dof+((dofrr-1)*dofz)+1)=(c24(1,dofrr)*c30(1,dofrr))/r(dofrr);
w0=zeros(2*doff,1);
figure('units','normalized','outerposition',[0 0 1 1])
for n=1:doft
    tspan=((n-1)*tstep):(tstep/2):(n*tstep);
    [t,w]=ode45(@(t,w) M*w+(q1*exp(-alpha*t)*sin(q2*t)).*F,tspan,w0);
    w0=w(3,:)';
    WW=reshape(w(3,1:dof)',[dofz,dofr]);
    UU=reshape(w(3,dof+1:doff)',[dofz,dofr]);
    subplot(1,2,1)
    pcolor(WW.*gs)
    colormap(jet)
    set(gca,'XAxisLocation','top','YAxisLocation','left','ydir','reverse')
    colorbar
    caxis([-(10^-3) (10^-3)])
    xticks([0 dofrr dofr])
    xticklabels([0 (dn/2) R])
    yticks([dofp dofz])
    yticklabels([Z-plug Zf])
    set(gca,'FontSize',15);
    axis equal
    axis tight
    set(gcf,'color','w');
    shading flat
    title(['W at t = ' sprintf('%0.5f',tv(n+1))],'FontSize',20)
    subplot(1,2,2)
    pcolor(UU.*gs)
    colormap(jet)
    set(gca,'XAxisLocation','top','YAxisLocation','left','ydir','reverse')
    colorbar
    caxis([-2*(10^-4) 2*(10^-4)])
    xticks([0 dofrr dofr])
    xticklabels([0 (dn/2) R])
    yticks([dofp dofz])
    yticklabels([Z-plug Zf])
    set(gca,'FontSize',15);
    axis equal
    axis tight
    set(gcf,'color','w');
    shading flat
    title(['U at t = ' sprintf('%0.5f',tv(n+1))],'FontSize',20)
    drawnow;
end
```